Actuation Power Efficiency Analysis for an Active Structure

by

Renfang Cao, M.S.

Dissertation submitted to the Faculty of the
Virginia Polytechnic Institute and State University
in partial fulfillment of the requirements for the degree of

Ph.D.

in

Mechanical Engineering

Donald J. Leo, Chair
William T. Baumman
Ricardo A. Burdisso
Daniel J. Inman
Harry Robertshaw

April 2001

Blacksburg, Virginia

Actuation Power Efficiency Analysis for an Active Structure

Renfang Cao

Virginia Polytechnic Institute and State University, 2001

Advisor: Donald J. Leo

Abstract

Methods for analyzing the structural-acoustic power efficiency of active structures are developed. For this work we define the power efficiency as the ratio of the sound power radiated by a structure to the maximum possible radiated sound power. An active structure is defined as one that has electromechanical actuators distributed over its surface for the purpose of structural-acoustic excitation. The power efficiency of planar, baffled structures with arbitrary boundary conditions is examined using a combination of methods based on numerical integration, variational principles, and finite element analysis.

The fundamental result of this work is that computing the power efficiency of an active structure reduces to the solution of two eigenvalue problems. The maximum possible sound power radiated by a planar, baffled structure is shown to be equivalent to the largest eigenvalue of the acoustic power transfer matrix. The structural-acoustic power efficiency is the solution of a separate generalized eigenvalue problem whose parameters include the location of the electromechanical actuators and the type of electromechanical actuation. The advantage of this metric over other measures of radiation efficiency is that 0 and 1 bound the structural-acoustic power efficiency. Furthermore, solving for the power efficiency as a function of frequency yields a measure of the bandwidth of the structural-acoustic actuator.

Power efficiency is analyzed for point force actuation and distributed moment actuation. Numerical simulations demonstrate that maximizing the power efficiency requires that the magnitude and phase of the structural modal velocity vector be matched to that of the eigenvector that corresponds to the maximum eigenvalue of the acoustic power transfer matrix. Matching the modal velocity to the maximizing eigenvector produces a vibration shape that maximizes the sound power radiation of the structure. Individual actuators are not able to achieve high efficiency over a broad frequency range for both types of electromechanical actuation. Multiple-actuator arrays are able to achieve higher average efficiency at the expense of increased number of actuators.

An optimization problem is then posed to maximize the structural-acoustic power efficiency by varying the location and size of distributed moment actuators. We demonstrate that an average efficiency on the order of 0.85 is possible over a large bandwidth through optimal placement and sizing of a set of four distributed moment actuators. Experimental results on a baffled plate demonstrate that correct phasing of the actuators results in velocity distributions that correlate well with predicted results.

Acknowledgments

First and foremost I would like to thank my advisor, Dr. Donald J. Leo for his wisdom and guidance throughout this process and all the supports through this study. I truly appreciate his confident in me at all stages of my research. His wonderful philosophy on the multiple areas in control, electronics, vibration and noise suppression, not only help me in the general advice but also the very much detailed the instructions. I would also like to specially thank Dr. Dan Inman for his valuable comments on my dissertation and Dr. Harry H. Robortshaw for his help to the study, and for both of them kind presence on my committee. Drs. Willam T. Baumann and Ricardo. A. Burdisso deserve a hearty thanks for kindly service as members of my committee and for their valuable suggestions throughout this endeavor and comments on the dissertation.

I wish to acknowledge all the staff and students at the Center for Intelligent Material Systems and Structures for their generous assistance and true understanding at all times. My special thanks go to Mr. Kenn Newbury and Dr. Gyuhae Park for his help both in the experimental suggestion and in his theoretical models. I would also like to thank Mark Malowicki for his kind help in proof-reading for most of this writing. I would also like to thank Ms. Beth Howell for helping fedexing the drafts to me.

I am specially grateful to my wife, Hailian Chen, for her understanding and supporting for my studies and her dedications to our family. Without those, I am sure that I could not complete this work. I am also greatly indebted to my daughter Jenny and Anna. Thank you, my parents, sister and brother-in-law for their support and encouragement in my pursue of higher degrees in the USA.

Thanks go to Dr. Gary S. Robinson for his allowing me to use anechoic chamber. Special thanks go to Drs. Jinwei Feng, Qinhong Chen, and Mr. Ming Dong for their kind help.

Renfang Cao

Virginia Polytechnic Institute and State University

April 2001

Contents

List of Tables

List of Figures

Chapter 1

Introduction

1.1 Background

Vibration and noise are persistent problems in many engineering applications. Various noise and vibration control techniques have been developed to alleviate problems in sound radiation and sound transmission. The large majority of these systems can be loosely defined as active or passive. Among these techniques, passive methods are widely used in industries and commercial products. Passive methods differ from active methods, in that they require no external power inputs for operation. Passive noise control either adds some noise reduction materials or devices to, or modifies the original system in such a way to reduce the unwanted the sound emission by the net system. Typical passive methods include sound absorbing materials and vibration damping materials. Mufflers, enclosures, and barriers are other examples of passive methods to reduce noise. Sound absorbing materials are commonly implemented for a large range of applications (such as buildings, machinery enclosures, and aircraft) to reduce sound propagation. As suggested by Kim and Song (1999), passive methods are often the most cost effective technique for suppressing noise in the mid to high frequencies, but they are less effective at low frequencies where the acoustical wavelength of the sound is relatively long compared to the thickness of the absorbing materials. Vibration damping materials can also be effective at suppressing structural sound radiation, but they also have limited effectiveness at frequencies well below the

critical frequency of the vibrating structure.

The limited effectiveness of passive noise suppression has resulted in the development of active control methods for the attenuation of low frequency noise. The possibility of active noise control was suggested by Lueg in 1936, but it was not until relatively recently that advances in digital signal processing have made active noise control a feasible alternative to passive techniques [Warnaka (1982)]. Active noise cancelation(ANC) is achieved by the intentional superposition of acoustic waves to create a destructive interference pattern so that attenuation of unwanted sound occurs. With this method, noise is canceled by an out of phase control signal generated by the control sources, such as speakers, directly added onto the acoustic field. Previous studies demonstrated that when the sound source is complex or distributed over multiple surfaces, many acoustic control sources are required in order to provide global control [C. R. Fuller and Nelson (1996)]. This disadvantage limited its engineering applications and motivated the development of a new technique, active structural-acoustic control(ASAC) for controlling structural sound radiation and structural sound transmission.

ASAC differs from active noise cancelation in the manner in which sound radiation and sound transmission is controlled. The seminal work in active structural-acoustic control was performed and reported by Fuller (1990) and , Jones and Fuller (1989) in their series of papers on controlling structural sound radiation and sound transmission. Since this study will not focus on the ASAC, this author will not present a detailed literature review on this field. However, a very comprehensive literature survey in the advancement of active noise control until 1990 can be found in the paper of Stevens and Ahuja (1991).

ANC uses acoustic sources directly added on the acoustic field to cancel the noise. Unlike ANC, ASAC relies on vibration sources, such as piezoelectric ceramic actuators and electromagnetic shakers, applied directly to the structure to control the noise. In general, this strategy requires a smaller number of control inputs for a global sound reduction in the acoustic field as compared to ANC. A common type of piezoelectric ceramic used in active noise control is the lead zirconate titanate

or short for PZT, a ferroelectric ceramic material with piezoelectric properties and reciprocal behavior that converts electrical energy into mechanical energy. Although a lot of scholars have successfully reduced the noise by the implementations of ASAC using different control algorithms: adaptive feedforward control algorithm [Widrow and Stearns (1985)], eigenvalue assignment [Burdisso et al. (1994)], linear-quadratic-Gaussian (LQG) [Ho and Robertshaw (1992)], not much emphasis has been paid to the effectiveness of an individual actuator or group actuators. As one can imagine, the effectiveness of the actuators plays a key role in the active noise control. Therefore, this work will focus on the maximization of the actuation power of the actuators.

A brief literature review in the immediately following sections will focus on the previous work on the sound radiation power analysis, the effectiveness of an actuator, and especially the sound radiation power and the actuation power efficiency of an actuator driven structure.

1.2 Sound Radiation from Plates

Early researchers studying the sound radiation of a structure focused on the radiation efficiency, which is defined as the ratio of the average acoustic power radiated per unit area of a vibrating surface to the average acoustic power radiated per unit area of a piston that is vibrating with the same average mean square velocity [Fahy (1985)]. Based on the similar definition, different approaches were applied to analyze the radiation of a beam and panel.

Using the Rayleigh integral and a far-field power integral, Wallace (1972) studied the far-field radiation efficiency of each low frequency mode without the coupling of different modes of a simply supported panel. One of the major disadvantages of his work was that the coupling between modes was ignored. Maillard (1974) advanced Wallace's work by cataloging the vibrational modes of the surface, edge, and corner modes in terms of modal radiation efficiency. Lomas and Hayek (1977) further advanced Wallace's work by including the numerical evaluation of the inertial cross-coupling terms oscillating functions. They also developed an approach to study the

sound radiation from an elastically supported plate. Keltie and Peng (1987) investigated the problem of the modal coupling and concluded that its effect on the radiated sound power was important to the degree that the modal coupling terms should not be ignored, especially for low frequency and off-resonance excitation cases. Instead of the direct evaluation on the Rayleigh integral, Levine (1984) developed a coordinate transformation that enables the exact evaluation of the integrals obtained in the use of spatial Fourier analysis applied to beams.

In another hand, some recent researchers further advanced Wallace's work by substituting the modal expansions into the Rayleigh integration and evaluated the sound radiation from radiation efficiency. Elliot and Johnson (1993) investigated the sound radiation power using the magnitude of mode shapes, and amplitudes of a number of elemental radiators. It was shown that velocity distributions which radiate independently can be calculated as the eigenvectors of an elemental radiation resistance matrix. The radiation efficiencies of these radiation modes were proportional to the corresponding eigenvalue of the radiation resistance matrix. Similarly, Naghshienh (1993), Snyder and Tanaka (1995)published their work on the study of sound power radiated from a simply supported structure. Based upon Wallace's work, they using a modal decomposition analysis of the acoustic power radiated from a simply-supported rectangular panel, represented the total acoustic power as summed contributions from the radiation efficiencies. They represented a power transfer matrix as their radiation operator. Within the power transfer matrix, the off-diagonal or mutual radiation terms were expressed as functions of the on-diagonal or self-radiation terms [Snyder and Tanaka (1995)]. Applying the modal decomposition analysis to their study, Leo and Paine (1997a) contributed to the field by deriving the maximum sound power radiation of a simply-supported plate as an eigenvalue decomposition problem. Their technique showed that the maximum radiation power was simply proportional to the largest eigenvalue of the power transfer matrix, which could be evaluated using numerical integration. It provided us with a easy way to evaluate the maximum sound radiation power of a simply supported structure. However, it could not be directly applied to a structure under non-simply supported boundary conditions.

While majority of the researchers focused on their study on the simply supported structures, a few scholars were considering noise reduction of the structures with a variation of boundary conditions from simply supporting. Based on a variational method and the Hamiltonian principle, Berry et al. (1990) presented a method using trial functions to study the radiation of the sound from a plate with edges elastically restrained against deflection and rotation. They applied their model to analyze the radiation efficiencies of modes of simply supported, clamped, free, and guided plates. Their results of a simply supported plate agreed with previous work. However, this method requires significant large terms of the trial functions [Berry et al. (1990); Song (1995)].

Based upon Galerkins method, Sung and Jan (1997) published their work on the active control of sound radiation from a clamped rectangular plate by piezoelectric moments. They proposed an approximate solution to the clamped plate using quasiorthogonal shape functions and the virtual work principal. The dynamic system response of the structure to the point force and piezomoments was approximately derived. They demonstrated that the piezomoment excitation effectively attenuated the global sound radiation power by approximately 24dB.

As an further application of the variational method and the Rayleigh-Ritz method, some researchers [Aksu and Ali (1976); Mead (1988a,b); Newbury and Leo (2000)] investigated the frequency or mode shape variation of plates with stiffeners, which are widely used in civil, marines, and aerospace structures because of their high strength-to-weight ratio. However, theses authors did not focus on the sound radiation power analysis of the stiffened structures.

As we could see from the literatures listed above that the majority of the sound radiation analysis did not focus on structure under the non-simply supported boundary conditions. Although some researchers' work on active noise control involved in the analysis of non-simply supported structure, it did not focus on the sound radiation analysis. Cao and Leo (1998) integrated the FEA, numerical integration, and eigenvalue decomposition technique into the sound radiation analysis of a structure under an arbitrary support. Submitting the normal mode analysis from FEA into

numerical integration, and integrated with eigenvalue decomposition technique, this method provides us with a general approach to analyze the sound radiation of a planar structure under any supports. Unfortunately, the FEA made it hard for the designers to get physical meaning from results. Therefore, a hybrid method integrated the variational approach with the numerical integration and eigenvalue technique will also be developed in this study.

1.3 The Effectiveness of Noise Reduction

Our above literature survey shows that the majority of the research related to the active noise control so far has not been directly related to the analysis of actuator efficiency. However, some of the work involves the effectiveness of noise reduction of the structure.

Fuller (1989) analyzed the active control of sound transmission through a circular plate clamped at the edges. Using active control, the plate will have a lower radiation efficiency. They inferred that the sound reduction is in some cases the results of redistributing the plate response, modal restructuring, and in others as suppressing plate modal vibration, modal suppression. They also experimentally investigated the effectiveness of using secondary acoustic sources and using control forces [Fuller (1990)]. It was found that the accelerometer locations were so critical to the control output that, at certain circumstance, the control system resulted in an increase in the sound pressure level.

Using distributed PZT actuators as control elements, Dimitriadis and Fuller (1989) suggested that the locations and sizes of the PZT actuators were very important to the control performance. Results from their study showed that the number of the control point forces required less than that of acoustic sources. Through an analytical study, Snyder and Hansen (1991) also reached the similar conclusion as above and they emphasized the importance of the actuator locations on the control performance of the system.

In the implementation of active noise control, different cost functions or con-

trol algorithms were used in the noise reduction. Built the cost function as being proportional to the radiated sound power, Dimitriadis and Fuller (1990) analyzed sound radiation control of a multiple PZT actuator driven simply supported plate. In their analysis, they concluded that the control would be much more effective with the use of multiple actuators. They also pointed out that the actuator locations were the key factor to the control effectiveness. Similarly, choosing a finite sum of the mean-squared sound pressure in the far field as the optimization objective function, Dimitriadis and Fuller (1990) developed an optimization approach for optimal locations of PZT actuators. It is demonstrated that with optimally located actuators, the control performance of the system is much better than that with the arbitrarily positioned actuators [Fuller and Dimitriadis (1991)].

Using the same cost function and filtered -x version of the adaptive LMS algorithm, Clark and Fuller (1991, 1992) developed an approach for the optimization of the sizes and locations of rectangular PVDF sensors in their investigation of the active noise control using polyvinylidene fluoride(PVDF) sensors. The experiments illustrate the importance of optimally locating the control transducers is of the same importance as the number of control channels.

Choosing the total sound radiation power, Varadan et al. (1997) combined a FEA with optimization to model and optimize sound attenuation of a piezoelectric active structure system. In their work, a group of actuators were used to reduce the sound radiated noise in a moderate frequency band, 200-400Hz. By changing the applied voltage to one of the single piezoelectric actuators, the sound radiation of the structure at first few natural frequencies was controlled. In their model, three-dimensional piezoelectric elements, flat shell elements, and transition element were used. It required large computer space and memory, and due to the size limitation of meshes, it is difficult to apply to a large structure.

Instead of using sound power as cost function, Meirovitch and Thangjithan (1990) chose the most active radiators as control strategy and then evaluated the attenuation level of the sound field with the high excitation frequencies of a large number of control actuator driven simply supported plate. Burdisso et al. (1994)

developed a technique to actively control the noise by responding with only the weakest set of modal radiators. They implemented the eigenvalue analysis for active noise control using a feedforward algorithm. This was demonstrated on a simply-supported, rectangular plate mounted in an infinite, rigid baffled. Cunefare (1991) presented an optimal velocity distribution for simply supported and clamped beams and the minimum radiation efficiencies in a set of orthogonal radiation modes. A modal expansion of the surface velocity in terms of unknown modal amplitude coefficients, the Rayleigh integration and a far-field intensity integration are employed to obtain a quadratic expression for the radiation efficiency of the beam. He concluded that the eigenvector of modal amplitude coefficients corresponding to the lowest eigenvalue yields the minimum radiation efficiency, while the eigenvalue itself is the actual value of the minimum radiation efficiency.

In another hand, some researchers use surface velocity as cost function in their implementation of noise reduction. Expressing the sound power as a function of the surface velocity, Ho and Robertshaw (1992) and Naghshienh (1993) used it to control broad band sound radiation from structures. Expressed the radiated power in the quadratic form of surface velocity, Naghshineh and Koopmann (1992) using a modal decomposition technique to actively control the noise of a clamped-clamped beam. The radiated power was summed contributions of eigenvalues determined from the linear combination of the eigenvectors, corresponding to the actual surface velocity. The radiated power was expressed in terms of primary and control forces on the nodes of the discrete node of the beam. With quadratic optimization the minium value of the power was achieved based on the spatial placement of the control forces, resulting in a set of optimum weights for the actuator forces. They also used eigenvectors acted as surface velocity filters to minimize the cost function using the control strategy determined by actively eliminating the most efficient radiators.

In addition, some work has also been performed in noise reduction by using linear control theory, such as linear quadratic regulator(LQR) or linear quadratic Gussion(LQG) in their controlling of noise. Ho and Robertshaw (1992) developed a method to estimate, in real time, the total radiated energy from measurements on

the structure and designed radiation filters and the feedback controller using LQR to suppress the acoustic energy radiated to the far field from a structure that has been excited by a short-duration pulse. The real time estimation of total acoustic energy was accomplished by spatially decomposing the structure and then decomposing the radiation of these spatial functions with respect to temporal frequency. A radiator filter was constructed based on these frequency responses. The radiation was estimated by converting the velocity measurements into the predetermined spatial functions. Computer simulation of a clamped-clamped beam demonstrated the effectiveness of the acoustic controller incorporated with radiation filter when compared to a vibration controller using the same control energy [Suanders and Robertshaw (1991)]. Furthermore, Ho and Robertshaw (1992) formulated the acoustic suppression problem for persistent broadband disturbance as a standard LQG problem and an optimal feedback controller was designed to minimize the radiation power of a clamped-clamped beam.

Song (1995) investigated the optimization of transducers for active control structural sound radiation from elastically supported plates under multiple-frequency excitation. In his study, two types of approaches have been developed to optimally design the error sensors. One is to design the sensors which can provide information about the radiated sound power. The other is based on the sufficient conditions developed in this work for the error criteria in the linear quadratic optimal control theory. For the second approach, an optimization procedure has been developed to determine the optimal locations of microphone sensors in the sound field. Moreover, a series of parametric studies have been conducted to evaluate the sensitivity of the control performance of the optimally designed actuator and sensor systems to the changes in important system parameters, such as the disturbance frequency, the plate support conditions. Its results show that even use of a small number of carefully located error sensors, it is possible to achieve global sound attenuation.

Problems with multiple actuators require a multiple input multiple output(MIMO) analysis. Some researchers tried to simplify the control problem using a directed combinatorial search, called Tabu search, to select an optimal configuration from a much

larger set of candidate locations, Dan, et al, optimized the locations for arrays of sensors and actuators. In their test 8 PZT actuators were installed on the interior shell of the cylinder, a total of 462 microphone locations were sampled. The goal is to derive and test optimum sensor and actuator arrays of dimension 8 x4, respectively, at three frequencies, which are relatively corresponding to the coupled strong acoustic and strong structural mode, weak acoustic and strong structural mode, and strong acoustic and weak structural mode [Palumbo and Cabell (2000)].

Instead of a conventional multichannel controller, Feng (1995) used one control channel to control multiple actuators by turning the subsidiary actuators to in phase or out of phase with the master actuator or simply switch off the subsidiary actuators and noise reduction is 15 -20 dB higher than that of the signal actuator method for a baffled, simply supported plate.

The above literature review showed that different methods have been successfully applied to the noise reduction control. However, the majority of the research focused on the noise reduction as a global measurement of the effectiveness of the control algorithm. There have been not enough emphases on the effectiveness of the actuator itself.

In order to analyze the effectiveness and maximize the performance of the actuators, Leo and Paine (1997a) suggested a definition of power efficiency as a standard to compare with for different actuators. The power efficiency is defined as the actual sound power radiated by the plate over the maximum possible sound power. It was evaluated using the eigenvalue decomposition for both the point force and the moment distributed PZT actuator driven plate. They also reduced the power efficiency of an air acoustic actuator array to a generalized eigenvalue problem, and they studied the maximum acoustic power output of the air-acoustic actuator array [Leo and Paine (1997b)].

Applying Leo and Paine's work to the study of the power efficiency of a general planar structure under an arbitrary supporting condition, Cao and Leo (1998) extended the eigenvalue decomposition technique to the study of power efficiency of an elastically supported general planar structure by integrating the finite element and

numerical integration. They also investigated the effect of boundary conditions, the number of actuators, as well as the location of the actuator on the power efficiency. Furthermore, they applied the eigenvalue decomposition and general eigenvalue decomposition technique to the radiation impedance calculation and power efficiency study of an elastic supported circular plate.

As the literatures suggested that there were little work focused on the power efficiency of the actuators, although a great deal of work has been successfully made to the noise reduction as a globe measurement. Therefore, this work will focus on the actuation power efficiency of the actuator(s) and the maximization of the actuator performance of an active structure.

1.4 Piezoceramic Actuator Modeling

With the development of ASAC, smart materials, such as shape memory alloys, electrostrictive materials, magnetostrictive materials and electro-rheological fluids, PVDF film, especially the piezoelectric ceramics, have been studied extensively for active control. When a control voltage is applied to PZT materials, it will generate mechanical strain. Conversely, it will generate a voltage when it is under mechanical deformation. Because of the coupling of the PZT materials with the host structure, the dynamics of the active system will vary from those of the plain host structure or PZT material itself. There also is energy transfer between mechanical energy and electric energy when the control voltage is applied.

Some researchers have investigated the mechanisms and modeling of smart materials, especially the piezoceramics.

Based on strain compatibility between the PZT patch and structure surface in contact, Crawley and Luis (1989) used both static model and dynamic models to predict the structural response when an external voltage was applied to PZT actuators. Their dynamic model was not strictly dynamic because it was generated by simply incorporating a dynamic model of the structure into a coupling static model of the PZT and its substructure. However, this model will give a reasonable

estimation of the force response if the PZT mass is much smaller than the total mass and the resonance frequency is much higher than the frequency of interest. As an extension of this work, Dimitriadis et al. (1991) derived a dynamic analysis model for an undamped thin rectangular plate with simply supported boundary conditions excited by a PZT patch.

By taking into account the free stress boundary conditions characterizing the finite size piezoelectric actuator, Pan et al. (1992) developed a dynamical model to predict the response of a beam driven by piezoelectric actuator. Their model agreed with the experiment results and had a good improvement on the prediction of the strain in the region close to the actuator. On other hand, some researchers moved to use FEA to analyze the active structure. Liang and Rogers (1992) used the finite element method to analyze the strain of shape memory alloy actuators embedded composite materials. Although this model is accurate in the strain calculation in the regions far away from the edge, it can not accurately estimate the strain value at the free edge because the boundary condition of the free stress in the surface is not satisfied in this model. Liang and Rogers (1994) also investigated the energy consumption and conversion of PZT actuators in active structures.

Based on a finite element analysis using a Rayleigh-Ritz energy formulation, Hagood et al. (1990) proposed a dynamic model that included the coupling between the actuator, structure, and electrical network. The corresponding state space models are developed and a comparison of theoretical derivations and validated experiment on an actively controlled cantilever beam shows a good agreement between the model and experimental results. However, his work does not discuss electromechanical power relationships in active structures, and the actuator force loading is not explicitly expressed as a function of the input impedance of the actuator itself [Zhou and Rogers (1995)]. In addition, Molyet et al. (1998) presented an experiment and finite element analysis on the induced strain transfer from PZT material to the metal substructure through a bonding layer. In order to include the electromechanical coupling of the active system, Sun et al. (1993) suggested a coupled electromechanical analysis for a piezoelectric actuator-driven spring-mass damper system, and discussed the concepts

of actuator power factor and energy transfer of the system. Zhou (1994) further expanded Liang's coupled electromechanical model to the 2D plate and cylinder. This model was also experimentally validated.

Combining the thermo coupling to piezoelectric-mechanical coupling, Chattopadlyoy (1999) developed a theormo-piezoelectric-mechanical model of composite laminates with surface bonded piezoelectric actuators by applying a higher-order displacement field to capture the transverse shear effects. Their model shows that significant deviations from the classical plate theory are observed for moderately thick and thick plates because classical theory neglects the presence of transverse shear effects.

Energy conversion is involved in both the piezoelectric and converse piezoelectric effects, therefore, how to model the power consumption in piezoelectric actuators attracted the attention of researchers. Giurgiutiu and Rogers (1996) used the dynamic analysis of an induced strain actuation stack coupled with external dynamic stiffness to study the maximum mechanical power and minimum power consumption.

Giurgiutiu (2000) reviewed the active-materials induced-strain actuation for aeroelastic vibration control, especially for aircraft. They inferred that the maximum energy output from the induced-strain actuator was calculated for the matched stiffness conditions. The overall efficiency of active-material actuation depends, to a great extent, on the efficiency of the entire system that includes not only the active-material transducer but also the displacement amplification and the power supply.

The above literature survey suggested the following: different actuation models, such as static model, dynamic model, FEA model, and coupled electro-mechanical model, have been used to investigate the mechanism and predict the response of the active system. Since a static model ignored the influence of the actuator on the system dynamic and the response predicted by a static model is frequency independent, therefore it is not accurate in all applications. A dynamic model is therefore necessary to the analysis of system response of active structure. However, most dynamic models are simply integrating the decoupled mechanical solution into a static model. The electro-mechanical coupling is ignored. As an alternative, a FEA model could be used to solve the coupled model with a good accuracy, but it typically has a high

requirement on the computer speed and memory. Since most commercial software did not have a suitable type of elements to handle the piezoelectric materials, it also limited its applications. Zhou and Rogers (1995) proposed a coupled electro-mechanical model by taking into account the coupling between the structure and actuators. Their model is verified by the experiment. Therefore, this model will be integrated in this work into actuation power efficiency analysis.

1.5 Motivation

In summary, the literature survey concerning the sound radiation, effectiveness of noise reduction, and actuation modeling suggests some of the limitations of current studies on the noise control and motivate this study on the followings:

1. The primary focus of noise control has not been power efficiency issues, although some researchers have used sound power output as a performance metric for active structural-acoustic control laws. The literature also shows that, under most circumstances, the planar structure under investigation concerning noise control is simply supported. Although a few researcher investigated on the clamped panels, their method lacked of a generality, and their work did not focus on issues of power efficiency [Sung and Jan (1997)]. The work by Berrys involved in the radiation power calculation of an elastically supported plate, but significant large terms of trial functions required by the model limited its applications [Berry et al. (1990), Song (1995)]. Furthermore, it is hard to apply this technique to a geometrically complex structure. Therefore, a more general method integrated the FEA/variational approach, numerical integration, and eigenvalue decomposition into the power radiation analysis will be developed.

2. On the other hand, great progress has been made in the implementation of active control and noise reduction, but few efforts have been contributed to the analysis of the effectiveness of the actuators. This motivates this work to expand the current actuation power efficiency studies of an active actuator driven

structure performed by Leo (1998) to include different boundary conditions and geometries.

3. As the rapid development of active noise control, smart materials are getting popular in the implementation of the control algorithm. Different actuation models have been developed to predict the response of an active system. Among them, the coupled electro-mechanical model developed by Zhou and Rogers (1995) incorporated the electro-mechanical coupling of the active system. However, few efforts have been made to study the power efficiency, especially the efficiency of active structure with electro-mechanical coupling. Although Liang and Rogers (1994) Dimitriadis et al. (1991) used the impedance models in their analyses of electromechanical energy conversion between the PZT actuator and the host structure, their results are sensitive to the damping ratios. In order to overcome the shortage of the current efficiency studies not accounting the dynamic coupling, this study is motivated to integrate the coupled electro-mechanical model into the power efficiency of the active structure.

4. As we knew, one of the disadvantages of active noise control in certain applications is the narrow bandwidth of performance. Although substantial progress has been made in noise control, very limited studies were focused on the improvement of the frequency bandwidth. Leo (1998) reduced the power efficiency of an active structure driven by the multiple actuators to a generalized eigenvalue problem. As suggested by previous studies, multiple actuators could not only improve the power efficency, but also increase the high efficiency bandwidth. However, research so far has shown that multiple actuators increasing the high frequency efficiency is far less successful than their performance in increasing low frequency efficiency. On the other hand, some researchers have successfully optimized the parameters of the multiple actuators to minimize the noise. However, their optimization procedures were tied to the control algorithms and did not focus on the performance of the actuators and nor the high efficiency bandwidth. This work is motivated to optimize the power efficiency

at a broad frequency bandwidth.

5. As for a typical active control applications, piezoceramic actuators or sensors are relatively small. Therefore, the efficiency analysis can be evaluated based on the power transfer matrix obtained from the normal mode analysis results of the host structure. Current efficiency studies did not take into account the normal mode and frequency variation on the influence of power efficiency. This study is motivated to investigate the power efficiency variation at some extremities, such as a multiple thick PZT actuator driven thin plate excited by multiple piezoceramic actuators.

1.6 Objective

As reviewed in the above sections, although considerable research work considering about the total noise reduction has been performed in the field of active control of sound radiation from the plates, there are some limitations on the research as following. Therefore, a general method could be used to calculate the sound radiation for any planar structure under arbitrary boundary conditions is worthwhile to study.

On the other hand, the increasing popular PZT actuation applications attracted a lot of investigators to study the reduction of noise using multiple actuators. However, very limited efforts have been made to evaluate the effectiveness of actuators. How effective of these smart materials is an important issue in the noise control. Previous studies focus on the noise reduction and not enough emphasis is paid on the effectiveness of actuation itself. As a results, in most cases the noise attenuation is problem dependent and only effective at a specific frequency bandwidth. Therefore, some fundamental investigation about the best location and number of the control actuators, as well as the performance of each actuator or the group actuators is still needed, especially with consideration of the active structure driven by PZT patches. In addition, the factors influencing the effectiveness, such as the electro-mechanical coupling of PZT actuators is worthwhile to study. Furthermore, the effect of system parameters, such as, edge support conditions and complex geometry, on the effective-

ness is deserving of investigation.

The goal of this work is to develop systematic methods to study the power efficiency of a baffled planar structure under various supporting conditions and to maximize the performance of actuators. It will provide the designers with a useful tool in the control design, especially the actuator design. On the basis of the literature review and study, the specific objectives of this dissertation are to:

1. Develop a general hybrid method that integrats the numerical integration, variational approach, and eigenvalue decomposition technique to predict sound radiation power for the complex plate under elastic supports;

2. Extend current sound radiation power analysis to the power efficiency issue of the active structure driven by a point force or distributed actuator. Further apply the power efficiency study to the multiple actuators driven structure;

3. Introduce a coupled dynamic eletro-mechanical model to the power efficiency analysis. The impedance model, reflecting the dynamic response of a point force actuator and its host structures, will be incorporated with the generalized eigenvalue decomposition technique to study power efficiency of the structure driven by actuator arrays;

4. Maximize the power efficiency by optimizing the PZT actuator sizes and locations, and analyze the influence factors such as the relative thickness of the PZT actuators on the power efficiency. Validate the power efficiency modal to the extremities such as relative thick PZT actuator driven thin plate.

1.7 Contributions

This work will focus on the power efficiency investigation of an actuator driven structure, especially the maximization of the actuator performance. The specific contribution of this study are as following:

1. First, one common method of sound radiation calculation using modal expansion is directly integrate the normal mode analysis results obtained from closed -form analysis. The specific contribution of this work is to introduce the normal mode analysis results from the variational approach or FEA to the above sound radiation analysis. Because of the generality of the variational approach and FEA, this hybrid sound calculation method can be easily applied to for any geometrical complex planar structure under elastic supports. In addition, similar to the previous maximum sound radiation analysis Leo (1998), this hybrid method is further integrated into eigenvalue decomposition technique to investigate the maximum power efficiency.

2. Another specific contribution is to introduce a coupled dynamical electro-mechanical model into the power efficiency analysis in order to take into account the influence of distributed PZT actuators on the power efficiency analysis caused by the electro-mechanical coupling.

3. In addition, this work contributes specifically to the power efficiency analysis by investigating the distributed PZT parameters, such as the relative thickness or size of PZT actuator to that of structure, on the power efficiency. This effort has been made by combining the variational method with the proposed hybrid sound radiation power analysis. The results show that the actuation power efficiency is much less influenced by the distributed PZT parameters than sound radiation power is.

4. The final contribution is to maximize the multiple PZT actuators performance using optimization based on the maximum efficiency. Although some efforts have been made on the optimization of actuator parameters, such as location and thickness , the majority of them was based on the noise reduction, not on the actuator performance. In addition, the optimization was based on narrow frequency range and was typically tied to the particular control algorithm. As a result, this optimization achieve a high efficiency at a much broader frequency bandwidth comparing to previous analyses.

1.8 Organization of This Dissertation

The work in this dissertation is broken up into several major sections.

Chapter 1 is concerned with an introduction of the background and a review of related work.

Chapter 2 deals with the analysis of the sound radiation power. A general method is proposed to analyze the sound radiation power for any planar structure under an arbitrary boundary. As derived by Snyder et al. (1995), the sound radiation power of a baffled planar structure can be expressed a function of the integration of the weighted mode shapes. By integrating the numerical integration approach with modal expansions, the sound radiation power could therefore be evaluated.

In order to make this analysis more genetic, a finite element analysis could be used to perform the normal mode analysis. Thereby the power transfer matrix can be evaluated with the mode shapes and frequencies using FEA or the variational method. According to the eigenvalue decomposition, the maximum sound radiation power is proportional to the maximum eigenvalue of the power transfer matrix. Therefore, the sound radiation power for any planar structure under arbitrary boundary conditions can be evaluated. Although a FEA generally provides a good accuracy of the normal mode analysis, it does not provide any physical insights. The variational method is alternatively used to analyze the normal mode. The sound radiation power is then calculated.

Chapter 3 studies the power efficiency of a point force actuator driven structure. In oder to compare the performance of a point force actuator quantitatively, the actuation efficiency of the point force driven structure is investigated using the eigenvalue decomposition technique. The efficiency is a function of the maximum power transfer matrix. The influence factors on the power efficiency are analyzed. Also, the radiation impedance of a rigid plate is derived and the corresponding results are compared with the rigid piston of the structure.

Chapter 4 applies the previous power efficiency of the point force actuator driven structure to the PZT actuator driven structure. As we know, the application

of the PZTs in the active control are getting popular and popular because of its small size and easy application. In order to take into account the electro-mechanical coupling, a dynamic electro-mechanical model is integrated into the power efficiency analysis. The effect factors of parameters such as PZT location are analyzed.

Chapter 5 extends the power efficiency from single actuator to multiple actuators. As previous studies illustrate that the multiple actuators could improve the power efficiency at a broad frequency ranges. Based upon the generalized eigenvalue technique, the maximum power efficiency of the multiple actuators is investigated. According to previous analysis the actuator locations are very crucial to the noise reduction, optimization is therefore be conducted. The corresponding maximum power is achieved with the optimized actuation location.

Chapter 6 studies the influence of the PZT size and thickness on the power efficiency. As we know, when a control voltage is applied to the PZT patches, the working procedure accompanies the energy changes, from mechanical to electrical , or vice verse. The added PZTs will also influence the dynamics of the original host structure. Using variational approach integrating the coupled dynamic impedance model, the power efficiency of the relative thick multiple PZT patch driven structure is then analyzed.

Chapter 7 discuses the experimental investigation of the influence of PZT patches on the frequencies, mode shapes, and damping ratios. Furthermore, the experimental results are used to verify the sound radiation power analytical modal.

Chapter 8 summarizes the major conclusions deducted from this work.

Chapter 2

Sound radiation power calculation

2.1 Introduction

Power requirements are a fundamental consideration in the application of active control systems to problems in noise and vibration suppression. Unlike a purely passive design, an active system converts electrical power into mechanical and acoustic power for the purpose of suppressing the unwanted sound or vibration. This energy conversion is performed using the sensors and actuators of the control system, and the amount of energy required is a function of how well the overall system can perform this electromechanical and electroacoutic conversion. Different actuators such as a point force actuator or a PZT actuator are used to excite the structure. How effective the actuation, which is defined later as the actuator power efficiency, will be a main topic of this work. Before we go deep into the efficiency analysis, we would first like to investigate the acoustic power generated by the active structure.

As discussed in the preceding chapter, a great amount of work has been performed to reduce the noise level using active noise control. Among the work, some research involved the sound radiation calculation and sound radiation power evaluation. Expressing the sound radiation power as the integral of the modal velocity, Snyder and Tanaka (1995) investigated the sound radiation power of a simply supported plate. The modal velocity vectors are a function of mode shapes. Integrating the mode expansions, the sound radiation power, therefore, could be evaluated.

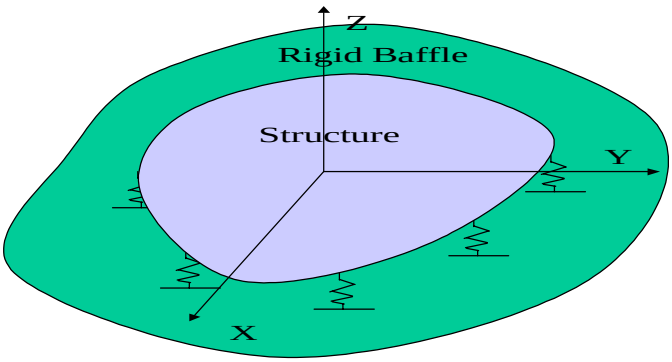

Figure 2.1: A plate under an infinite baffle.

However, for a geometrically complex plate or a plate under elastic support, it is not suitable to evaluate the sound radiation power directly using the same formulation.

This chapter will derive a general hybrid approach to compute the sound radiation power of a planar structure, as shown in Figure 2.1. This planar structure could be in any shape and it could be under an arbitrary boundary condition. As it will be known later that the sound radiation power of a planar structure could be evaluated using numerical integration by expressing the sound radiation power as a quadratic form of the integration of the mode velocity [Snyder and Tanaka (1995)]. By integrating the normal mode analysis from the finite element analysis or variational approach with numerical integration, a more general method is achieved.

2.2 Problem Ddescription

In this chapter, it is assumed that the structural vibration is controlled by a set of actuator(s) that apply point force inputs normal to the plate surface. A systematic method will be derived to compute sound power radiation. As examples, this method will be applied to the analysis of sound radiation of a rectangular plate under different boundary conditions.

2.3 Sound radiation power formulation

For the planar structure in an infinite baffle, as shown in Figure 2.1, there are two common approaches to calculate the sound power radiation. The first approach is to integrate the far-field acoustic intensity over a hemisphere enclosing the sound resource and the other approach is to integrate the real part of the acoustic intensity over the surface of the vibrating structure. Here the second approach will be taken, as it leads more directly to the desired result. For the planar structure being considered here, the acoustic power output can be expressed as the following integral [Snyder et al. (1995)],

$$W = \frac{1}{2}\int_s Re(p(\boldsymbol{X})^* v(\boldsymbol{X}))d\boldsymbol{X} \tag{2.1}$$

where S denotes integration over the surface of the vibrating structure, $v(\boldsymbol{X})$ is the complex surface velocity at a location $\boldsymbol{X}(x,y)$ on the structure, with $z=0$ defining the plane of the structure, and Re denotes the real part of the expression.

Using the Rayleigh integral, the acoustic pressure of the planar structure, $p(\boldsymbol{X})$ can be expressed in terms of surface velocity [Snyder et al. (1995)],

$$p(x) = \frac{j\omega\rho_0}{2\pi}\int_S V(\boldsymbol{X}')\frac{e^{-jkr}}{\mathsf{r}}d\boldsymbol{X}' \tag{2.2}$$

where k is the acoustic wave number, which is defined as angular frequency normalized with respect to the speed of sound, c and r is the distance between the source location $\boldsymbol{X}^{\mathsf{0}}$ and the receiver location $\boldsymbol{X}$, respectively. After simplification, the sound power radiated into far field can be expressed as followings [Snyder and Tanaka (1995)]:

$$W = \frac{\omega\rho_0}{4\pi}\int_S\int_S V^H(\boldsymbol{X}',t)\frac{\sin(kr)}{r}V(\boldsymbol{X},t)d\boldsymbol{X}'d\boldsymbol{X}, \tag{2.3}$$

where ^{H} stands for the complex conjugate transpose, ω the angular frequency, the variable S denotes the integration over the surface of the plate, and $V(\boldsymbol{X},t)$ is the physical velocity at a given location $\boldsymbol{X}$ and time t. The physical velocity $V(\boldsymbol{X},t)$ is expressed as the linear combination of a modal velocity $v(t)$ and mode shape $\psi(\boldsymbol{X})$. The

velocity $V(\boldsymbol{X}, t)$ at any location $\boldsymbol{X}$ can be expressed in the modal expansions [Snyder et al. (1995)]

$$V(\boldsymbol{X}, t) = \sum_{i=1}^{N} \psi_i(\boldsymbol{X}) v_i(t), \tag{2.4}$$

where N is the number of the modes in modal expansions, the variable v_i is the ith the modal velocity, and $\psi_i(\boldsymbol{X})$ is the ith mode shape. As an example, sound power radiation of a planar structure is derived as follows. If we normalize the dimensions with respect to the maximum length and maximum width of the plate, respectively, then we have

$$\begin{aligned} \xi &= \tfrac{x}{a} \\ \zeta &= \tfrac{y}{b} \end{aligned} \tag{2.5}$$

and express r as:

$$r = a\sqrt{(\xi - \xi')^2 + \varrho^2(\zeta - \zeta')^2} = a\eta, \tag{2.6}$$

where ϱ is the aspect ratio. The differential element is expressed in nondimensionalized form

$$d\boldsymbol{X} = dxdy = abd\xi d\zeta = abd\boldsymbol{\xi}. \tag{2.7}$$

After inserting Equation(2.6) and Equation(2.7) into Equation(2.3), the sound power can be expressed as:

$$W = \frac{\omega \rho_0 a b^2}{4\pi} V^H \int_S \int_S \psi^T(\boldsymbol{\xi}') \frac{\sin(\kappa\eta)}{\eta} \psi(\boldsymbol{\xi}) d\boldsymbol{\xi}' d\boldsymbol{\xi} V, \tag{2.8}$$

where ^{T} stands for the transpose. If we define α as:

$$\alpha = \int_S \int_S \psi^T(\boldsymbol{\xi}') \frac{\sin(\kappa\eta)}{\eta} \psi(\boldsymbol{\xi}) d\boldsymbol{\xi}' d\boldsymbol{\xi}, \tag{2.9}$$

then the sound radiation power can be expressed as:

$$W = \gamma \frac{2\kappa\varrho}{\pi} v^H \alpha v, \tag{2.10}$$

where $\gamma = \frac{\rho_0 cab}{4}$ is equivalent to the sound power output of a rigid piston normalized with respect to the velocity of the piston. Therefore, sound radiation power is a quadratic function of modal velocity and a function of power transfer matrix. In the following sections, we will propose a general method to evaluate the sound power radiation.

2.4 A General Hybrid Method

In previous analysis, it is shown that the sound power radiation can be evaluated using numerical integration with equation (2.8). However, due to the irregularity of the geometry and the varying boundary conditions, we may not be able to obtain the closed-form frequencies and mode shapes necessary to evaluate the integrals. In order to evaluate the sound radiation of a general planar structure, we first need a general method to solve for normal modes and then a general procedure to evaluate the two double integrations over the surface of the structure. For the normal modal analysis, the commonly used finite element analysis [Liang et al. (1992)] and the variational approach [Charette and Berry (1997); Newbury and Leo (2000)] will be employed. As for the evaluation of the two double integrations, a numerical integration subroutine is developed for the rectangular plate. Furthermore, the more general approach of using the approximate summation of the integration elements over small areas instead of the direct integration over the surfaces is also proposed. One advantage of this approximation is that it could be applied to any planar structure. As a contribution, this work will integrate the modal analysis data with numerical integration to evaluate sound radiation, and later on the power efficiency for any planar structure. In the following sections, we will address the FEA, variational approach for normal modal analysis and the numerical integration procedures of the two double integrations.

2.5 Normal Mode Analysis

In his section, two methods, FEA and variational approach will be applied to the normal mode analysis to obtain the natural frequencies and mode shapes which are needed in the sound radiation power analysis. Natural frequencies alone are usually sufficient for applications in which the primary concern is avoiding a structural resonance. In noise and vibration control applications, though, the mode shapes play an equally important role in the design of effective passive and active treatments [Newbury and Leo (2000)]. It is well known that structural sound radiation is related to the radiation efficiency of the vibration modes [Wallace (1972)]. In this study, normal mode analysis will be directly related to the sound radiation power of the structure. In addition, due to the fact that damping is ignored during normal mode analysis, experimental modal analysis of damping ratios will be used in the acoustic analysis to increase its accuracy.

2.5.1 Finite element analysis

Finite element analysis is a popular engineering tool with a proven high degree of accuracy for the modal analysis of a structure. Actually, some researchers, to name a few, Liang and Rogers (1994); Varadan et al. (1997), have also advanced one step further and analyzed the dynamic response of the PZT actuator-driven active structure. However, a dynamic FEA model requires fine meshes around PZT regions and most commercial software does not have the proper elements to handle the PZT. Due to the above reasons, in this section, we will use FEA as one of the approaches to obtain the normal mode analysis needed in the sound radiation analysis instead of direct modeling the acoustics of the structure.

Natural Frequency

A FEA model is first used to determine the natural frequencies and mode shapes of the structure under different supports. In order to simulate the different boundary conditions, a group of rotational springs and translational springs are placed along the

Table 2.1: The mode shapes and damping ratios

Index	Notation	Physical meaning	Value	Unit
1	ω_i	Angular frequency of the plate		
2	M,N	Modal indices		
3	ν	Poisson's rate	0.3	
4	a	Length of the plate	1.88	m
5	b	Width of the plate	0.88	m
6	h	Plate thickness	0.009	m
7	E	Young's modulus	254	GPa
8	ρ_s	The density of the plate	7800	kg/m^3
9	ϱ	The rate of the side length	b/a	
10	ρ_a	Density of air	1.34	kg/m^3
11	C	Air velocity	340	m/s

edges. In order to simulate the boundary condition variation from simply supported to clamped, the translation of all nodes on the edge of the plate is constrained to be zero and the torsional spring supports whose stiffness is varied with the boundary conditions are placed on the rotational degrees of freedom. For the simply supported, the plate rotational stiffness is set to zero and for the clamped, the rotational stiffness is a very large number. In order to verify the accuracy of normal mode analysis, a 1.88 x 0.88 x 0.09 meter steel rectangular plate listed in Table 2.1 is used as an example.

A 1.88x0.8x0.009 m rectangular plate is used as the study objective. Its corresponding parameters and their definitions used for the numerical analyses are listed in Table 2.1.

Different commercial software, such as SDRC-IDEAS and MSC/NASTRAN, has been used for normal mode analysis. Table 2.1 lists the plate parameters and their definitions used for the numerical analyses. As an example, a FEA model consisting of a 21 x 21 grid of the elements is developed for the normal mode analysis. The accuracy of the FEA is checked against the closed-form solution in the simply-supported case. The undamped closed-form solution for the natural frequency of a simply supported

plate can be calculated from following expression [Inman (1994)]:

$$\omega = \sqrt{\frac{D\pi^4}{\rho_s h a^4}\left(M^2 + \frac{N^2}{\varrho^2}\right)} \tag{2.11}$$

where D is the bending stiffness of the plate:

$$D = \frac{Eh^3}{12(1-\nu^2)} \tag{2.12}$$

The above expression demonstrates that the natural frequency is a function of material properties, geometries and side length ratio, but the side length ratio of the plate ϱ is the only parameter that affects the order of the vibration modes. For the simply supported case, the closed-form solution of frequencies and finite element analytical results are listed in Table 2.2. The numerical calculation shows that the error is less than one percent for each of the first six natural frequencies. The accuracy of the FEA model in the simulation of boundary conditions is also checked against the closed-form solution. This check is performed by increasing the stiffness of the torsional springs and comparing the results to the closed-form solutions for a simply-supported and clamped plate. As shown in Figure 2.2, the first natural frequency changes as the stiffness of the torsional springs vary. The FEA frequencies of the large spring stiffness supported plate matched those of a clamped plate. Similarly, the FEA frequencies of the small stiffness supporting matched those of a simply supported plate. The above analysis demonstrates that the FEA model to simulate the variation of boundary is acceptable.

Mode shapes

As discussed previously, sound radiation power is a function of mode shapes. Therefore, the accuracy of the mode shape is crucial in the analysis. The accuracy of the previous model is checked only in respect to the natural frequencies. Now we will also check the accuracy of the mode shapes. This check is performed for a special case, i.e, simply supported. The mode shapes of the FEA are compared with those of

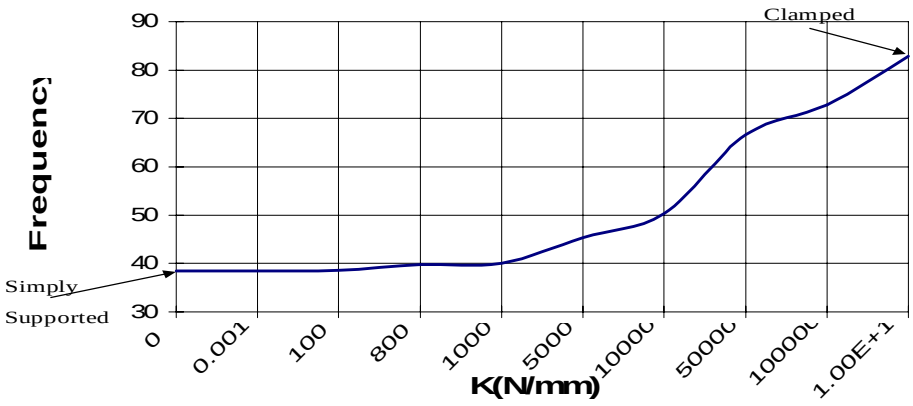

Figure 2.2: The first mode frequency of the plate under different spring stiffnesses.

closed-form solution. For a simply- supported plate, the mode shapes are sinusoidal functions given by the expression.

$$\psi_i(x, y) = sin(M_i \pi x_j) sin(N_i \pi y_j). \tag{2.13}$$

where x, y are coordinates. The variable i and j are mode index and location index, respectively. Detailed numerical analysis demonstrates that the FEA mode shapes have a high accuracy comparing to those of closed-form analysis.

After verifying of the accuracy of the FEA model, it is applied to the study of normal mode analysis for the structure under different boundary conditions, such as clamped and spring supported plate. By constraining the translational degrees freedoms and varying the torsional stiffness of the supporting springs, the FEA model can easily simulate boundary conditions from simply-supported to clamped. As an example, the second mode shape of the plate under the simply -supported and clamped conditions are plotted in Figure 2.3 and Figure 2.4, respectively. As seen from these figures, the mode shape of the clamped plate looks similar to that of a simply-supported plate except that it has relatively smaller displacement along the edges. These mode shape analyses will be the basis for the sound radiation and power efficiency analysis presented in the later sections.

Table 2.2: A comparison of the closed-form and finite element analytical frequencies

Index	Closed-form	FEA	Error (%)
1	38.41	38.41	0.0
2	59.12	59.01	0.2
3	93.63	93.42	0.2
4	132.93	133.39	0.3
5	141.96	141.77	0.7
6	153.70	153.58	0.0

2.5.2 Variational Approach

The FEA method is a general method with good accuracy, however, a variational approach with the Hamilton principle could also be used as an alternative to solve for the normal modes. Similar to the FEA model, this approach is able to accommodate a wide variety of geometries and boundary conditions. Based on the Hamilton's principle and Lagrange's equation of motion, the formulation derivation for the system is briefly summarized from reference as follows. The Hamilton's principle can be expressed as following [Meirovitch (1997)]

$$\begin{gathered} \int_{t_1}^{t_2}(\delta T + \delta W)dt = 0 \\ \delta q_k(t_1) = \delta q_k(t_2) = 0 \quad k = 1, 2, ..., n \end{gathered} \tag{2.14}$$

where δT is the system kinetic energy, δW is the virtual work done by the applied force, q_k is the generalized coordinates, and k is the number of the degree of freedoms. The above equation can be simplified as Lagrange's equations of motion

$$\frac{d}{dt}(\frac{\partial L}{\partial \dot{q_k}}) - \frac{\partial L}{\partial q_k} = Q_k, \quad k = 1, 2, ..., n \tag{2.15}$$

where $L = T - V$, V is the potential energy, and Q is the external force. If we use a polynomial trial function, the out-of-plane displacement of the structure can be

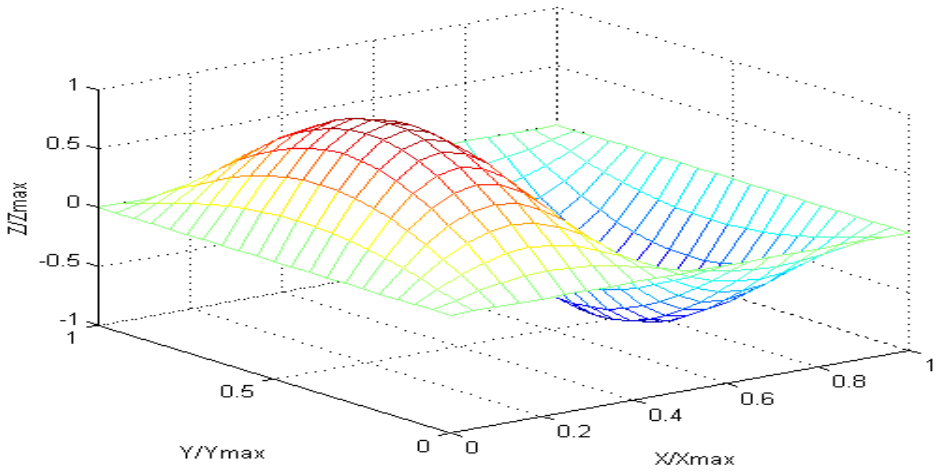

Figure 2.3: The second mode shape of a simply -supported plate.

approximated as:

$$W(x,y,t) = \sum_{m=1}^{N}\sum_{n=1}^{N} a_{mn} e^{j\omega t} (\frac{2x}{a})^{m-1} (\frac{2y}{b})^{n-1} \tag{2.16}$$

Furthermore, the system's potential energy, kinetic energy, and external force can be expressed in terms of W. After inserting these terms into Lagrange's equation of motion, the system will yield an eigenvalue problem.

$$(-\omega^2 M + K)U = Q \tag{2.17}$$

which is an N by N degree of freedom model of the system that can be solved for the system frequencies and corresponding eigenvectors. Where M and K are the system mass matrix and stiffness matrix, respectively. These matrices are contributed by several factors such as plate, PZT patches, and boundary conditions.

Mass matrix and stiffness matrix formulations

In order to solve the eigenvalue problem, equation (2.17), we should evaluate the matrices first. In the interest of simplicities, equation (2.16) is expressed in a more compact form [Newbury and Leo (2000)]:

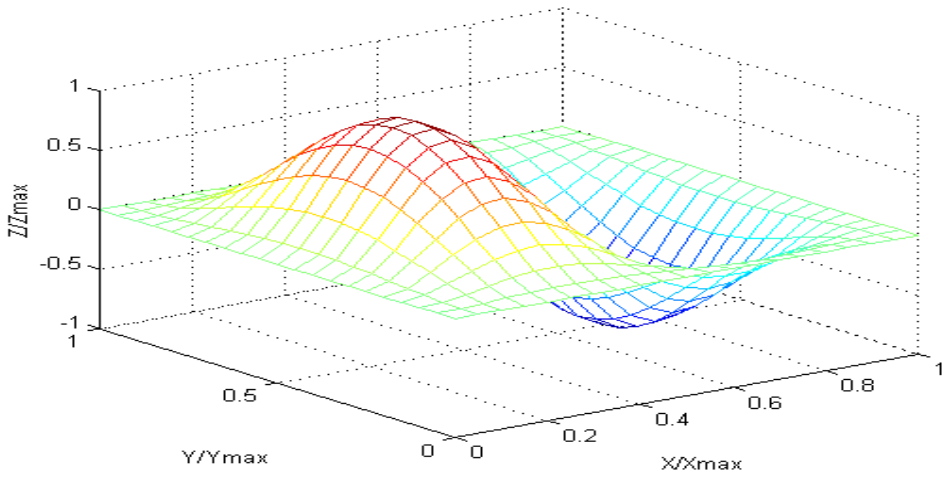

Figure 2.4: The second mode shape of a clamped plate.

$$W = U^T \Phi e^{(j\omega t)}$$
$$\Phi = [\sigma^0\vartheta^0 \quad \sigma^0\vartheta^1 \quad \ldots \quad \sigma^0\vartheta^{N-1} \quad \sigma^1\vartheta^0 \quad \ldots \quad \sigma^{N-1}\vartheta^{N-1}]; \tag{2.18}$$

where $\sigma = \frac{2x}{a}$ and $\vartheta = \frac{2y}{b}$ are non-dimensional spatial coordinates. $\mathsf{r} = \frac{a}{b}$ is the aspect ratio.

Based on the small deflection theory of thin plates, Charette and Berry (1997) derived the plate stiffness matrix in terms of the motion of the mid-plane of the plate W. The plate's contribution to the structure's stiffness matrix is expressed as the following [Newbury and Leo (2000)]:

$$K_{plt} = \frac{4D}{ra^2} \int\int_{A_{plt}} \left[\Phi_{\sigma\sigma}\Phi_{\sigma\sigma}^T + r^4\Phi_{\vartheta\vartheta}\Phi_{\vartheta\vartheta}^T + \nu r^2(\Phi_{\sigma\sigma}\Phi_{\vartheta\vartheta}^T + \Phi_{\vartheta\vartheta}\Phi_{\sigma\sigma}^T) + 2r^2(1-\nu)\Phi_{\sigma\vartheta}\Phi_{\sigma\vartheta}^T\right] d\sigma d\vartheta \tag{2.19}$$

where subscript $_{plt}$ stands for the plate parameters, h is the thickness, $\Phi_{\sigma\sigma}$, $\Phi_{\vartheta\vartheta}$ is the second derivatives of trial functions Φ with respect to σ and ϑ, respectively and $\Phi_{\sigma\vartheta}$ is the second derivative with respect first to σ and then to ϑ. The PZT also

contributes to the stiffness matrix in the following manner.

$$K_{pzt} = \left(\frac{h_{pzt}^2}{12} + \frac{(h_{pzt}+h_{plt})^2}{4}\right) h_{pzt}\frac{4}{ra^2}\int\int_{A_{pzt}}(C_{11}\left[\Phi_{\sigma\sigma}\Phi_{\sigma\sigma}^T + r^2\Phi_{\vartheta\vartheta}\Phi_{\vartheta\vartheta}^T\right] + C_{12}r^2\left[\Phi_{\sigma\sigma}\Phi_{\vartheta\vartheta}^T + \Phi_{\vartheta\vartheta}\Phi_{\sigma\sigma}^T\right] + C_{44}4r^2\Phi_{\sigma\vartheta}\Phi_{\sigma\vartheta}^T)d\sigma d\vartheta \tag{2.20}$$

where subscript $_{pzt}$ stands for the parameter of the PZT patches.

Boundary conditions also contribute to the stiffness matrix. For an edge at $\vartheta = \vartheta_0$, the stiffness matrix is:

$$K_{bc} = \frac{kD}{2a^2}\int_{\sigma_0}^{\sigma_1}\Phi(\sigma,\vartheta=\vartheta_0)\Phi^T(\sigma,\vartheta=\vartheta_0)d\sigma + \frac{2Dcr}{a^2}\int_{\sigma_0}^{\sigma_\vartheta}\Phi_\vartheta(\sigma,\vartheta=\vartheta_0)\Phi_\vartheta^T(\sigma,\vartheta=\vartheta_0)d\sigma \tag{2.21}$$

where $k = \frac{Ka^3}{D}$ and $c = \frac{Ca}{D}$. By varying K and C, we can simulate any kinds of boundary conditions. For example, a simply-supported boundary condition can be easily simulated by assigning the translational spring constant K a value approaching infinity and the rotational spring stiffness C zero at the edge. Since the supporting condition at each edge will contribute to the stiffness matrix, the total matrix stiffness related to boundary conditions is simply the total of the stiffness matrix contributed by the boundary conditions for all edges.

The final stiffness matrix is the summation of above stiffness caused by plate, PZTs, and boundary conditions.

Similarly, the mass matrix can also be formulated based upon the contributions of the plate and the PZT. The boundary condition will not influence the stiffness. The mass matrix for the plate is

$$M_{plt} = \rho_{plt}h_{plt}\frac{a^2}{4r}\int\int_{A_{plt}}\Phi\Phi^T d\sigma d\vartheta \tag{2.22}$$

The mass matrix for the PZT is

$$M_{pzt} = \frac{\rho_{pzt}h_{pzt}a^2}{4r}\int\int_{A_pzt}\Phi\Phi^T d\sigma d\vartheta \tag{2.23}$$

A_{pzt} denotes integration area over the transducer surface. The total mass matrix is

$$M = M_{plt} + M_{pzt} \tag{2.24}$$

With above N by N mass matrix and stiffness matrix, the homogenous equation of equation (2.17) can be solved for natural frequencies and eigenvectors.

The next step is to solve for the modal shapes. The modal shapes can be evaluated using the following expression:

$$\psi_i(\sigma, \vartheta) = u_i^T \Phi \tag{2.25}$$

where u_i is the column eigenvectors corresponding to the ith frequency and ψ_i is the mode displacement of ith mode at location (σ, ϑ).

Forcing functions

Two types of excitations are considered in this study: the concentrated impact loads that are perpendicular to the plate, and induced in-plane strains resulting from electrical excitation of the piezoceramic actuator(s). An impact load is represented by an impulsive force acting at a single point on the plate. The point force can be represented by this concentrated force. The corresponding force vector Q is found by differentiating the virtual work that corresponds to a displacement at the point of the applied force with respect to the expansion coefficient U [Newbury and Leo (2000)]:

$$Q = \frac{\delta W}{\delta U} = F\Phi(X_F, Y_F) \tag{2.26}$$

where F is the magnitude of the force. Similarly, the force vector corresponding to voltage excitation of the piezoelectric actuator is

$$Q_{PZT} = \frac{V d_{31}}{2r}(C_{11} + C_{12})(h_{pat} + h_{plat}) \int\int (\Phi_{\sigma\sigma} + r^2 \Phi_{\vartheta\vartheta}) d\sigma d\vartheta \tag{2.27}$$

where V is the applied voltage and d_{31} is the piezoelectric coefficient of the actuator material.

Applications of variational approach in modal analysis

In this subsection, the variational model presented in previous section can be used to calculate the natural frequencies and mode shapes of a plate with a PZT actuator.

Table 2.3: Properties of the plate and PZT actuator

Index	Notation	Physical meaning	Value	Unit
		Plate		
1	L_x	Length	480	mm
2	L_y	Width	420	mm
3	h_{plt}	Thickness	3.22	mm
4	ρ	Density	2700	kg/m^3
5	E	Young's modulus	$66.5 * 10^9$	N/m^2
6	ν	Poisson's coefficient	0.33	
		PZT		
1	l_x	Length	38.1	mm
2	l_y	Width	31.8	mm
3	h_{pzt}	Thickness	0.254	mm
4	ρ	Density	7750	kg/m^3
5	E	Young's modulus	$63 * 10^9$	N/m^2
6	ν	Poisson's coefficient	0.33	
7	d_{31}		$210 * 10^{-12}$	m/v

For the purpose of convenience for the comparison, the structure used in the work of Charette and Berry (1997) whose parameters are listed in Table 2.3 is used as example to compute the natural frequencies.

Using the above variational model with a truncation of $N = 9$ terms of trial functions, the system equation is evaluated and solved for the eigenvalue problem. The corresponding first ten frequencies are listed in the following Table 2.4. As one advantage, the variational approach can also be used to solve the normal modes for a plate without PZT patches. The frequencies with PZT and without PZT are compared to that of analytical solutions and the corresponding percentage errors are also listed in the same table for reference.

The error is defined as

$$E_f = \frac{|Freq - F_{ana}|}{F_{ana}} * 100 \tag{2.28}$$

where $Freq$ stands for the natural frequency of the structure, F_{ana} is the theoretical

Table 2.4: A comparison of frequencies of a plate with or without PZT

Modal Index	$Fana$	$FwoPZT$	Error(%)	$FwPZT$	$Error(\%)$
1	77.064	77.042	0.033	77.039	0.03
2	177.316	177.261	0.031	177.261	0.03
3	208.005	207.942	0.031	207.942	0.03
4	308.257	308.090	0.049	308.106	0.05
5	344.402	344.334	0.021	344.331	0.02
6	426.240	426.135	0.028	426.123	0.03
7	475.343	475.048	0.062	475.048	0.06
8	526.492	526.176	0.060	526.176	0.06
9	578.323	599.665	3.690	599.665	3.69
10	693.578	692.947	0.095	692.916	0.10

values of natural frequencies. As Table 2.4 shown, most frequencies predicted by the variational model is very close to that of analytical model. The maximum frequency error is less than 3.7 percent, occurs at the $9th$ mode, while most frequency errors are below 0.1 percent. The above numerical analysis results demonstrate that the variational model is very accurate in predict the natural frequency.

Table 2.4 also lists the natural frequencies of the same plate with a PZT patch whose dimension is 1" x 1.5" by 0.01", which is located at the center of the plate. As we could see from the table, the frequencies predicted by the variational model is almost identical to that of the plate without PZT patch predicted by the same approach. It shows that a relatively small PZT patch does not influence the natural frequencies much. The frequencies predicted by this variational model matches with the experimental results conducted by Charette and Berry (1997).

We also like to make a comparison between the variational mode shapes and analytical mode shapes. Here we define that the mode shape error as following:

$$E_{ms} = \sum_{l=1}^{N_0} \frac{||Z| - |Z_{ana}||}{|Z_{ana}|} \tag{2.29}$$

where N_0 is the total number of the grids of the plate, Z, Z_{ana} is the mode displace-

Table 2.5: A comparison of mode shape error for different thickness of PZT patches

Single PZT $\frac{h_{pzt}}{h}$	$Error(\%)$	Double PZT $\frac{h_{pzt}}{h}$	Error(%)
0.5	0.114		
1.0	0.367		
2.0	2.085	2.0	3.65
3.0	4.919		
5.0	9.495		

ment normal to the plate surface at each grid for the mode desired to compare with and the analytical mode, respectively. A numerical evaluation shows that the error for the first ten modes between the analytical and variational model is 1.8 percent. Thus it is reasonable for us to use the modal analysis result obtained from the variational method in our later sound radiation analysis.

Based on the structure and parameters given by Charette and Berry (1997), the natural frequencies and modal shapes are evaluated using variational approach. The parameters for the plate and PZTs are listed in Table 2.3. Assuming the center of the PZT patch is collocated with the center of the plate. The area of ratio of PZT to plate is about 0.6%. By varying the thickness of PZT patch, the modal shapes are evaluated and the error based on the definition, equation (2.29), is computed. The corresponding errors are listed in Table 2.5.

The results demonstrates that for regular control applications, PZT size is about an order of 0.5% of the structure, the mode shape error is ignorable if the relative thickness of PZT patches to the thickness of the plate are less than 3. However, if the relative thickness is great than 5, the mode shape may need compensation. For the collocated PZTs, the mode shape error is relatively large, for example, the mode shape error is 3.65% for a double PZT patches instead of 2.0% for a single PZT patch. Increasing the term of trial functions will increase the accuracy of variational approach at a cost of computing time. In addition, Matlab may have difficulty in per-

forming Gaussian elimination in solving the eigenvalue problem in the large degree of freedoms when N is greater than 12 [Newbury and Leo (2000)].

2.6 Evaluation of the Double Integrals

With the frequencies and modal shapes obtained either from FEA or variational approach, we can use mode expansions to evaluate the double integrals and therefore, the sound radiation analysis. As discussed previous, either a direct numerical integration or an approximation of summation of the integral over the surface can be used to evaluate the integrals, equation (2.3) or (2.9).

For a rectangular plate, a direct integration subroutine over the surface is written. The integration meshes must correspond to those of normal modal analysis. In this analysis, a 21 by 21 mesh is used for the rectangular plate. Since this subroutine is only valid on a rectangular plate, another more general method will also be employed to approximately evaluate the double integrals.

Because of the complexity of the geometry, a different approach is employed to evaluate the double surface integrals by breaking down it into the summation of an integral function over small elements. For example, the component of the matrix α, equation (2.9), can therefore be approximated as

$$\alpha_{i,j} = \sum_m \sum_n \psi_i(\xi_m, \eta_m)^T \frac{sin(\kappa\eta)}{\eta} \psi_j(\xi_n, \eta_n) S'_m S_n, \tag{2.30}$$

where S_m is the normalized area of the mth element and $\psi_i(\xi_m, \eta_m)$ is the ith mode shape at location (ξ_m,η_m). In order to verify the accuracy of this method, the above approximation method and the directly numerical integration approach are used to evaluate the power transfer matrix of a rectangular plate which is divided into 21 by 21 elements. Results indicate that only 0.5 percent error exists between these two methods. Comparing to the direct integration, this method is applicable to any planar structures.

2.7 Sound Radiation Calculations

Previous sections presented a methodology to compute sound radiation for a baffled general structure under arbitrary conditions. In this section, we will first apply this method to study the influence of boundary conditions on the sound radiation for a rectangular plate, and then to investigate the sound radiation of a circular plate under elastic support.

The material properties and dimensions are listed in Table 2.1. In order to compute the sound radiation power, equation (2.10), we need to evaluate the two double integrals, equation (2.9), first. The natural frequencies and mode shapes are computed using either FEA or variational approach. With the modal analysis results, a subroutine for the two double integrations over a rectangular panel is written to perform a numerical integration. Before we apply this method to the study of sound radiation analysis, the power transfer matrix of a simply supported plate is computed and compared with that of publication by Snyder and Tanaka (1995). The sound transfer matrix is defined as

$$A = \frac{\omega \rho_0 a b^2}{4\pi} \int_S \int_S \psi^T(\boldsymbol{\xi}') \frac{\sin(\kappa\eta)}{\eta} \psi(\boldsymbol{\xi}) d\boldsymbol{\xi}' d\boldsymbol{\xi}. \tag{2.31}$$

It is calculated with numerical integration for the same structure as used by Snyder and Tanaka (1995) with the first ten mode truncations and the 30 by 30 mesh grids for the double integration.

$$\begin{pmatrix}
10.5344 & 0.0000 & 3.1981 & 0.0000 & 0.0000 & 0.0000 & 0.0000 & 1.8771 & 0.0000 & 3.4138 \\
0.0000 & 0.5996 & 0.0000 & 0.0000 & 0.2869 & 0.0000 & 0.0000 & 0.0000 & 0.0000 & 0.0000 \\
3.1981 & 0.0000 & 0.9775 & 0.0000 & 0.0000 & 0.0000 & 0.0000 & 0.5740 & 0.0000 & 1.0356 \\
0.0000 & 0.0000 & 0.0000 & 0.1464 & 0.0000 & 0.0000 & 0.0460 & 0.0000 & 0.0000 & 0.0000 \\
0.0000 & 0.2869 & 0.0000 & 0.0000 & 0.1373 & 0.0000 & 0.0000 & 0.0000 & 0.0000 & 0.0000 \\
0.0000 & 0.0000 & 0.0000 & 0.0000 & 0.0000 & 0.0050 & 0.0000 & 0.0000 & 0.0024 & 0.0000 \\
0.0000 & 0.0000 & 0.0000 & 0.046 & 0.0000 & 0.0000 & 0.0145 & 0.0000 & 0.0000 & 0.0000 \\
1.8771 & 0.0000 & 0.5740 & 0.0000 & 0.0000 & 0.0000 & 0.0000 & 0.3370 & 0.0000 & 0.6078 \\
0.0000 & 0.0000 & 0.0000 & 0.0000 & 0.0000 & 0.0024 & 0.0000 & 0.0000 & 0.0012 & 0.0000 \\
3.4138 & 0.0000 & 1.0356 & 0.0000 & 0.0000 & 0.0000 & 0.0000 & 0.6078 & 0.0000 & 1.1067
\end{pmatrix}$$

Snyder calculated the power transfer matrix and the total acoustic power output of a simply supported rectangular plate using modal radiation efficiencies by including the first ten modes in the mode expansion. The corresponding power transfer matrix of Snyder's calculation can be found from the work of Snyder and Tanaka (1995). Results show that the corresponding between these two approaches is extremely good with the maximum error less than 4 percent.

Then we move to the study of the sound radiation of a point force actuator-driven panel. For a simply supported plate, the modal velocity of the ith mode can be expressed as [Snyder and Tanaka (1995)]

$$v_i = j\omega \frac{sin(M_i \pi \xi_a) sin(N_i \pi \varsigma)}{m_i Z_i}, \tag{2.32}$$

where $m_i = \frac{\rho_0 hab}{4}$, $Z_i = \omega_i^2 - \omega^2$, and (M_i, N_i) are the modal indices of the ith mode. General speaking, for a non-damping system

$$M\dot{X} + KX = B^T F \tag{2.33}$$

with mode coordinate, the modal velocity can be evaluated using follow expression:

$$V = s(\psi^T M \psi s^2 + \psi^T M \psi)^{-1} \psi^T B^T F \tag{2.34}$$

where $s = j\omega$ and B is the force location vectors. With modal velocity and matrix α, equation (2.9), the sound radiation power can be evaluated using equation (2.10).

Figure 2.5 is a plot of sound radiation power of the rectangular plate under simply supported and clamped, respectively. The plate is driven by a point force actuator at the center of the plate. The peaks are corresponding to the resonance frequencies. Since the clamped plate has a larger resonance frequencies, the sound radiation power shifts against frequencies to the right comparing to the simply supported plate. Therefore, we conclude that the boundary conditions will affect the sound radiation.

In this chapter a general hybrid approach is proposed to calculate the sound radiation power of a baffled plate under arbitrary boundary conditions. In this approach, the FEA or variational approach is first used to analyze the normal modes

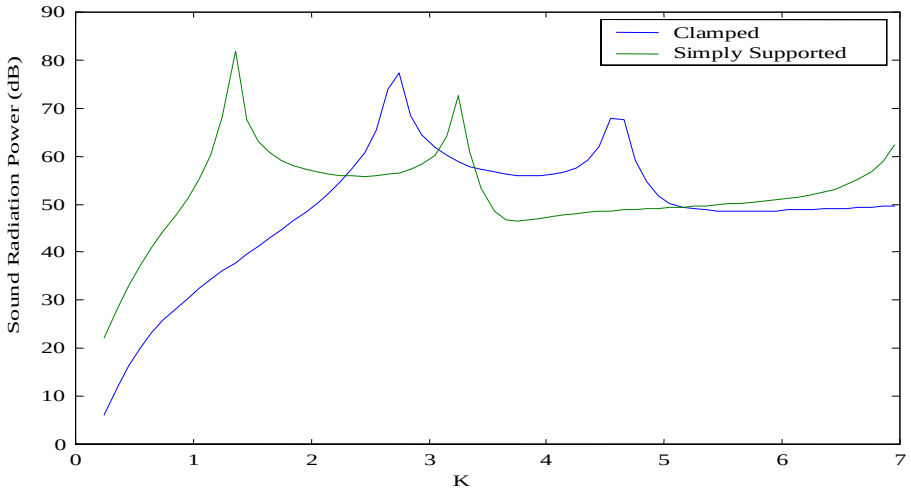

Figure 2.5: The sound radiation power.

of the structure. In order to simulate any boundary supports, translational and rotational springs are used in these models. With the normal mode analytical results, a direct numerical integration or an approximate summation is applied to integrate the sound power radiation. Numerical comparison shows that the above approach has a good accuracy. Therefore, this approach could be applied to the actuation power efficiency analysis in later chapters.

Chapter 3

Power Efficiency Analysis of a Point Force Actuator-Driven Plate

3.1 Introduction

As outlined in the introduction in Chapter 1, research into the active noise control has drawn substantial attention in recent years. The analytical and experimental work on active noise control sound radiation has shown the advantage of the ASAC strategy [Dimitriadis and Fuller (1990); Fuller and Dimitriadis (1991)]. However, most of the active noise control focused on the implementation of the active control and the noise reduction is mainly used as the target of the control. As discussed previously, the global noise reduction does not accurately reflect the effectiveness of the specific actuator, especially the effectiveness of an individual actuator among a group of actuators.

Acoustic radiation from planar vibrating structures into free space is a topic of continuing research in the structural acoustics community, from the standpoint of both prediction and control. One common measure employed to qualify the low-frequency radiation characteristics of structures is radiation efficiency [Snyder and Tanaka (1995)]. There are, however, limitations to the use of these modal radiation efficiencies to characterize the radiation of a vibrating structure; they could not be used to directly calculate the total acoustic power and they do not account the cou-

pling among different modes. Furthermore, the radiation efficiency is not bounded by unity.

Because of the above limitations of radiation efficiency, Leo (1998) defined a maximum actuation power efficiency to investigate the effectiveness of the actuator. The maximum power efficiency is defined as the actual sound power radiated by the structure over the maximum possible sound power. Based on this definition, this chapter will analyze the power efficiency to identify the effectiveness of a single point force actuator and the factors which influence efficiency by integrating the general method for sound radiation power calculation discussed in the preceding chapter with an eigenvalue decomposition technique. The power efficiency analysis, in this Chapter, will focus on the point force-driven complex structure which is shown in Figure 2.1. In addition, the radiation impedances of the structures will also be derived. As examples, the radiation impedance and power efficiency will be numerically evaluated using the previous mentioned general method for both rectangular and circular plates. The radiation impedance at special cases could also be served as a purpose of the modal validation. This efficiency analysis could be used as a reference in comparing the effectiveness of different actuators. It will also help the designer to choose and place actuators.

The basis for this investigation power efficiency of a point force actuator driven structure will be a sound power model developed by several researchers, including Snyder et al. (1995); Snyder and Tanaka (1995); C. R. Fuller and Nelson (1996), for the acoustic radiation from a planar baffled structure . It was demonstrated that the sound power radiation from a baffled structure could be expressed as a quadratic function of the structural modal velocities [Snyder et al. (1995)]. This sound power model provides a convenient means for studying the control authority due to the simple relationship between the structural vibration and the sound power radiation. Another basis for analyzing power efficiency is the eigenvalue technique. Instead of applying the eigenvalue technique to the noise control effort [Burdisso et al. (1994); Ho and Robertshaw (1992); Cunefare (1991); Naghshienh (1993)], this chapter will focus on the power efficiency of the point force actuator driven structure using eigenvalue

techniques. Leo and Paine (1997a) developed an eigenvalue technique for studying the acoustic control authority of point force and distributed moment actuators. Cao and Leo (1998, 1999a,b) extend the technique to study the power efficiency for a baffled planar structure for any geometry under different support conditions.

3.2 Eigenvalue Decomposition Technique for Maximum Radiation Power

In the previous chapter, a formulation of sound radiation power for a baffled planar structure is expressed as

$$W = \gamma \frac{2\kappa\varrho}{\pi} v^H \alpha v, \tag{3.1}$$

or, equivalently

$$W = v^H A v, \tag{3.2}$$

where $A = \gamma \frac{2\kappa\varrho}{\pi}$ and $\gamma = \frac{\rho_0 cab}{4}$ is equivalent to the sound power output of a rigid piston normalized with respect to the velocity of the piston and α is defined as:

$$\alpha = \int_S \int_S \psi^T(\boldsymbol{\xi}') \frac{\sin(\kappa\eta)}{\eta} \psi(\boldsymbol{\xi}) d\boldsymbol{\xi}' d\boldsymbol{\xi}. \tag{3.3}$$

The matrix α or A is frequency dependent and real symmetric. For the purpose of convenience, we expressed the modal velocity as: $v = v_m V_q$ and normalized it in such a way that $V_q^T V_q =$ unity. Where v and V_q represent the magnitude and phase of modal velocity, respectively. Now we try to find the extremty of

$$max v^H \alpha v = max ||v_m||^2 V_q^H \alpha V_q \tag{3.4}$$

According to Lancaster (1969)(interested reader may find the derivation procedure in Appendix A), $max V_q^H \alpha V_q = \lambda_1$ while $V_q = q_1$, which is the eigenvectors corresponding to the largest eigenvalue λ_1. Therefore,

$$max v^H \alpha v = ||v_m||^2 \lambda_1 \tag{3.5}$$

For the purpose of concise, we drop the subscript $_m$ in v_m and

$$max v^H \alpha v = ||v||^2 \lambda_1 \tag{3.6}$$

As we see from equation (3.1), when equation (3.3) achieves its maximum value, the sound power radiation is also maximized. Therefore, the maximum sound radiation power can be expressed as:

$$W_{max} = \gamma ||v||^2 \frac{2\kappa\varrho}{\pi} \lambda_1. \tag{3.7}$$

The maximum radiation sound power output can be normalized with respect to the power output of a rigid piston by dividing both sides of the equation by $\gamma||v||^2$:

$$\frac{W_{max}}{\gamma||v||^2} = \frac{2\kappa\varrho}{\pi} \lambda_1. \tag{3.8}$$

The above derivation shows that the maximum sound power radiation can be simplified as an eigenvalue problem of the matrix α, which is defined by equation (3.3).

3.3 Actuation Power Efficiency

In previous sections, the sound power generated by a point force actuator-driven structure has been derived. The maximum sound power radiated from a plate driven by a point force actuator is normalized with respect to the maximum power that could be generated by the plate, this quantity, denoted actuator efficiency, is examined in this section as a function of frequency and also as a function of actuator location on the plate.

The point force actuation is modeled as a dirac delta function located at (ξ_a, ζ_a):

$$f(\xi, \zeta) = \delta(\xi - \xi_a)\delta(\zeta - \zeta_a), \tag{3.9}$$

therefore, the modal velocity of the ith mode is [Snyder et al. (1995)]

$$v_i = j\omega \frac{sin(M_i \pi \xi_a) sin(N_i \pi \zeta_a)}{m_i Z_i}, \tag{3.10}$$

where $m_i = \frac{\rho_s hab}{4}$ and $Z_i = \omega_i^2 - \omega^2$, and (M, N) are the modal indices. Based upon the above definition, the power efficiency can be expressed as:

$$\eta = \frac{W}{W_{max}}. \tag{3.11}$$

Inserting equation (3.1) and equation (3.7) into equation (3.11), the efficiency can be simplified as:

$$\eta = \frac{v^H \alpha v}{v^H v \lambda_1}. \tag{3.12}$$

Comparing to the previous efficiency definition, this expression is directly related the power efficiency to the maximum eigenvalue of the power transfer matrix. It also clearly shows that the power efficiency is a function of modal velocities.

This equation demonstrates that efficiency is a function of frequency, modal velocity, matrix α, as well as the largest eigenvalue of the matrix. Since the matrix α and modal velocities are a function of mode shapes and natural frequencies, we can numerically relate the power efficiency to the modes and frequencies. By controlling certain modes, we are able to achieve the desired efficiency. Unlike the radiation efficiency that could be higher than unity, this power efficiency is not great than 1. According to equation (3.6), the maximum value of the numerator of equation (3.12) is $||v||^2 \lambda_1$ or equivalently $v^H \alpha v < v^H v \lambda_1$. Therefore, the efficiency is not greater than unity. As for a special case, if a rigid piston vibrates in the first rigid mode, i.e. the normal displacement at each node is uniform, then all the components of power transfer matrix will be the same. According to equation (3.12), the efficiency is unity.

As we can see from equation (3.12), the numerator of the efficiency is the sound radiation power; the denominator is the maximum possible value of the power could be generated at that particular frequency. The maximum efficiency occurs while the modal velocity components are propotional to the components of the eigenvectors of the largest eigenvalue of the matrix α. There are some advantages of this efficiency definition

1. The value is bounded by unity;

Table 3.1: Frequency indices.

Index	$M^2 + \frac{N^2}{\varrho^2}$	M	N
1	5.56	1	1
2	8.56	2	1
3	13.56	3	1
4	19.26	1	2
5	20.56	4	1
6	22.26	2	2
7	27.26	3	2
8	29.56	5	1
9	34.26	4	2
10	40.56	6	1

2. It provides an easy tool to compute the efficiencies and make comparisons among different actuators or various placements;

3. It can also be extended to compare the efficiency of multiple actuators. The disadvantage is that it is hard to experimentally verify the efficiency directly, because of the difficulty of measuring the maximum possible radiation power.

3.4 Numerical Analysis

In this section, we will first verify the above general approach of the calculation of sound radiation power and then apply this approach to analyze the power efficiency of a point force actuator driven plate. It is known that there are an infinite number of mode shapes for a plate with a specified boundary condition. However, previous studies show that only the (odd, odd) modes will contribute to the increase of the maximum eigenvalue of the matrix acoustic power [Leo and Paine (1997a); Snyder and Tanaka (1995)]. For this reason, only the first few frequencies and their mode shapes used in the numerical calculation are converged sufficiently [Leo and Paine (1997a)]. Table 3.1 demonstrated how the index affects the order of the frequencies.

Table 3.2: The converge analysis of the normalized maximum power.

Index	No. of Modes	Normalized Maximum Sound Power	Error (%)
1	10	0.8540	6.4
2	15	0.9123	0.1
3	20	0.9123	0.1
4	30	0.9124	0.0
5	50	0.9124	

As we could see from the Table 3.1, the (odd, odd) modes: (1,1), (3,1) and (5,1), are among the first ten modes. For this particular problem, the effect of the number of the modes on the convergence is shown in Table 3.2. Numerical results demonstrate that the normalized maximum sound power converges fast with the increasing of the number of mode expansions.

Including only the first ten modes in the mode expansion will result in a maximum 6.4 percent error for this particular structure in the sound radiation power analysis. Including less modes will make the power transfer matrix less accurate. Since the maximum eigenvalue is proportional to the matrix, therefore, the largest eigenvalue will be decreased correspondingly. In another words, including less modes will make both the numerator and the denominator of the power efficiency expression, equation (3.12), decrease. Thereby there is a relatively smaller error of power efficiency compared to the error of sound radiation power.

3.4.1 Radiation Impedance

Although this work will not focus on the radiation, the calculation of the radiation impedance acting on the vibrating surface is fundamental to the prediction of its acoustic behavior. The purpose of this analysis is to verify the model at special cases using radiation impedance. Usually effects of the radiation impedance on the sound radiation is ignored by assuming small radiation impedance. This simplification is

acceptable at low frequencies, but it will cause errors at high frequencies. Even for a simple structure, it's hard to compute the radiation impedance. In this section, the radiation impedance of the structure will be derived in terms of the maximum eigenvalue of the power transfer matrix. We will not only apply the previously derived general method of sound radiation to the radiation impedance, but also verify the model accuracy by comparing the radiation impedance with published values for special cases.

The mechanical radiation impedance of a baffled piston is defined as the ratio of the force amplitude to the normal velocity amplitude of the piston. It equals to the area integral of the specific radiation impedance [Pierce (1994)]:

$$Z_{m,rad} = \frac{-i\omega\rho_0}{2\pi} \int_S \int_S r^{-1} e^{ikr} ds' ds. \tag{3.13}$$

On the other hand, the sound power radiation of a rigid piston can also be expressed as [Kinsley (1982)]:

$$W = \frac{1}{2} U_0^2 Z_r, \tag{3.14}$$

where Z_r is the real part of the radiation impedance or radiation resistance and U_0 the magnitude of the physical velocity. For a rigid piston, the velocity U_0 is equal to the modal velocity v. If we substitute W with $\frac{2\kappa\varrho}{\pi}\lambda_1\gamma||v||^2$, then the real part of the radiation impedance can be simplified as:

$$Z_r = \frac{4\kappa\varrho}{\pi}\gamma\lambda_1. \tag{3.15}$$

Equation (3.15) shows that the radiation resistance is proportional to the largest eigenvalue of the matrix α. It provides us an effective way to calculate the radiation impedance.

As suggested by equation (3.15), the radiation impedance is proportional to the maximum eigenvalue of the matrix α. Using the normal modes and numerical

integrations, the radiation impedance for a rigid rectangular plate and circular plates are evaluated, respectively. Then, as in special cases, this radiation impedance is compared to that of other publications.

In this work, the mode shape ψ is normalized against its maximum component, i.e. the maximum $\psi(m,n) = 1$. For a circular plate, if we use a unit mode shape at each node to simulate the rigid mode solution, the corresponding radiation resistance can be evaluated using equations (3.22) and (3.12). In this work, the mode shape ψ is normalized against its maximum component, i.e. the maximum $\psi(m,n) = 1$. The radiation resistance obtained using the eigenvalue decomposition technique is plotted against non-dimensional wave number κ, in Figure 3.1.

For the rigid circular plate, we can compare the radiation resistance between our model and the corresponding closed-form solution. The radiation impedance is defined as the ratio of the force amplitude to the normal velocity amplitude for a baffled piston. Generally speaking, there is no closed-form solution of the radiation impedance for a rigid piston of any arbitrary geometry. However, for the circular baffled piston, the real part of the radiation impedance, Z_r, is a Bessel function of the first kind [Pierce (1994)]

$$Z_r = \rho_0 c \pi a^2 [1 - \frac{2J_1(2ka)}{2ka}], \tag{3.16}$$

where J_1 is the Bessel function. The corresponding radiation impedance is evaluated using equation (3.16) and plotted versus that predicted by the general model in the Figure 3.1. The maximum error between the solutions is less than 2.5 percent. The difference is attributed to several factors, such as the number of modes used in the modal truncation, the size of the finite element mesh, and using the average area of the finite element instead of the individual element area in the numerical integration. This analysis shows that the general method has a good accuracy and can be applied to the radiation analysis of a rigid planar structure.

As for the rectangular plate, some researchers have investigated the radiation impedance, which could be used as references to validate the above model. Morse and Ingard (1968) evaluated the radiation impedance for rectangular large aspect ratio

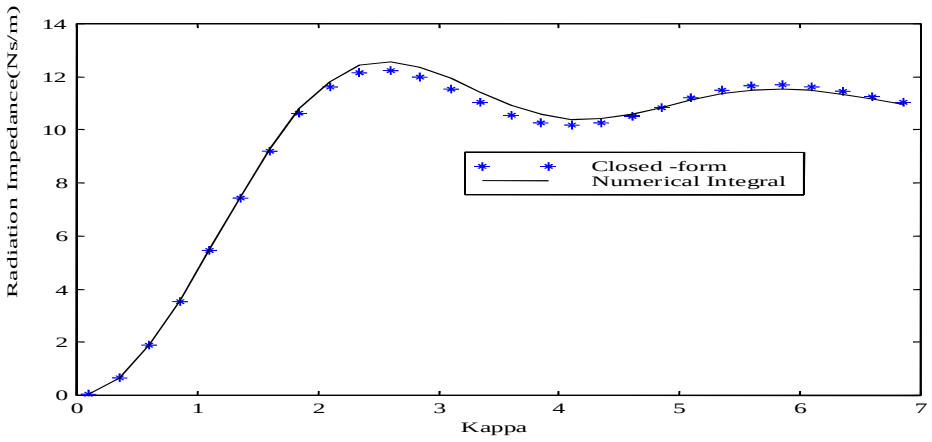

Figure 3.1: The radiation impedance of a circular plate: $*$–closed-form solution of a rigid piston, solid line–evaluated by the eigenvalue decomposition with rigid mode

pistons. Ford presented a theoretical expression for the intensity at a distance from an infinitely long narrow ribbon, and deduced the resistive part of the impedance function. Using Simpson's approximation, Bank and Wright (1995) evaluated the radiation impedance of a rectangular piston with two double surface integrals over the four divided surface areas. Following the procedures suggested by Bank and Wright, the radiation resistance of the rectangular plate is computed using Simpson's approximation. Meanwhile, equation (3.15) is evaluated using the eigenvalue decomposition technique. Both results are plotted in Figure 3.2. *Simpson* stands for the radiation resistance evaluated by equation (3.13) using the Simpson approximation , *Approxi* the approximation using equation (3.15). The error between these two methods is less than 0.5 percent. The error is mainly caused by the step of the integration. These examples demonstrate that the eigenvalue decomposition technique can be used to evaluate the sound radiation of a rigid planar structure with a good accuracy.

Applications in a circular plate

As in a special case, the sound radiation power, radiation impedance, as well as power efficiency of a point force driven circular plate can be easily derived. In order to validate the above analytical model, the radiation impedance will be examined

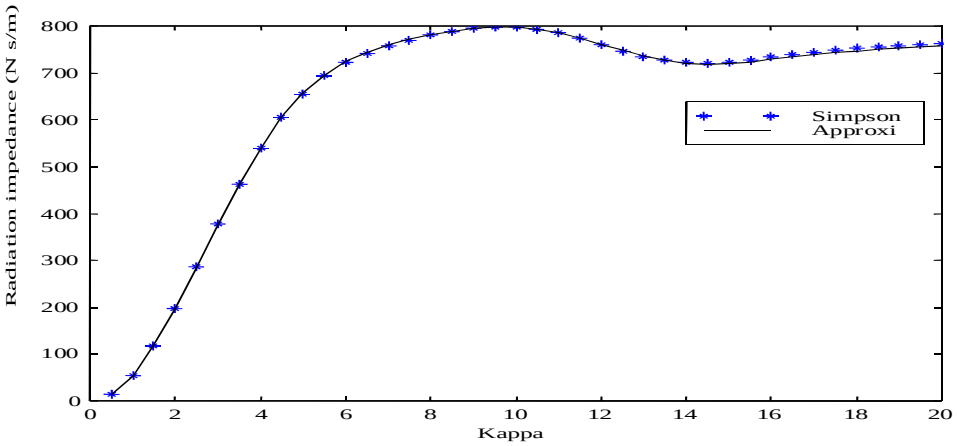

Figure 3.2: A comparison of radiation resistance of a rigid rectangular plate:∗–Simpson method, solid line– eigenvalue decomposition technique

against the close form solution. For the purpose of simplicity, the detailed derivation process is omitted [Cao and Leo (1999a)]. The following is a brief description of the formulation of sound radiation power and radiation resistance of a circular plate.

Instead of normalizing x, y with respect to the maximum length and maximum width of the structure for the case of a rectangular plate, respectively, they are normalized with respect to the radius of the plate, R,

$$\begin{aligned} \xi &= \tfrac{x}{R} \\ \zeta &= \tfrac{y}{R} \end{aligned} \tag{3.17}$$

Using equation (3.14) The sound power can be simplified as

$$W = \frac{\omega \varrho}{4\pi} v^H \alpha v, \tag{3.18}$$

where,

$$\alpha = \int_S \int_{S^0} R^3 \psi^T(\xi,\zeta) \frac{sin(\kappa\eta)}{\eta} \psi(\xi,\zeta) d\mathrm{S}' d\mathrm{S}. \tag{3.19}$$

where $dS = d\xi d\zeta$. The maximum sound power for the circular plate is

$$W = ||v||^2 \frac{\omega \varrho}{4\pi} \lambda_1. \tag{3.20}$$

The radiation resistance can be expressed as

$$Z_r = \frac{\omega \varrho}{2\pi} \lambda_1. \tag{3.21}$$

Because of the complex geometry, an approximate approach is employed to evaluate the double surface integrals by breaking it down into the summation of an integral function over small elements. The component of the matrix α can therefore be approximated as

$$\alpha_{i,j} = R^3 \sum_m \sum_n \kappa \psi_i(\xi_m, \eta_m)^T \frac{sin(\kappa\eta)}{\eta} \psi_j(\xi_n, \eta_n) S'_m S_n, \tag{3.22}$$

where m, n are the indices of location coordinate. In order to verify the accuracy of this method, the above approximation method and the direct numerical integration approach are used to evaluate the matrix α of a rectangular plate which is divided into 21 by 21 elements, respectively. Results indicate that only 0.5 percent error exists between these two methods. Therefore, we can use the procedure suggested by equation (3.22) to evaluate sound radiation power, equation (3.1), for any planar structures.

3.4.2 Normalized maximum power

For the planar structure in an infinite baffle, as shown in Figure 2.1, the expression for the radiated power is shown by equation (2.3). For a simply -supported plate, matrix α can be evaluated using the above two double integrations. However, if the plate is not simply -supported, it is not possible to obtain a closed -form solution for frequencies and mode shapes. Therefore, the sound radiation calculation approach based on the closed-form normal modes is impractical. Thereby an finite element method or variational method will be introduced into the frequency and mode shape computation.

Figures 3.3 and 3.4 are plots of the normalized maximum radiated sound power as a function of the side length ratio and the supporting boundary conditions. In the FEA, a 21 by 21 grid is used. As with the finite element analysis, the same

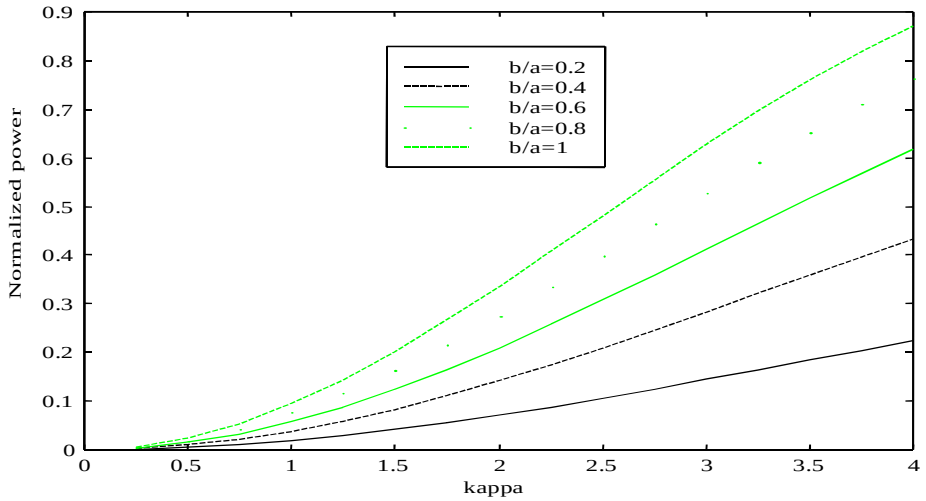

Figure 3.3: A comparison of the normalized maximum power of a simply-supported plate with different length ratios.

pattern of grid was also used for the numerical integration of equation (3.3). From the curves of maximum power as a function of the nondimensional frequency, we conclude that the maximum radiated power increases with frequency. The κ term in the expression of maximum power ensures that the quantities will increase with frequency. However, the increase is not linear because it is also related to the integral term of κ . For a given frequency, the normalized maximum power decreases with the stiffness of rotational spring, Figure 3.4. The notations used in the legend are explained as follows :$SSSS$ stands for simply-supported along all edges, $1K$ and $5K$ a spring with a stiffness of 1 KN/m and 5KN/m at each node along all edges, respectively, and $CCCC$ clamped at all edges. The maximum power is the largest for the simply supported case and the smallest for the clamped support and varies between these upper and lower boundaries for different rotational spring stiffnesses. Because the clamped edges constraint the motion of the edge, the plate mode shape is relatively smaller along the edge comparing to the mode shapes at corresponding nodes when the plate is simply-supported. The mode shapes different along edges of the plate for the simply-support and clamped can be refereed at Figure 2.3 and 2.4. In another words, a simply -supported plate radiate sound power easier than the

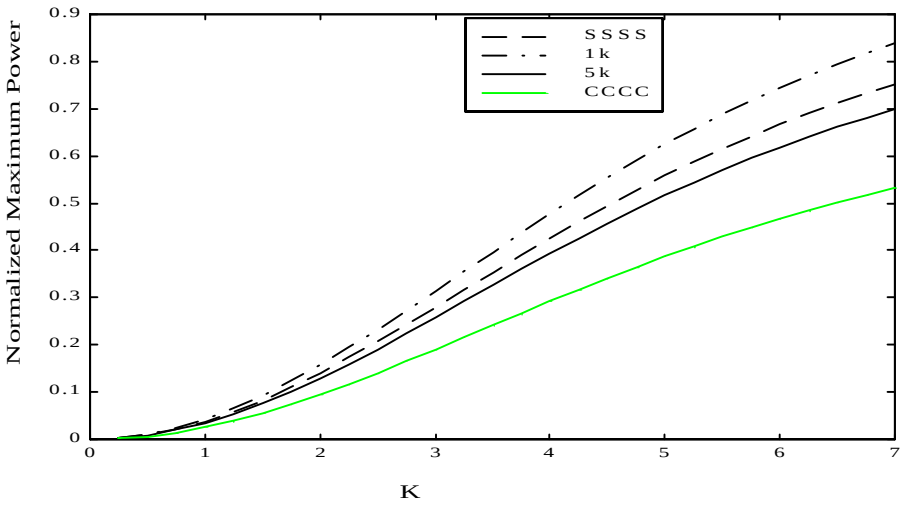

Figure 3.4: A comparison of normalized sound power under different boundary conditions.

clamped the case. Similarly, the stiffer the supporting spring, the less effective of the sound radiation.

As shown in Table 3.1, the side length ratio will affect the order of frequencies. Detailed investigation suggests that it would influence the sound power radiation. Figures 3.3 demonstrates that the normalized maximum power increases with side length ratio. The maximum power increases as the side length rate increases to 1 when the plate is clamped. It has similar results when it is simply supported or under spring supports. The increasing sound power as a function of side length ratio is attributed to the fact that the efficient radiator modes, e.g., the (1,3), and (3,1) modes, coalesce towards the same frequency as the side length ratio approaches 1.

3.5 Power Efficiency

Not only can the actuator power efficiency be used as an index of the performance of single actuator itself, but also it can be used to quantitively to compare the performance among different actuators. Therefore, it is worthwhile to investigate the power efficiency.

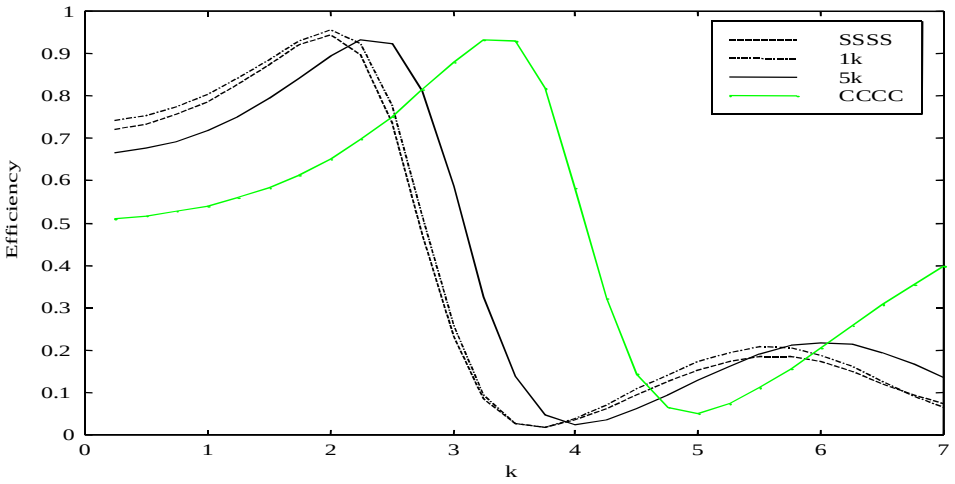

Figure 3.5: A comparison of the influence of the boundary conditions on the actuation power efficiency.

3.5.1 Efficiency calculation procedure

In order to compute the power efficiency, the sound radiation power or power transfer matrix is first evaluated. Then the eigenvalue decomposition technique is applied to the power efficiency analysis. For a given plate driven by a point force actuator, the sound radiation can be calculated using the general hybrid method described at the previous Chapter. First, normal mode analysis is conducted using either the FEA or variational approach. For the simply-supported rectangular plate, a closed-form normal mode analysis could be directly computed. As the of normal mode analysis, frequencies and mode shapes of the structure are thereby obtained.

Next step is to compute the power transfer matrix using the two double integrals. For the rectangular plate, a direct numerical integration is performed. Therefore, the matrix α is evaluated. If the geometry is not rectangular, a direct, numerical integration may be not practical, the approximation described by equation (2.30) will be used instead of the direct numerical integration to evaluate the matrix α.

Then the power efficiency is computed using the eigenvalue decomposition of matrix α and modal velocities, or equation (3.12).

3.5.2 Numerical results

As a numerical example, the power efficiency generated by an actuator located at nondimensional coordinate (1/2, 1/2) under different boundary conditions is shown in Figures 3.5. In general, the power efficiency curves are similar for different rotational spring stiffnesses with the highest value about the same, 90 percent. For a given frequency and structure, the maximum radiated power achieved by a point force is a function of the structural boundary conditions. As we see, the power efficiency is high at low frequencies and low at high frequencies. Increasing the rotational stiffness will increase the resonance frequencies. Figure 3.5 demonstrates the power efficiency shifts to higher frequencies as stiffness increases. At low frequencies, the clamped case has the smallest power efficiency while the highest the power efficiency is about the same, 90%, for the different spring stiffnesses. The reason for the higher efficiency at low frequencies is that the first mode shape is dominate at low frequencies and the modal velocity has a good correspondence to the eigenvectors related to the first eigenvalue. For the clamped case, the first natural frequency increases comparing to that of the simply-supported case. Therefore, the efficiency peak shifts to a higher frequency correspondingly.

As we see from Figure 2.3 and 2.4, for different boundary condition, the mode shapes are different, but they are very similar except near the edges. Since the mode shapes are similar, the power efficiency will be similar but with a frequency shift to the right with a higher stiffness spring supports. As we knew from the FEA model, the rotational spring stiffness is very small for the simply support and the stiffness is very high for the clamped. We also knew that the natural frequency is relatively lower for the simply supported plate comparing to the frequency at the corresponding order of the same plate under the clamped case. Since the efficiency is proportional to the mode velocity, which is proportional to $\frac{1}{(\omega^2-\omega_n^2)}$. Therefore, for the clamped case, the efficiency high peak will shift to a higher frequency.

The above analysis concludes that boundary condition will affect the power efficiency. Although the maximum efficiency is almost identical for different bound-

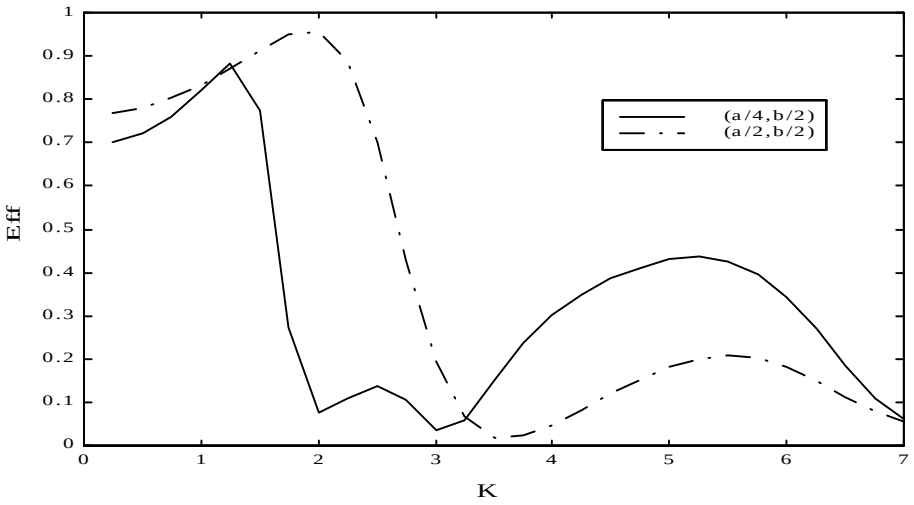

Figure 3.6: A comparison of power efficiency for a simply supported plate when actuator is located at center or (a/4, b/2).

ary conditions, the efficiency will shift with the resonance frequencies for a support condition that approaches clamped. For a small variation of boundary conditions, it will not change the efficiency significantly. However, for larger variation of boundary conditions, the power efficiency will shift with the resonance frequencies. Therefore, for small boundary condition variation, such as the variation of experimental setup for the same structure at different times, the efficiency will not change significantly.

We now move one step further to study the effect of actuator location on the maximum actuator power efficiency. Figure 3.6 shows that efficiency for actuator at nondimensional location $(1/4, 1/4)$ and $(1/2, 1/2)$, respectively.

It is obvious from that Figure 3.6 actuator location has a strong effect on the actuator power efficiency. From equation (3.12), the actuator power efficiency is a function of modal velocity, which, in turn, is a function of the actuator position. If the actuator is placed at a node of a structural mode, then the modal velocity of this mode will be zero. In this case this particular mode will not have any contribution to the maximum achievable power, or the power efficiency. For an actuator located at the center of the plate, the efficiency is higher at lower frequencies than that of actuator at the center of the quarter plate, because the latter actuator effectively excites the first

resonance and it is the dominate vibrating mode. However, at higher frequencies the efficiency decreases because it cannot effectively excite other modes such as $(1,3)$, or $(3,1)$ modes which are dominated at their resonances. As shown in Figure 3.6, when the actuator is placed at the center of the plate, the power efficiency is maximized at approximately $\kappa = 2.0$. The power efficiency changes from 68% to 95% from $\kappa = 0.25$ to 2.25, but drops off rapidly at higher frequencies and only achieves a value greater than 20% in the region near $\kappa = 5.25$. The shape of the curve is different for an actuator located at nondimensional coordinator$(1/4, 1/2)$. For this actuator location the maximum power efficiency shows a remarkable increase near the nondimensional frequency of $\kappa = 5.25$, and achieves a value that is approximately a factor of two greater than the value achieved by the actuator nondimensional location $(1/2, 1/2)$. The reason for the efficiency increase around $\kappa = 5.25$ is that the actuator located at $(1/4, 1/2)$ excites more modes, such as $(, 2, 1), (1, 2)$, and $(2, 2)$. These modes which could not be excited by the actuator located at the center of the plate contribute the sound radiation and improves the power efficiency. This analysis demonstrates that the maximum power efficiency is strongly related to actuator location for a specified structural boundary condition. For the efficiency of the plate driven by an actuator at $(1/4, 1/4)$, the efficiency is high until the first resonance, afterwards it drops, since the actuator not only excite the first frequency, but also excites the other low modes, and none of these excited modes are dominated. Therefore, the efficiency decreases.

Figure 3.6 also demonstrates that the actuator power efficiency varies significantly with the nondimensional frequency. The peaks and valleys in the actuator efficiency do not necessarily correspond to the frequencies of the plate modes, since near structural resonance, the magnitude of one modal component will most likely dominate because $\omega_i = \omega$, but this will not necessarily result in a modal velocity vector that is co-linear with q_1.

This and next paragraphs further explain the efficiency difference at different frequencies based on the modal velocity vector and vector q_1. Figure 3.7 is the power efficiency of the simply supported plate (1.88 by 0.88 by 0.09m) driven by a central point force actuator with two vertical lines showing the first two (odd, odd)

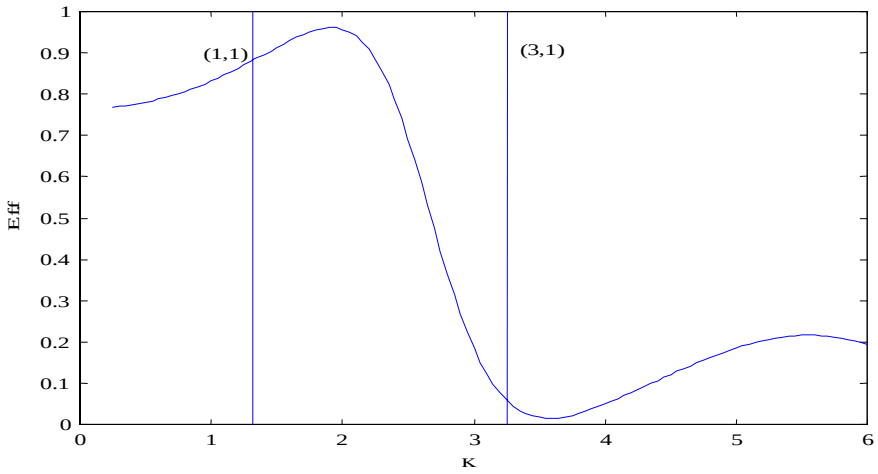

Figure 3.7: The power efficiency for a single actuator located at the center of the plate

resonances. The results illustrate that the maximum and minima do not correspond to the plate radiated resonant frequencies. The maximum power efficiency occurs at $\kappa = 1.95$, not the first mode $\kappa = 1.32$ or the (3,1) mode $\kappa = 3.25$. Similarly, the minimum power efficiency does not occur at exactly resonant frequencies.

The difference results from the fact that the power efficiency is related to the direction and magnitude of the modal velocity vector, and not simply any one component of the vector. For the present analysis, the largest element of the vector q_1 is the coefficient of the (1,1) vibration mode. This is true over the whole frequency range of interest. Figure 3.8 illustrates that the modal velocity vector is dominated by the (1,1) coefficient at low frequencies, thus explaining the relatively high power efficiency over this range. For the none (odd, odd) modes, the corresponding modal velocities are three or four order lower than those of (odd, odd) modes. In contrast, near the resonance of the second (odd, odd) structural mode, this coefficient, not the coefficient related to the first mode, dominates the modal velocity vector and results in a relatively low value of the power efficiency. These results show that the power efficiency, unlike the sound power output, is not directly related to any one of the structural natural frequencies.

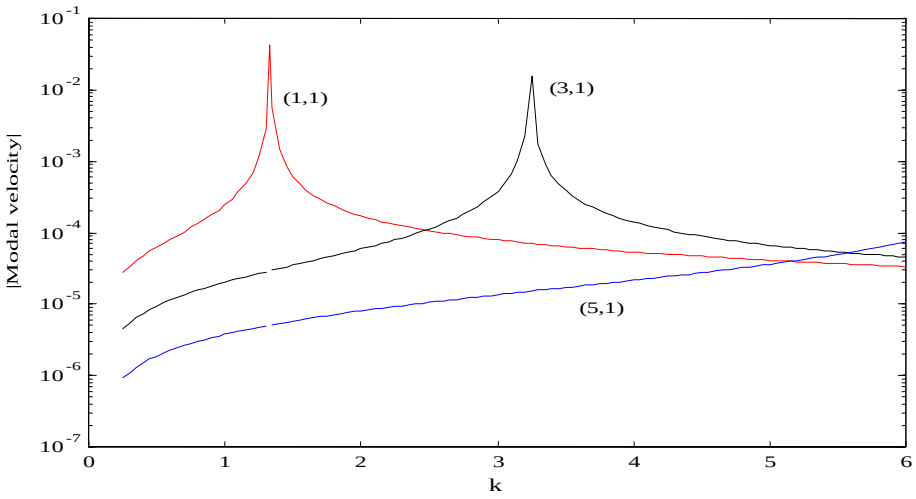

Figure 3.8: The modal velocities of radiated modes for a single actuator located at the center of the plate

In Figure 3.9, 3.10, and 3.11 are the vector q_1 and the modal velocities related to first three (odd, odd) modes at $\kappa = 2, 7$, and 3.25, respectively. Vector q_1 is the eigenvector corresponding to the maximum eigenvalue of the matrix α at a certain frequency. For this particular point force location (at the center of the plate), the first three non-zero components which correspond to the first three (odd, odd) modes are plotted. The horizontal axis 1, 2, and 3 are correlated to (1,1), (3,1), and (5,1) modes, respectively. The corresponding non-zero modal velocities related to first three (odd, odd) numbers are also plotted in the same figure. As we could see from Figure 3.9, the modal velocity components have a very good corelation between the (1,1) and (3,1) modes, in other words, the phase and the magnitude of modal velocity vector are well matched with q_1 and it is this match between the modal velocity components and eigenvector q_1 that results in a high efficiency. Nevertheless, when the frequency increases, the first mode is not the dominant vibrating mode and its first modal velocity component decreases while the $(3, 1)$ and $(5, 1)$ mode component increase, see Figure 3.10, and 3.11. It is these magnitude changes that cause the phase change between the q_1 vector and modal velocity. The efficiency drops to 6% and 5.5% at $\kappa = 3.25$ and 7, respectively.

we could conclude

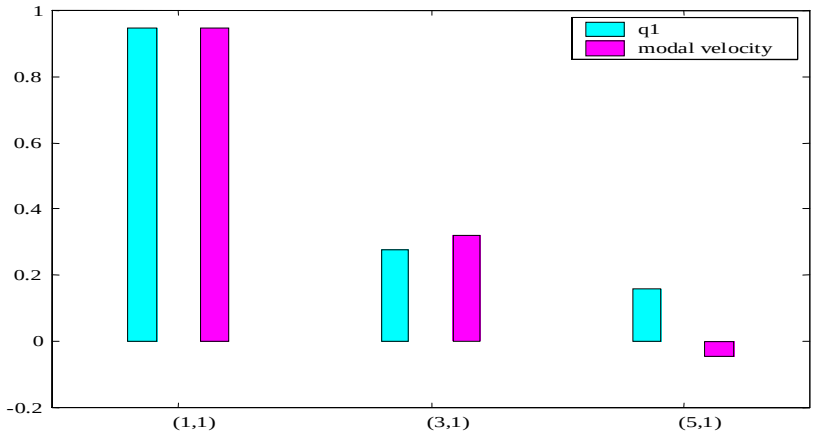

Figure 3.9: The q_1 vector and modal velocity at $\kappa = 2$ of radiated modes for a single actuator located at the center of the plate

The efficiency analysis illustrates that the general approach of sound radiation calculation can be applied to power efficiency analysis of a point force driven structure. Meanwhile, the efficiency analyses also demonstrate that the power efficiency is highly dependent on the coupling of the modal velocity and eigenvector q_1 corresponding to the largest eigenvalue of matrix α, which are related to the actuator locations. Usually, the efficiency is high at low frequencies because of the good match between the modal velocity components and vector q_1. However, unlike the sound power output, the maximum efficiency is not necessary co-linear with that of resonance frequencies because the magnitude and phase of these two vectors mentioned above plays a key role in the efficiency contributions.

3.6 Summary

The eigenvalue decomposition was reviewed in this chapter. This technique shows that the maximum eigenvalue was simply proportional to the largest eigenvalue of matrix α. Integrating the general approach of sound radiation power analysis into

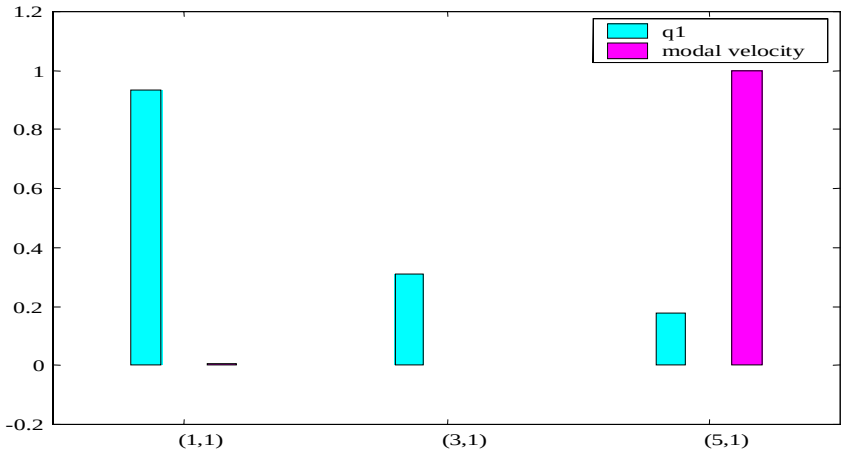

Figure 3.10: The q_1 vector and modal velocity at $\kappa = 3.25$ of radiated modes for a single actuator located at the center of the plate

the eigenvalue decomposition, a general approach is developed and applied to study the maximum radiation power and actuation power efficiency analysis.

The maximum power analysis demonstrates that aspect ratio will affect the maximum power. For a chosen area of a rectangular plate, increasing the aspect ratio will increase the maximum power since the $(1, 3)$ and $(3, 1)$ modes will approach the same frequency. In addition, the FEA and variational approach are used respectively to analyze the influence of the boundary condition on the maximum radiation power. As we learned from the case studies, the normalized sound radiation power is bounded by the limitations of simply supported and clamped, if a rotational spring stiffness is used to simulate the boundary conditions from simply-support and clamped.

In addition, a derivation of sound radiation impedance shows that the general approach of sound radiation power could also be applied to study the radiation impedance of a rigid structure. Numerical analysis suggests that the general approach integrating with the eigenvalue decomposition could be used to predict the sound radiation impedance with a good accuracy. Meanwhile, the radiation impedance evaluation of a rectangular plate and circular plate shows the above general model is accurate. After the maximum sound radiation analysis and model validation, the

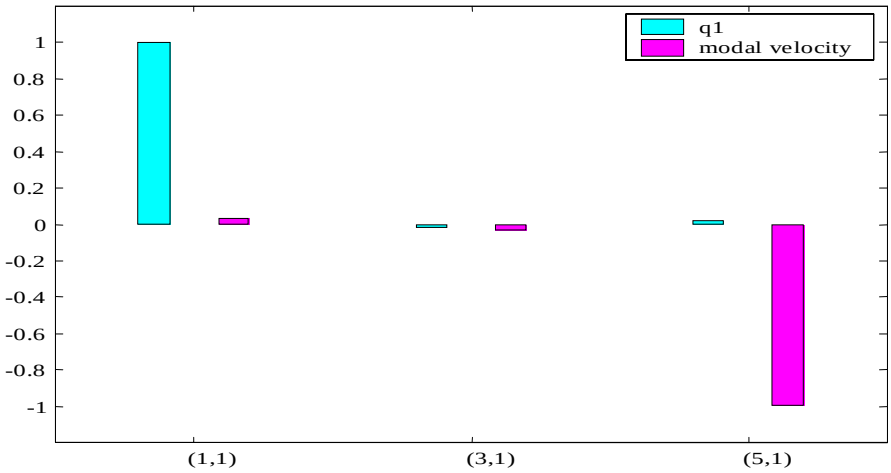

Figure 3.11: The q_1 vector and modal velocity at $\kappa = 7$ of radiated modes for a single actuator located at the center of the plate

above general approach for the sound radiation calculation integrated with the eigenvalue is applied to the power efficiency analysis. The power efficiency evaluation of the rectangular plate driven by a point force shows that efficiency is a strong function of frequency and actuator location. It is also related to boundary conditions. Generally speaking the efficiency is high at low frequencies and low at high frequencies. The maximum efficiency is near but does not necessary correspond to the first resonance frequency. It depends on the matrix α and the modal velocity, especially the correspondence of the modal velocity vectors and the eigenvector related to the largest eigenvalue of the matrix α. The relative phase between the vector q_1 and the modal velocity vector will significantly affect the power. In fact, it is their relative magnitude and phase that will determine the sound power efficiency.

The location of actuator will also influence the modal velocity vector and the power transfer matrix, and in turn they will affect the power efficiency. However, just by placing a point force at a specific location to effectively excite certain radiation modes will not necessary result in a high efficiency, it is especially true when a broad frequency range is considered. The placement of an actuator to maximize the power efficiency should therefore be emphasized not only on effectively exciting the radiated

modes, but also on such a way that the generated modal velocity vector has a good match with the eigenvector of the first eigenvalue of the matrix α.

From above analysis, we may also infer that a single actuator is not enough to achieve a good match between these two vectors both in the magnitude and in phase at a broad frequency range. Therefore, a multiple actuator may be needed for some applications.

Chapter 4

Power Efficiency Analysis for Structures with Distributed Moment Actuators

4.1 Introduction

In the preceding chapter, we have analyzed the power efficiency of a point force actuator driven structure, which provides us with a systematic method to analyze the actuator power efficiency and help designers in their implementation of active noise control. Because of their small size and easy applications, PZT materials are becoming popular in replacing point force actuators or shakers in the noise and vibration suppression. Furthermore, PZT materials can also be used as sensors because of their converse piezoelectric effect. So far a great deal of progress has been made in the modeling and predicting the equivalent force or moments of a PZT acting on the host structure. In addition, some scholars, such as Clark (1992); Dimitriadis et al. (1991); Ho and Robertshaw (1992); Burdisso et al. (1994), working in the active noise control areas, especially in ASAC, have successfully analyzed and optimized the performance of PZT transducers in the implementation of active control. Nevertheless, very few researchers have focused on the power efficiency of a PZT actuator driven structure.

Among them, Leo (1998) compared the point force and PZT actuators based on the efficiency.

In spite of the above progress in noise reduction by using the PZT actuators, a majority of the research did not focus on the performance of PZT actuators themselves. The total noise reduction does not give much insight into the effectiveness of the individual PZT actuator. In addition, the coupling models have not been integrated into the power efficiency analysis, which lowers the credibility at certain circumstances, such as when strong electro-mechanical coupling exists. In this chapter we will extend the power efficiency analysis concerning the point force driven structure to that of the structure driven by a distributed moment actuator. Unlike previous studies, a dynamic coupling model will be integrated into the power efficiency analysis. How to maximize the performance of each PZT actuator is an important aspect in the implementation of ASAC, especially for large structures [Zhou and Rogers (1995)]. This chapter can be used as basis for the later study on maximizing the performance of actuators.

4.2 PZT Distributed Moment Actuator Modeling

A number of PZT actuator models have been studied: static model, dynamic model, FEA model, and coupled electro-mechanical model, etc, have been developed to investigate the force interaction between a PZT and its host structure.

The static model refers to the method of using a statically determined equivalent force or moment as the amplitude of the forcing function to determine the dynamic response due to the activation of integrated induced strain actuators. In a static model, it is assumed that the PZT actuators do not significantly alter the inertia mass and the stiffness of the host structures and the dynamic interaction between PZT actuators and their host structures is thus ignored. Therefore, the amplitude of the excitation force of the PZT actuator predicted by these static models is frequency independent.

Crawley and Luis (1989) developed a one-dimensional static model to predict

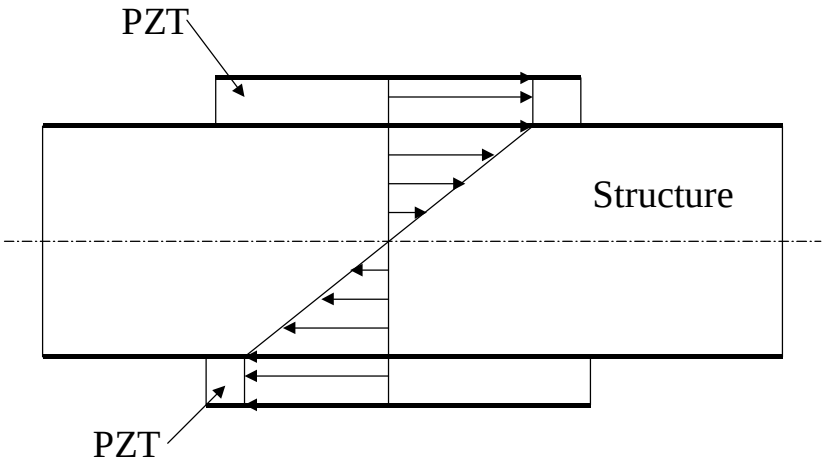

Figure 4.1: A static model assuming uniform strain within the actuator and linear variation of strain within the substrate structure

.

the equivalent force or moment acting to the structure, see Figure 4.1 and Figure 4.2. As an extension of Crawleys work, Dimitriadis et al. (1991) derived an analytic model for a PZT driven undamped rectangular plate. Once again, the force or moment is calculated based on the stiffness of the structure at that point where the actuators are attached and the resultant induced force or moment is independent of frequency, even for the dynamic analysis.

In addition, some researchers, for example, Hagood et al. (1990) Liang and Rogers (1992), Liang and Rogers (1994), Molyet et al. (1998), Varadan et al. (1997), used finite element based models to predict the system response of an active structure. Typically, FEA models require larger number of meshes. Although the results may be accurate, it did not capture the physical essence of the dynamic interaction between the actuator and structure [Liang and Rogers (1994)].

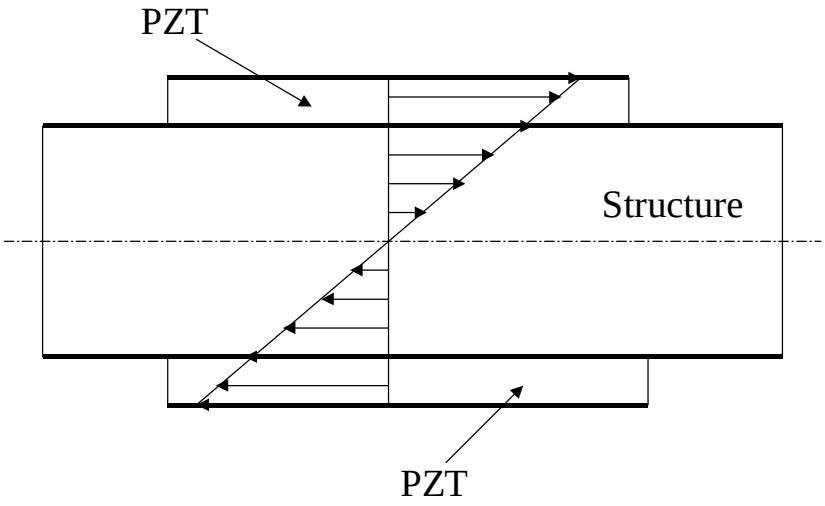

Figure 4.2: A static model assuming linear variation of strain through the thickness of the substrate structure and actuator

.

As an advancement from a static model, some dynamic models have been developed to predict the response of a structure driven by a piezoelectric actuator [Pan et al. (1992)]. However, most dynamic model did not account the electromechanical coupling. When a control voltage is applied to the PZT actuators, the strain is induced on the host structure. To avoid the disadvantage of the static models, dynamic analytical approaches have been developed to predict the force or moment output of the PZT actuator. The active force is therefore generated as a result of the mechanical interaction between the actuator and host structure. As we know, when a control voltage is applied to the PZT patch along the polarization direction, a force is generated as a result of the mechanical interaction between the actuator and the structure; the PZT actuator itself is also driven by the force. This process is involved in energy conversion from electronic energy to mechanical energy, and vice

versa. Therefore, a coupled electro- mechanical impedance model is desired and some dynamic models concerning the electromechanical coupling have been suggested [Sun et al. (1993); Giurgiutiu and Rogers (1996)]. Among these models, Zhou and Rogers (1995) built a PZT model for actuator -driven plate and shell cylinder.

The focus of this chapter is to incorporate a more accurate coupled-impedance model developed by Zhou (1994) with the eigenvalue technique to analyze the acoustic control authority of distrubuted moment actuators. As demonstrated by Leo and Paine (1997a), the problem of determining the sound power efficiency of one distributed moment actuator could be reduced to an eigenvalue problem and the maximum power radiation efficiency of distributed moment actuators could be simplified as a general eigenvalue problem. These eigenvalue techniques provide a straightforward method for studying the tradeoffs in the location and number of actuators in the air-acoustic array consisting of multiple actuators.

4.2.1 Dynamic impedance model

The impedance method of analyzing the dynamic response of active material systems can be used to describe the interactions between actuators and structures by including the electro-mechanical coupling. In this chapter, a coupled electro-mechanical model developed by Zhou (1994) will be used to analyze the actuator power efficiency of the distributed moment actuator. The following is a brief review of the formulation of the impedance model for power efficiency analysis. As shown in Figure 4.3, two PZT patches are placed on the opposite sides of the plate. A control voltage was applied to excite the structure.

As discussed in the previous chapters, we need modal velocity vectors and a power transfer matrix to evaluate the efficiency. These parameters could be obtained by solving the system partial differential equations using constitutive equation and boundary conditions to take into account the electro-mechanical coupling. The following is a brief review of the coupled electro-mechanical model as applied to determining frequencies and equivalent moments, which are the key to model velocity solutions .

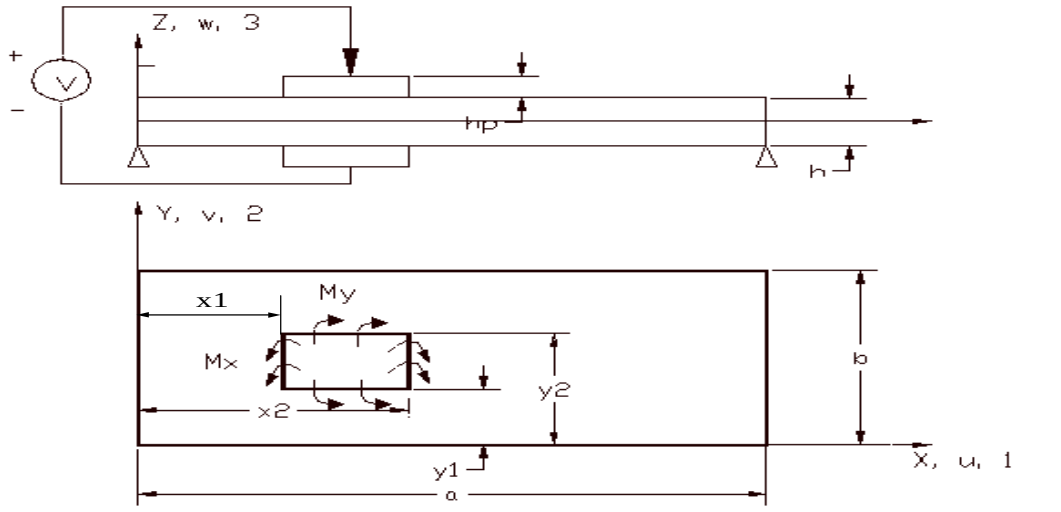

Figure 4.3: Geometric configuration of a simply-supported thin plate with surfaced boned PZT actuators.

The equivalent force, F_{mn}, can be expressed as [Zhou (1994)]:

$$F_{mn} = \frac{4}{ab\varrho h}(\frac{bm}{an}\overline{M_x} + \frac{an}{bm}\overline{M_y})C_xC_y, \tag{4.1}$$

where $C_x = cos(\frac{m\pi}{a}x_2) - cos(\frac{m\pi}{a}x_1)$, and $C_y = cos(\frac{n\pi}{b}y_1) - cos(\frac{n\pi}{b}y_2)$, (x_1, y_1) ,(x_2, y_2) are the coordinates of the PZT, see Figure 4.3, where a, b is the plate's length and width, respectively, and m and n are the mode indices. The constant

$$D = \frac{h^3Y}{12(1-\nu^2)} \tag{4.2}$$

is the flexural stiffness of the plate, h is the thickness of the plate, and Y is the Young's modulus. ϱ, ν is density, Poisson's ratio of the plate, respectively. and $\overline{M_{x(y)}}$ is the amplitude of the line moments per unit length created by a pair of PZT actuators and can be computed by:

$$\begin{bmatrix} \overline{M_x} \\ \overline{M_y} \end{bmatrix} = -j\omega \begin{bmatrix} a_pZ_{xx} & a_pZ_{xy} \\ b_pZ_{yx} & b_pZ_{yy} \end{bmatrix} \begin{bmatrix} A \\ C \end{bmatrix} \begin{bmatrix} sin(k_pa_p) \\ sin(k_pb_p) \end{bmatrix} \tag{4.3}$$

where ω is the excited angular frequency, and the resonant frequency, ω_{mn}, is determined from the homogenous equation of the transverse motion of the plate:

$$\omega_{mn} = \pi^2\sqrt{\frac{D}{\varrho h}}\left[(\frac{m}{a})^2 + (\frac{n}{b})^2\right]. \tag{4.4}$$

The variable k_p is the wave number and can be expressed as:

$$k_p = \omega \sqrt{\frac{\varrho_p}{Y_p^E}}, \tag{4.5}$$

where the subscript p refers to the parameters of the PZT patch, ϱ_p is the mass density, and Y_p^E is the complex Young's modulus at a constant field:

$$Y_p^E = Y_p(1 + j\eta), \tag{4.6}$$

where η is the structural loss factor and j is the complex number. The constants a_p, b_p, and t_p are the length, width, and thickness of the PZT patch, respectively. The constant A and C can be solved by the following expression:

$$\begin{bmatrix} A \\ \\ C \end{bmatrix} = -\frac{1}{k_p} \begin{bmatrix} cos(k_p a_p)(1 - \frac{\nu_p Z_{xy}}{r_p Z_{pxx}} + \frac{Z_{xx}}{Z_{pxx}}) & cos(k_p b_p)(r_p \frac{Z_{yx}}{Z_{pyy}} - \nu_p \frac{Z_{yx}}{Z_{pyy}}) \\ \\ cos(k_p a_p)(\frac{Z_{xy}}{r_p Z_{pxx}} - \nu_p \frac{Z_{xx}}{Z_{pxx}}) & cos(k_p b_p)(1 - \nu_p r_p \frac{Z_{xy}}{Z_{pxx}} + \frac{Z_{xx}}{Z_{pxx}}) \end{bmatrix}^{-1} \begin{bmatrix} d_{31} \\ \\ d_{32} \end{bmatrix} E, \tag{4.7}$$

where ν_p is the Poisson's ratio of the PZT material, $r_p = \frac{a_p}{b_p}$ is the ratio of the length to the width of the PZT patch, d_{31} and d_{32} are the piezoelectric constants of the PZT actuator, and Z_{pxx} and Z_{pyy} are the short-circuit input impedance of the PZT actuator in the x and y directions, defined as:

$$\begin{aligned} Z_{pxx} &= -j \frac{K_{px}}{\omega} \frac{k_p a_p}{tan(k_p a_p)} \\ Z_{pyy} &= -j \frac{K_{py}}{\omega} \frac{k_p b_p}{tan(k_p b_p)} \end{aligned} \tag{4.8}$$

where the K_{px}, K_{py} is the static extension stiffness of the PZT actuator in the x and y directions, can be calculated as:

$$\begin{aligned} K_{px} &= \frac{Y_p^E b_p t_p}{a_p} \\ K_{py} &= \frac{Y_p^E a_p t_p}{b_p} \end{aligned} \tag{4.9}$$

The direct and cross force admittance of the plate at the edge of the PZT patch can be evaluated by the following expressions:

$$Q = \frac{2\pi(h+t_p)^2}{\varrho h}\sum_{m=1}^{\infty}\sum_{n=1}^{\infty}\begin{bmatrix} \frac{m^2C_x^2 sin\frac{n\pi(y_1+y_2)}{2b}C_y}{a^3b_p n(\omega_{mn}^2-\omega^2)} & \frac{mC_x sin\frac{m\pi(x_1+x_2)}{2a}C_y^2}{(a^2bb_p\omega_{mn}^2-\omega^2)} \\ \frac{nC_x^2 sin\frac{n\pi(y_1+y_2)}{2b}C_y^2}{(ab^2a_p\omega_{mn}^2-\omega^2)} & \frac{n^2C_x sin\frac{m\pi(x_1+x_2)}{2a}C_y^2}{b^3a_p m(\omega_{mn}^2-\omega^2)} \end{bmatrix} e^{j\omega\pi/2}. \quad (4.10)$$

where t_p is the thickness of the PZT. The corresponding force impedance matrix is determined by:

$$Z = \begin{bmatrix} Z_{xx} & Z_{xy} \\ Z_{yx} & Z_{yy} \end{bmatrix} = [Q]^{-1} \quad (4.11)$$

where Z_{xx}, Z_{yy} is the direct impedance in the x and y direction, respectively; Z_{xy}, Z_{yx} is the cross impedance.

Based on the coupled electro-mechanical model, if we ignore the change of mode shapes caused by PZT actuators, the power transfer matrix and eigenvalue decomposition can be evaluated by the mode expansions using the same procedures as in previous Chapters. In a later Chapter, a similar study concerning the power efficiency will be conducted by incorporating the mode shapes and frequency changes caused by PZT actuators. After evaluating the admittance using equation (4.10) or the inverse of the impedance matrix and the constants A and C, the magnitude of the line moments can be calculated by equation (4.3) and the equivalent force can be computed using equation (4.1). Therefore, the mode velocity can be determined by the following expression:

$$v_{mn} = j\omega\frac{F_{mn}sin(\frac{m\pi}{a}x)sin(\frac{n\pi}{b}y)}{\omega_{mn}^2-\omega^2}, \quad (4.12)$$

With mode velocities, we will then be able to use the same formulae to calculate the sound radiation power, equation (2.10), and power efficiency, equation (3.12).

The steady-state solution of the forced vibration of the plate can be expressed as a function of mode shape $W_{mn}(x,y) = sin(\frac{m\pi}{a}x)sin(\frac{n\pi}{b}y)$:

$$w(x,y,t) = \sum_{m=1}^{\infty}\sum_{n=1}^{\infty}\frac{F_{mn}sin(\frac{m\pi}{a}x)sin(\frac{n\pi}{b}y)e^{j\omega t}}{\omega_{mn}^2-\omega^2}, \quad (4.13)$$

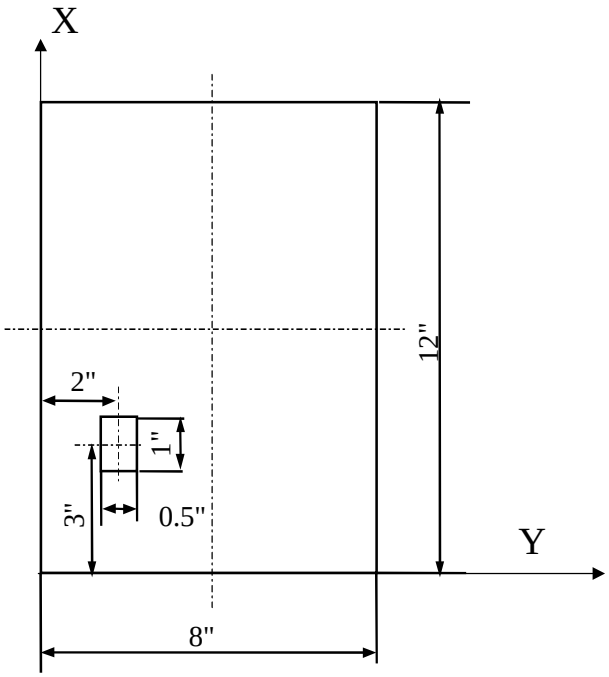

Figure 4.4: The test plate 8"x12"x0.12" with a patched PZT actuator (0.5"x1"x0.01")

.

4.3 Power Efficiency Analysis

In this section, the sound radiation power and power efficiency of a structure driven by one distributed moment actuator will be evaluated using the above formulae. An investigation on the effect of locations of PZT actuators on the efficiency will also be performed.

Before we apply the coupled electro-mechanical impedance model to analyze the power efficiency of a patched PZT actuator-driven active system, this model is first checked against the experimental results. An experimental modal analysis was performed on a small plate, 0.203x0.305x0.003 m (8" x 12"x0.12"), on which a patched PZT was placed in one corner, see Figure 4.4. The dimension of the PZT patch is 0.5"x1"x0.01". The plate dimensions and material properties are listed in Table 2.1.

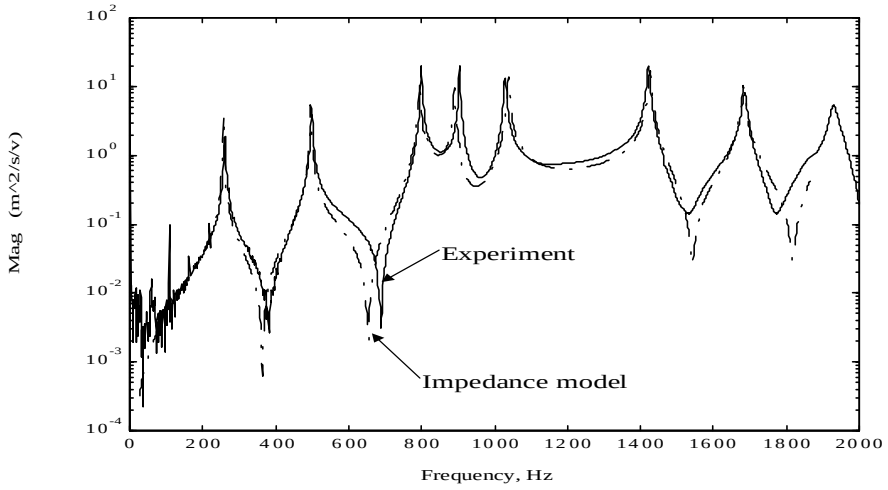

Figure 4.5: A comparison of the acceleration of a patched PZT actuator -driven plate: solid line–experimental results;dash-dot line–coupled electro-mechanical model.

The experimental acceleration and analytic acceleration at location $x = 3", y = 5"$ predicted by the coupled electro-mechanical model were plotted in Figure 4.5. The plot demonstrates that there was a close match both in resonance frequencies and accelerations of the structure.

After above validation of the model, the equivalent moment is now calculated using equation (4.3). The normalized magnitude of moments along the x and y axes predicted by the coupled electro-mechanical model is shown in Figure 4.6. The magnitudes of the moment at resonances are significantly larger than those of off-resonance. At off-resonance, the moment is relatively constant. There is also a noticeable difference between the moments along the X and Y axes at each frequency. The difference increases with higher frequencies.

Table 4.3 lists the experimental frequencies and analytical frequencies predicted by the impedance model. The maximum percentage frequency error is 1.23 %.

As we could see from Figure 4.6, at off-resonance frequencies, the variation of the equivalent moment is very small and the magnitude along the x and y axes are almost identical. However, there are high peaks corresponding to resonance frequencies. In addition the magnitude of the moments are not equal in the x and y directions.

Table 4.1: A comparison of experimental frequencies and analytical frequencies with impedance model

Index	Experiment	Impedance	Error (%)
1	261.2	258.0	1.23
2	500.0	495.3	0.94
3	800.0	794.9	0.64
4	1028.8	1037.2	0.82
5	1422.5	1421.7	0.06
6	1686.3	1682	0.25
7	1931.2	1926	0.27

Therefore, a frequency independent static actuation model will generate errors at resonance frequencies, although it may have a good accuracy at off-resonance. Because the modal velocity is proportional to the equivalent force, equation (4.1), the sound radiation is also a function of equivalent moments.

After verifying the accuracy of the coupled electro-mechanical model by comparing the experimental and analytic acceleration of a PZT actuator-driven structure, we will apply this impedance model to the power efficiency analysis following the procedure presented in Section 4.2.1. Figure 4.7 is a plot of the sound radiation power level of a PZT actuator -driven testing plate using this impedance model. The Solid line is the sound radiation power generated by a PZT patch which is placed at $(a/4, b/4)$. Since this particular PZT effectively excites most low frequency modes, such as $(1,1)$, $(3,1)$, etc., there are peaks corresponding to the peaks of the high resonance. On other hand, a centrally located PZT can not effectively excite the low frequencies except for the $(1,1)$ modes. Therefore, only a high peak is found near the first natural frequency. By changing the locations of the PZT, we can control the modes of vibration, and therefore, the sound radiation power.

After a simple example of sound radiation power analysis, we will apply the coupled electro-mechanical model to analyze the power efficiency of the simply supported plate whose dimensions and material properties are listed in Table 2.1. This

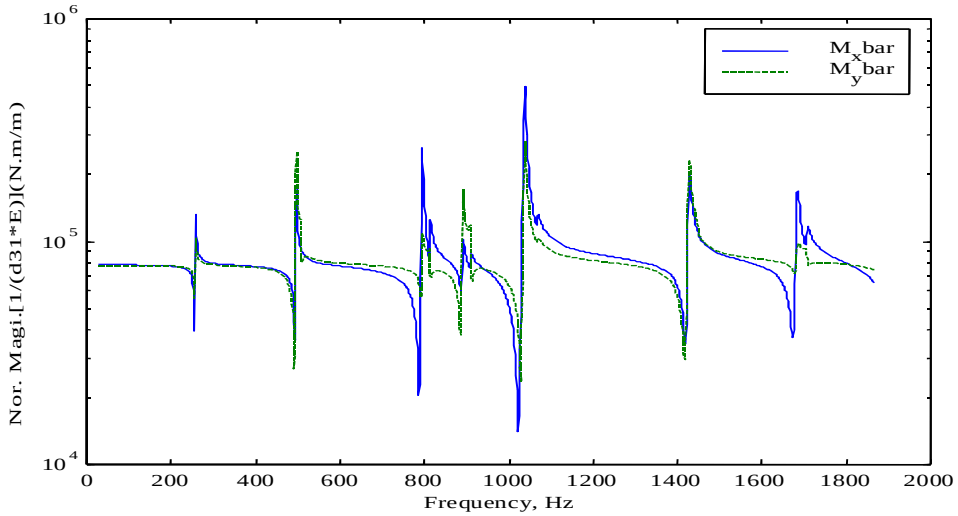

Figure 4.6: The magnitude of moment generated by a PZT actuator , solid line–M_x, and dash line– M_y.

plate was driven by a patched PZT actuator. The investigation will focus on the influence of factors such as the location of the PZT actuator and the number of the actuators on the power efficiency.

The influence of the location of PZT actuators on the efficiency was examined using two PZT patches separately to drive the plate. First, a PZT patch, 0.0254x0.0125x0.003 m (1"x0.5"x0.01"), was placed in the same pattern as shown in Figure 4.4, but its center was co-located at the center of the plate. A certain voltage was applied to the PZT to excite the plate. The corresponding efficiency was computed using equation (3.12) after evaluating the equivalent moments and modal velocities. Similarly, the efficiency of a same size control PZT patch whose center was at nondimensional location (1/4, 1/4) was also calculated. The corresponding efficiency was plotted against non-dimensional wave number κ in Figure 4.8. As we can see, similar to the efficiency of point force actuator, the efficiency is a strong function of frequency. It has a high peak at low frequencies, and it is low at high frequencies. Generally speaking, the efficiency for a PZT at the center of the quarter plate is higher than that of a central PZT at low frequencies. As we expected , the efficiency is related to the direction of the modal velocity. For a central PZT, the

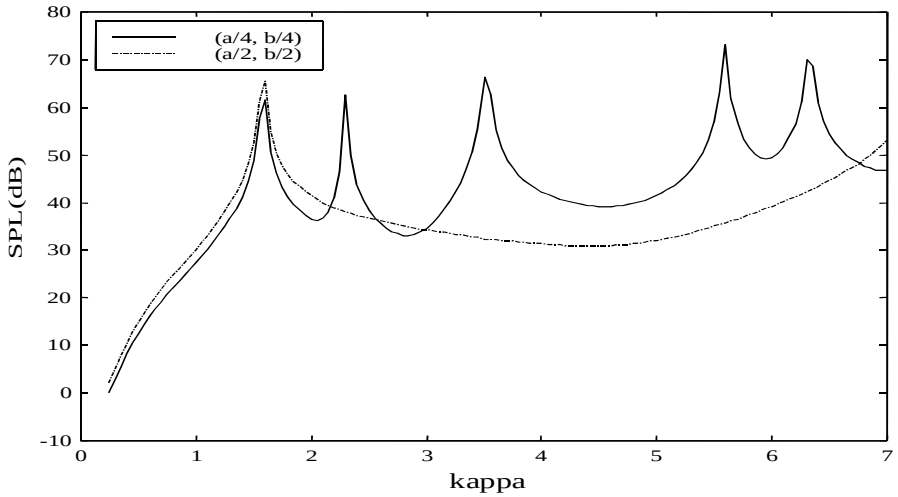

Figure 4.7: The sound radiation power generated by a PZT actuator at different locations , solid line$-(a/4, b/4)$, and dash line$-(a/2, b/2)$.

first mode is effectively excited and most other radiation modes are not,i.e., there is a large magnitude of the first mode. The large amplitude of the first modal amplitude decreases the angle between the modal velocity and vector q_1, thereby increasing the efficiency. However, at higher frequencies, the amplitude of the structural modes other than the first mode dominates and the efficiency is decreased.

For the plate driven by an actuator located at nondimensional location(1/2, 1/2), the efficiency is improved only up to the first mode. Therefore, the efficiency is higher at low frequencies, since at low frequencies the first resonance frequency is the only dominant mode. For the actuator at(1/4,1/4), the efficiency is high before it reaches the first resonance. However, it drops since the PZT also excites other modes along with the first mode. All of these modes contribute to the efficiency, but none of them was dominating, i.e. q_1 is not collinear so that the efficiency decreases. According to our definition of power efficiency, equation (3.12), efficiency is improved. For a central PZT, the actuation power efficiency increases with non-dimensional wave number, κ, up to $\kappa \approx 2$.

In addition, if we compare Figure 4.7 and 4.8, it is easily seen that the maximum power efficiency does not correspond to the first resonance frequency. The

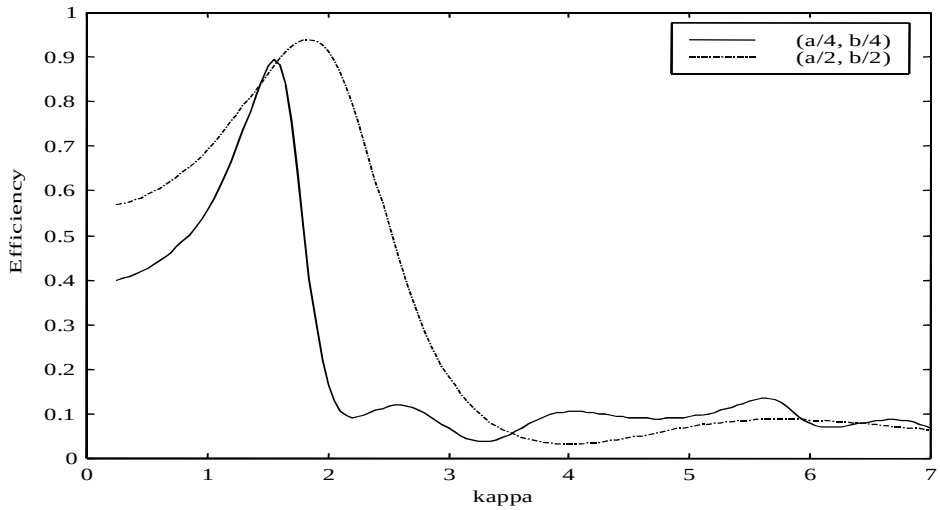

Figure 4.8: The power efficiency of the simply-supported rectangular plate driven by a centrally PZT actuator, solid line–PZT at $(a/4, b/4)$, and dash line–at center of the plate.

reason for this is that the efficiency is related to the direction of the modal velocity and not simply the magnitude of any one component. Near a structural resonance, the magnitude of one modal component will most likely dominate because $\omega_i \approx \omega$, although this will not necessarily result in a modal vector that is collinear with q_1.

Leo and Paine (1997a) computed the power efficiency of a distributed moment PZT actuator driven plate. In their model, the actuation force was modeled as a pure moment applied about the neutral axis of the plate and the formulation of the modal velocity was based on the reference [Clark (1992)]. The ith transfer function component $H(\kappa)$ related to the jth PZT patch can be computed using the following expression [Leo (1998)]:

$$H(\kappa)_{ij} = \frac{j\varrho a\kappa}{c(\kappa^2 - c_r^2(M^2 + \frac{N^2}{\varrho^2}))}\left[(\frac{M}{N} + \frac{N}{M\varrho^2})(cos(M\pi\xi_j^2) - cos(M\pi\xi_j^1))\right]\left[cos(N\pi\zeta_j^1) - cos(N\pi\zeta_j^2)\right] \tag{4.14}$$

where $c_r^2 = (D\pi^4)/(\rho_s h a^2 c^2)$, and (ξ_j^1, ζ_j^1), (ξ_j^1, ζ_j^1). are the corner locations of the jth actuator.

Figure 4.11 is a comparison of sound pressure level of Leo's model and coupled dynamic model, respectively. As we could see, SPL predicted from both models are

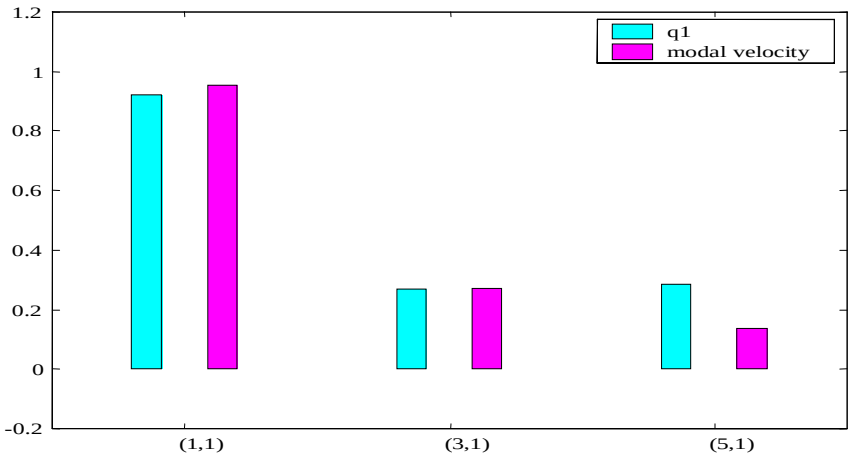

Figure 4.9: The q_1 vector and modal velocity at $\kappa = 2$ or 355Hz of radiated modes for a single actuator located at the center of the plate

closely matched at most frequencies. However, the dynamic model did predict a SPL peak approximately at 1,838Hz, which corresponding to (2 , 3) mode. This mode is not predicted by the static model.

The corresponding efficiencies predicted by these two models are plotted in Figure 4.12. As we can see from this plot, the two efficiency curves are almost overlapped, due to the cancelation in the numerator and denominator of the efficiency expression, equation (3.12).

4.4 Summary and Conclusions

In general, the coupled electro-mechanical impedance model was integrated with the general approach of sound radiation and eigenvalue technique to study the power efficiency of the PZT actuator-driven structure. The representative example of a simply-supported rectangular plate in an infinite baffle was used to demonstrate the utility of the technique. The experiment shown that the model had a good accuracy in dynamic responses. After the coupled electro-mechanical model was validated with the experimental acceleration, it was applied to the power efficiency analysis of one

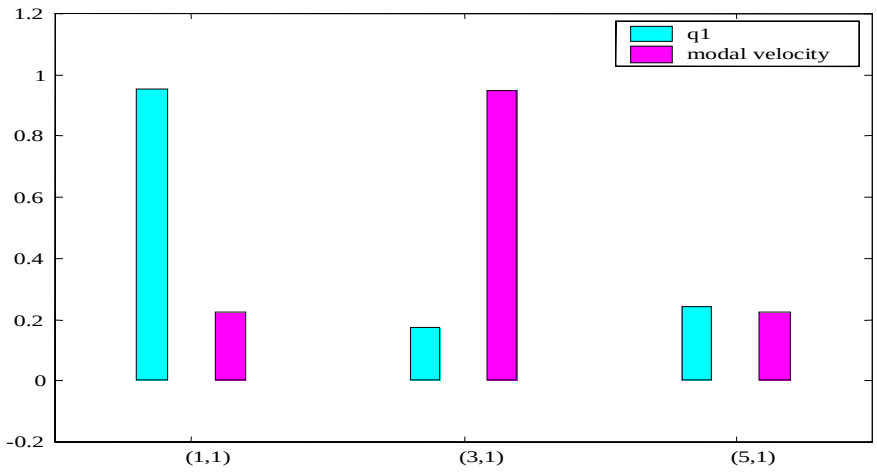

Figure 4.10: The q_1 vector and modal velocity at $\kappa = 4$ or 710 Hz of radiated modes for a single actuator located at the center of the plate

PZT patch-driven plate using the eigenvalue technique.

The coupled dynamic impedance model shows that moment generated by a pair of collocated PZT actuator is strongly depend on the frequencies. The magnitude of moments near the resonances are significantly differ from that of off-resonance, where the magnitude is almost identical. In addition, the moments generated by the PZT actuator along X and Y axes are not necessary equivalent as it predicted by a static model. Because of these two reasons, this model is more accurate in the prediction of the moments and system responses, therefore the sound radiation power. If there exists a strong coupling, then the dynamic impedance model should be applied.

Power efficiency analysis demonstrates that the efficiency is strongly dependent on the frequency and location; a similar conclusion was drawn form the previous chapter. Generally speaking, the frequency of one PZT actuator has a narrow bandwidth of high efficiency at low frequencies and low efficiency at high frequencies. It is apparent that changing a PZT actuator position will affect efficiency because it will excite certain modes and therefore influence modal velocity and sound radiation power. However, the detailed efficiency analysis shows that real reason is far more complicated. Similar to the power efficiency of the point force actuator driven plate,

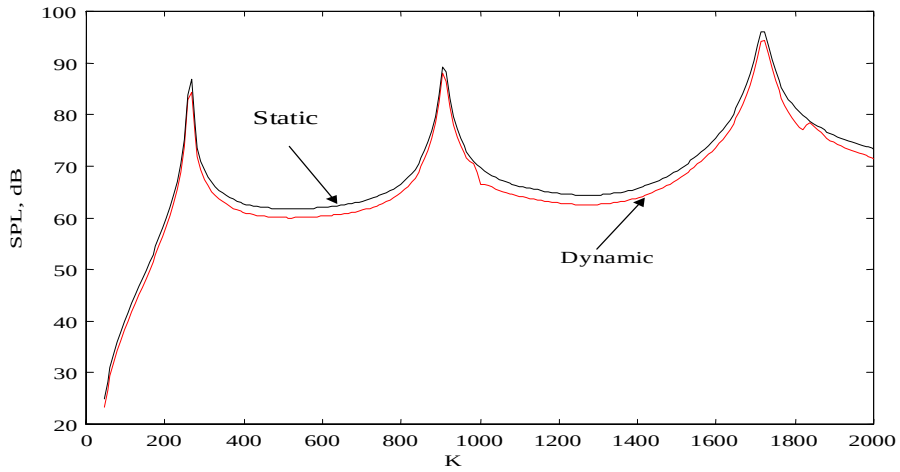

Figure 4.11: SPL of the simply-supported rectangular plate driven by a centrally placed PZT actuator predicted by the static model and dynamic model.

it is the correlation of the modal velocity vectors and the eigenvectors q_1 related to the largest eigenvalue of the matrix α that influences the efficiency greatly.

Power efficiency analysis further demonstrates that the efficiency difference between the coupled dynamic modal prediction and static model prediction is much smaller than that of sound radiation power. The reason is that the significant difference of moment generation predicted by the two models is proportionally presented at both the numerator and the denominator. Therefore, the efficiency is consistent with that predicted by Leo and Paine (1997a) in their power efficiency analysis by integrating the actuation model from the work of Clark and Fuller (1992), although the coupled electro-mechanical model is more accurate in the sound power prediction. In another words, we do not have to use the coupled dynamic model to perform the efficiency analysis if we are only interested in calculating the power efficiency of the actuation.

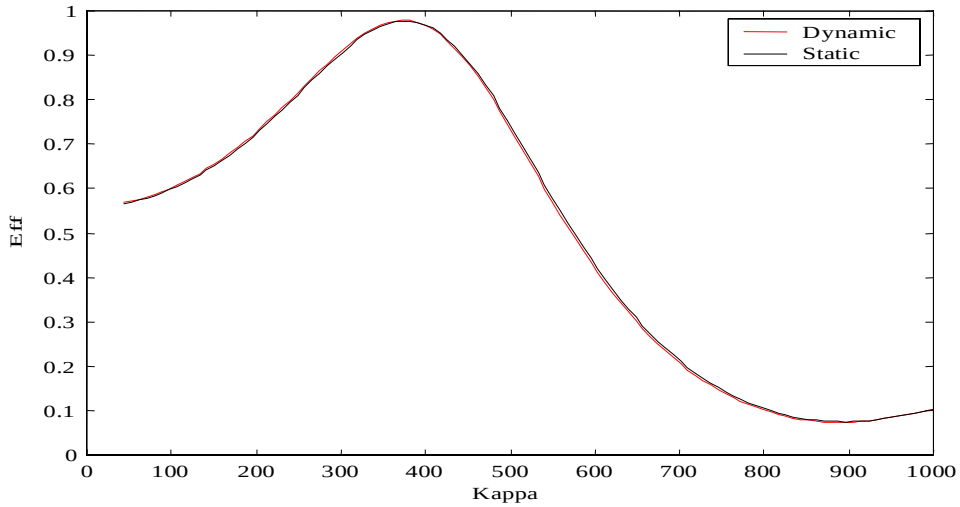

Figure 4.12: Efficiency of the simply-supported rectangular plate driven by a centrally placed PZT actuator predicted by the static model and dynamic model.

Chapter 5

Power efficiency of the multiple actuator air-acoustic array

In the previous chapters we have analyzed the power efficiency of a single actuator and distributed moment actuator using an eigenvalue decomposition technique. Results show that the efficiency is high at low frequencies, but low at high frequencies, see Figure 3.6 and Figure 4.8. In other words, the bandwidth is narrow for a single point force or distributed moment PZT actuator. In order to improve the efficiency bandwidth, a multiple actuator air-acoustic array consisting of a group of actuators can be employed.

In this chapter, we will extend the previous efficiency analysis to the multiple actuator air-acoustic array. For this work we define a multiple actuator air-acoustic array as a multiple actuators placed in a certain pattern and used to excited the structure. Both the point force actuator array and the distributed moment PZT actuators will be analyzed. Furthermore, an efficiency comparison will be conducted between one actuator and actuator arrays.

5.1 Generalized Eigenvalue Technique

As discussed in the previous chapters, the maximum radiated sound power for a baffled plate is proportional to the maximum eigenvalue of the power transfer matrix,

α. Similarly, the maximum radiated power of a multiple air acoustic array can be reduced to a generalized eigenvalue problem. The maximum power is also proportional to the maximum eigenvalue of this generalized eigenvalue problem. The corresponding force input can be determined by expressing modal velocities of the baffled plate as a function of the force inputs to the structure [Leo (1999)]. For a system, the system equation can be expressed as follows:

$$M\dot{\dot{X}} + C\dot{X} + KX = Bf \tag{5.1}$$

where M, C, and K are the mass, damping, and stiffness matrices of the structure, respectively, B is the location vector for the forcing inputs, and f is the input vector. If we use notations of ψ and Z as modal shape and mode coordinate, respectively, the following relationship exists

$$X = \psi Z \tag{5.2}$$

and the modal velocities can be solved through the following expression,

$$v(j\omega) = H(j\omega)F(j\omega), \tag{5.3}$$

where $H(j\omega)$ and $F(j\omega)$ are the system transfer function and Fourier transformation of the applied force of the active structure system,

$$H(j\omega) = j\omega(\Lambda_s - I\omega^2)^{-1}\psi^T B. \tag{5.4}$$

The matrix Λ_s is a diagonal matrix of eigenvalues that corresponds to the square of the natural frequencies of the structure. Substituting the nondimensional expressions:

$$\kappa = \frac{\omega a}{c} \quad \tilde{\Lambda}_s = \Lambda_s \frac{a^2}{c^2} \tag{5.5}$$

into equation (5.4) yields:

$$H(j\omega) = j\kappa(\frac{a}{c})(\tilde{\Lambda}_s - I\kappa^2)^{-1}\phi^T B. \tag{5.6}$$

Thus, the modal velocities can be written as a function of the nondimensonal wavenumber as [Leo (1998)]

$$v(j\kappa) = j\kappa(\frac{a}{c})H(j\kappa)F(j\kappa). \tag{5.7}$$

The power efficiency is defined previously as the ratio of the maximum power generated by the actuator driven plate to the maximum achievable sound power of the plate:

$$\eta = \frac{v^H \alpha v}{\lambda_1 v^H v}. \tag{5.8}$$

After inserting equation (5.7) into equation (5.8), the power efficiency is

$$\eta(j\omega) = \frac{F^T(-j\kappa)A(\kappa)F(j\kappa)}{F^T(-j\kappa)B(\kappa)F(j\kappa)}, \tag{5.9}$$

where $A(\kappa)$ and $B(\kappa)$ are defined by the following expressions

$$\begin{aligned} A(\kappa) &= H^T(\kappa)\alpha H(\kappa) \\ &\quad . \\ B(\kappa) &= \lambda_1 H^T(\kappa)H(\kappa) \end{aligned} \tag{5.10}$$

Since $H^T(\kappa)\alpha H(\kappa)$ and $H^T(\kappa)H(\kappa)$ are real-symmetric matrices at each value of κ, equation (5.9) represents a generalized eigenvalue problem at each value of κ, where the maximum eigenvalue is the maximum power efficiency at that frequency. The eigenvector corresponding to the maximum eigenvalue represents the relative magnitude of the forcing inputs that achieves the maximum power efficiency at that frequency.

5.2 Point Force Actuator Array Efficiency

As discussed in the previous section, the power efficiency of a multiple point force actuator driven plate reduces to the solution of a generalized eigenvalue problem. First, we will study the power efficiency of four actuators which are placed at nondimensional coordinates $(0.1, 0.1)$, $(0.1, 0.9)$, $(0.9, 0.1)$, and $(0.9, 0.9)$. The matrix $H(\kappa)$ can be evaluated using the following expression:

$$H(\kappa) = \begin{bmatrix} \frac{1}{(\frac{a}{c}\omega_1)^2-\kappa^2} & \dots & 0 \\ 0 & \dots & 0 \\ \dots & \frac{1}{(\frac{a}{c}\omega_i)^2-\kappa^2} & \dots \\ 0 & \dots & 0 \\ 0 & \dots & \frac{1}{(\frac{a}{c}\omega_n)^2-\kappa^2} \end{bmatrix} \psi^T B(\kappa) \tag{5.11}$$

The matrices $A(\kappa)$ and $B(\kappa)$ are computed using equation (5.10) from the α matrix defined by equation (3.3) and the expression for $H(\kappa)$, equation (5.11).

As discussed previously, if we assume that the point force applies an ideal force to the structure, the power efficiency of the point force actuators could be computed using equation (5.9). Figure 5.1 is a plot of the power efficiency for this set of four point force actuators driving the plate with a dimension of 12"x8"x0.1235". The four actuators are placed at the center of each quarter of the plate. The efficiency of one actuator placed at the center of the plate is also shown in the plot for the purpose of comparison. For the case of four actuators, the efficiency is very close to unity when κ is less than 1. However, it decreases rapidly between $\kappa = 1$ and 2 and is very low after $\kappa > 2$. However, for a structure driven by one central actuator , the efficiency is slightly lower than that of four actuators before $\kappa = 1.5$ but higher afterward until $\kappa = 2.75$. The curve shifts to right a little bit, i.e. the bandwidth is larger than that of four corner actuators. Similar to that of four actuators, the efficiency is very low at higher frequencies. Meanwhile, the figure demonstrates that at certain frequencies a single actuator placed at the center is more efficient in terms of power generation than four actuators placed near the corners because they could not efficiently excite the first mode of the structure.

Figure 5.1 also includes the power efficiency curve of the same plate driven by five actuators simultaneously. These five actuators consist of the previously mentioned four actuators plus one central actuator. As we can see from the plot, these five actuators not only increase the power efficiency but also increase the bandwidth of the efficiency.

We now compare the effect of the actuator locations on the power efficiency. Figure 5.2 plots the efficiency for two groups of actuators. Both groups have four actuators. One group is placed at nondimensional coordinates $(0.1, 0.1)$, $(0.1, 0.9)$, $(0.9, 0.1)$, and $(0.9, 0.9)$, while the other is placed at the center of each quarter of the plate.

Figure 5.2 shows that there is a higher efficiency for the group actuators at centers of quarter plates at most frequencies as compared to the efficiency of four

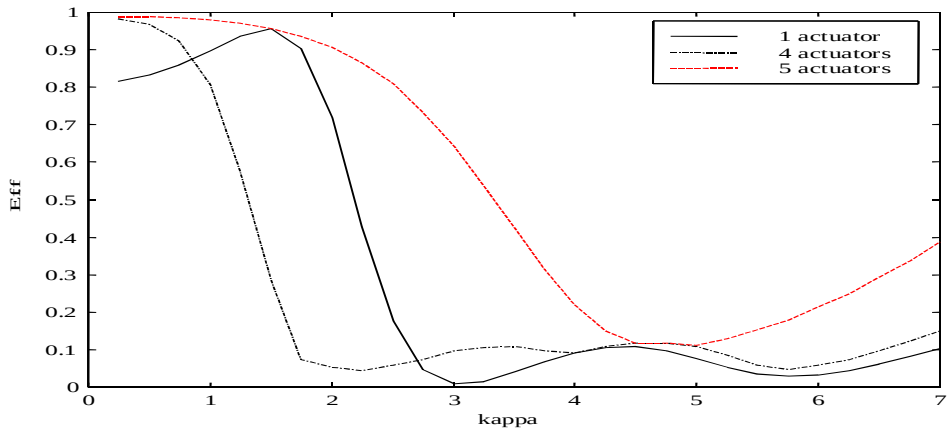

Figure 5.1: A comparison of efficiency for different number of actuators.

corner actuators. The reason is apparent because the actuators close to the corners could not effectively excite the structure.

In order to analyze the effect of the number of actuators on the power efficiency, a central actuator was added to the previously mentioned two groups of actuators. The corresponding efficiency for these two groups are plotted in Figure 5.3. If we compare the power efficiency of the group of four actuators to that of the group of five, Figure 5.2 and 5.3 respectively, it is obvious that adding a center actuator will significantly increase the efficiency, especially for those actuators located at the center of each quarter plate. The figure also shows that the efficiency for the five actuator driven plate is almost unity. It shows that it is not necessarily to add too many actuators to increase the efficiency. Depending on the structure and actuator locations, there is a limit to the number of actuators that are required to achieve the maximum power efficiency.

In general, the above numerical analysis demonstrates that the number and location of the actuators will significantly affect the power efficiency. Increasing the numbers of actuators could, but not necessarily increase the power efficiency since the location may outweigh the influence of the number of actuators.

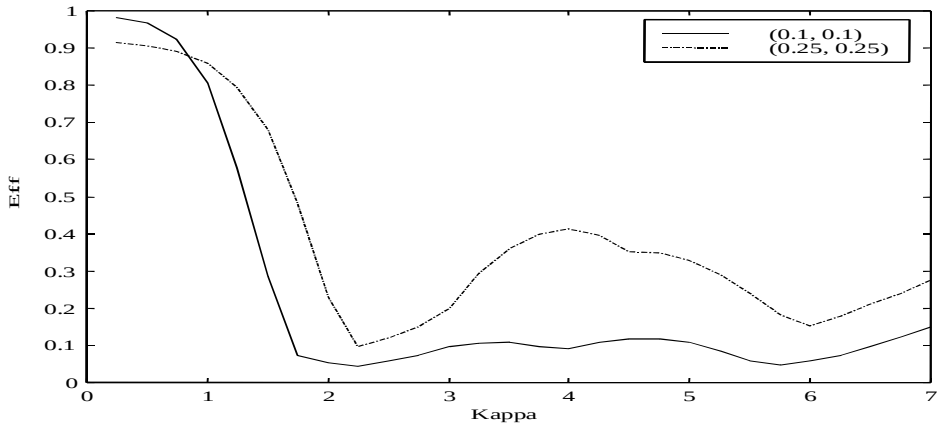

Figure 5.2: A comparison of efficiency of four actuators for different locations.

5.3 Patched PZT Actuator Array Efficiency Analysis

Similar to the point force actuators, multiple distributed moment PZT patches could also be adopted to increase the power efficiency. Because of the easy application of the PZT actuators, it is very popular in the implementation of ANC. Since a single PZT actuator is usually not enough to achieve the expected noise reduction in a real structure, the group PZT actuators are widely applied in the actual vibration and noise control. Therefore, it is worthwhile to study group actuator efficiency so that the maximum power efficiency could be achieved. The power efficiency analysis of the PZT actuators can be performed in the same manner as for the point force actuators using the generalized eigenvalue technique. As discussed in the preceeding chapter, different actuation models,including static and dynamic models, could be chosen in the efficiency analysis.

Based on a frequency independent equivalent force model, Leo (1998) analyzed the power efficiency of distributed moment actuators. In this work, the coupled dynamic model discussed in previous chapters will be used in the power efficiency analysis. Since the dynamic coupling between the PZT actuators and its host structure is taken into account, this model should improve the accuracy of power analy-

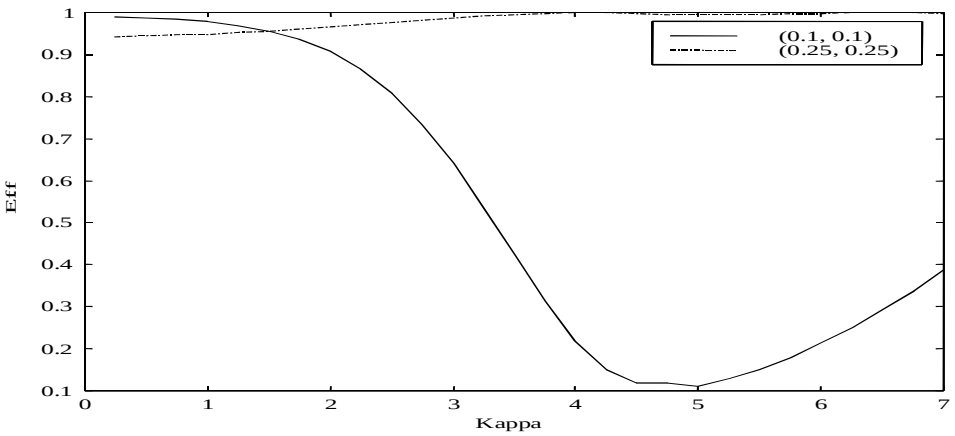

Figure 5.3: A comparison of efficiency of five actuators for different locations

sis, especially at resonance frequencies. However, for the power efficiency analysis, we conclude from previous chapter that the efficiency analysis for the static model and dynamic model is almost identical. Based on the coupled electro-mechanical impedance model, the modal velocities are first evaluated and then the transfer function $H(j\omega)$ is computed. The efficiency is finally computed using equation (5.9).

The following is a very brief procedure to compute the power efficiency of patched PZT actuators. Based on the PZT patch and structure information and boundary conditions, the force admittance matrix is evaluated, using equation (4.10). The amplitude of the line moments is evaluated, using equation (4.3), after solving constants A, and C, equation (4.7). Therefore, the equivalent force and modal velocities can be calculated using equation (4.1) and (4.12), respectively. Since our focus is mainly on the power efficiency, the transfer function $H(\kappa)$ can be evaluated using the following expression:

$$H(\kappa) = [v_1 ... v_i ... v_n]\,; \tag{5.12}$$

where v_i is the modal velocity caused by each PZT actuator. If we assume the PZT actuator does not cause significant variation in mode shape and natural frequency, we can still use equation (3.3) to compute the matrix α. Therefore, $A(\kappa)$ and $B(\kappa)$ can be evaluated using equation (5.10). Figure 5.5 illustrates the power efficiency for

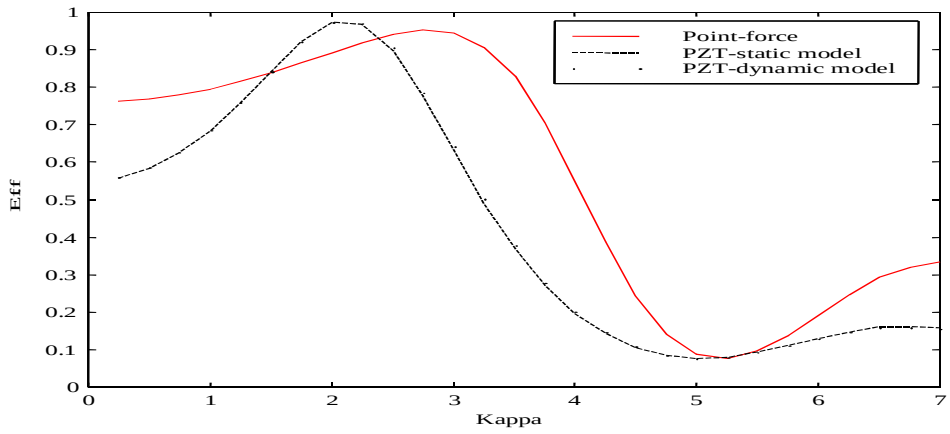

Figure 5.4: A comparison of efficiency of PZT actuators.

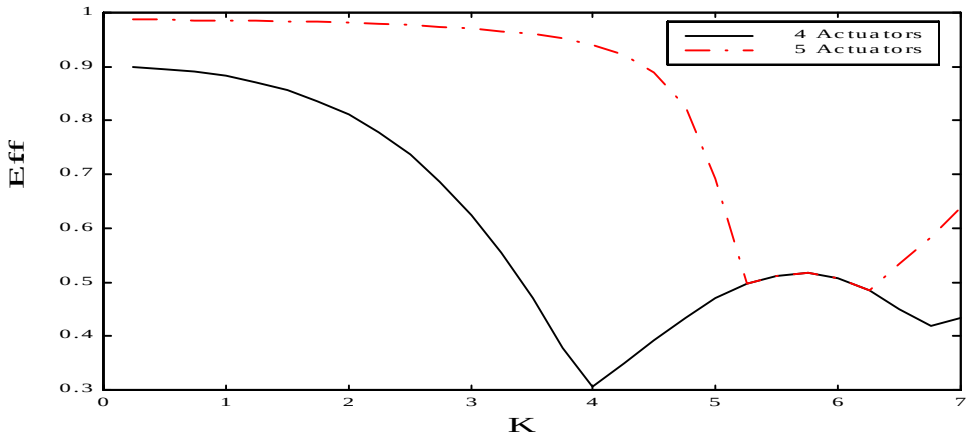

Figure 5.5: A comparison of efficiency for different numbers of PZT actuators.

four and five PZT patch driven plates, respectively. The four actuators are placed at the center of each quarter plate respectively and the fifth actuator is at the center of the plate. The PZT size is 1" by 1.5".

5.4 The Optimization of PZT Patch Actuator Locations

As the previous numerical analysis shows, the power efficiency is a strong function of actuator location. In this section, we will perform the optimization on the power efficiency for the PZT patch actuators driven structure. The objective of this study is to maximize the performance of the actuators at a broader frequency range.

Since we are more concerned about the actuation efficiency, we will choose the maximum power efficiency, or equivalently the minimum of the negative efficiency as an objective function. Because the bandwidth affects the efficency, a frequency of interest is chosen in conjunction with the objective function. As we can see from previous efficiency, Figure 5.1, we could optimize the power efficiency simply by maximizing the area over the chosen frequency range. In other words, this maximized the average value of efficiency over an interested nondimensional frequency κ range. The optimal objective function can therefore be mathematically expressed as follows:

$$\eta_{opt} = -min \quad \eta = -min\frac{\sum_i^N \eta_i}{N} \tag{5.13}$$

where, N is the total number of discrete frequencies, and η_i is the efficiency at ith discrete frequency. A variety of parameters can be chosen as optimization variables. In order to simplify the problem, we may assume that only four actuators are used and these four actuators are symmetrical to the central axes. We will focus on the optimization of the location and size of PZT patches. The optimization variables are: dx, dy, a_p, and r_p, where dx and dy are the distance from the center of the plate to the center to the PZT patches along X and Y axes, respectively. The variables a_p, and r_p are the length and aspect ratio of PZT patch, respectively. The width of PZT patch is $b_p = \frac{a_p}{r_p}$.

The constraints are as follows:

$$\frac{a_p}{2} < dx < \frac{a}{2} \tag{5.14}$$

$$\frac{b_p}{2} < dy < \frac{b}{2} \tag{5.15}$$

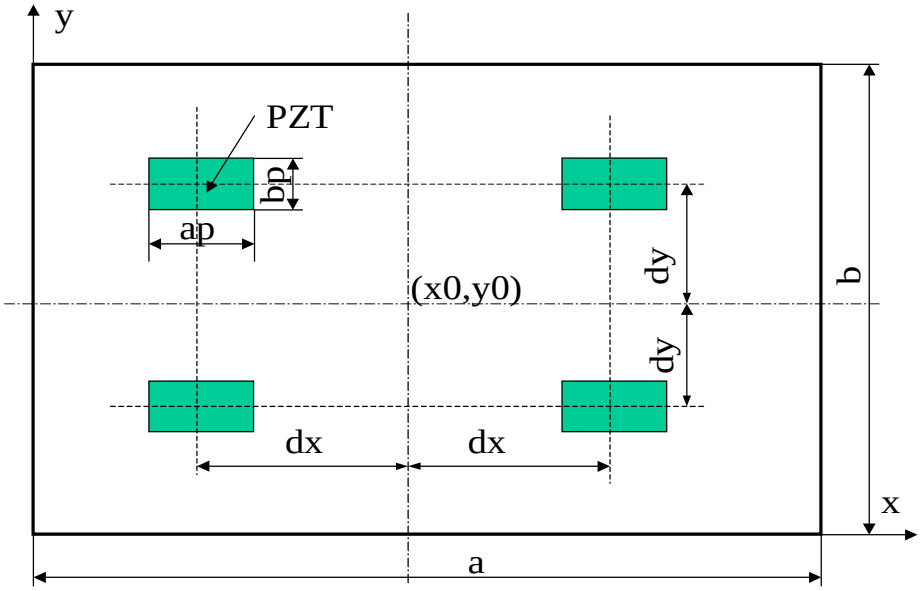

Figure 5.6: The placement pattern of PZT patches.

$$1" < a_p < 2" \tag{5.16}$$

$$0.75" < r_p < 1.5" \tag{5.17}$$

The first two constraints will prevent the PZT from overlapping or moving out of the plate surface. In other words, these constraints will guarantee the optimized solution is feasible. The constraints three and four are the possible length and width of PZT actuators. After choosing the initial conditions, a program is written to solve this constrained optimization problem.

Because of the limitation of PZT sizes, we fix $a_p = 1.5"$ and $b_p = 1"$ and optimize the locations of PZT patch centers only. Table 5.1 lists the optimized locations for the PZT centers based on the optimization of efficiency at the frequency range up to $\kappa = 4$ or 6, respectively.

If we increase the κ to 6 (κ=5.6 corresponding to $1,000$Hz), the optimization is listed in Table 5.2.

Table 5.1: The optimization of 4 PZT patches for $\kappa < 4$

Initial Conditions	dx	dy	Objective function	note
$a/8, b/8$	0.0482m	0.0320m	0.89	

Table 5.2: The optimization of 4 PZT patches for $\kappa < 6$

Initial Conditions	dx	dy	Unit	Objective function
$a/8, b/8$	0.0508	0.0359	meter	0.8490
$a/8, b/5$	0.0508	0.0359	meter	0.8490

After the optimization, the coordinates of the PZTs can be easily evaluated. For example, for the bottom left PZT patch, the bottom left corner coordinate is:

$$\begin{aligned} x &= x0 - dx - ap/2 \\ y &= y0 - dy - bp/2 \end{aligned} \tag{5.18}$$

where $x0 = a/2$ and $y0 = b/2$. After inserting values, the coordinate of the bottom left corner (corresponding to the optimization in the range of $\kappa < 6$) is $(0.0825, 0.0530)$ m, or $(3.25", 2.09")$. The optimized locations for four actuators are plotted at Figure 5.7 (κ up to 4).

Figures 5.9 and 5.10 are the power efficiency for the four actuators at the optimization locations corresponding to $\kappa < 4$ and $\kappa < 6$, respectively. The optimized locations for four actuators are plotted at Figure 5.8 (κ up to 6).

Figure 5.11 is a plot of power efficiency of the four PZT patch actuator driven plate with actuators at the optimized and non-optimized locations, respectively. The non-optimized location of each PZT patch's center is collocated with the center of each quarter of the plate. As we could see from this plot, although the efficiency for

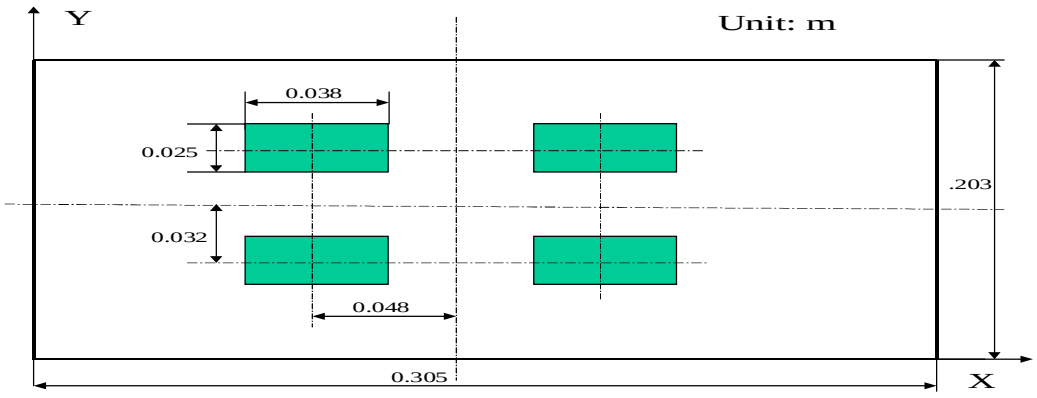

Figure 5.7: The optimized PZT locations for 4 actuators corresponding to κ up to 4.

non-optimization is high at very low frequencies, the optimization does generate a much higher efficiency at most frequencies other than the very low frequencies.

Figures 5.12 and 5.13 are the plot of q_1 and non-zero modal velocity components at $\kappa = 2$ and 4, respectively. In both cases the q_1 and modal velocity vectors have a good correlation. In other words, the phase between q_1 and modal velocity components is almost in-phase. Table 5.3 lists the first 3 non-zero components of the eigenvector and modal velocity vectors for $\kappa = 2$ and $\kappa = 6$, respectively. As we could see from Figure 5.12 and Table 5.3, the first component corresponding to the largest eigenvalue of power transfer matrix is 0.9207 and the corresponding normalized modal velocity vector component is 0.9701. The other two non-zero components of the largest eigenvectors are 0.2663 and 0.2855, respectively. The other related modal velocity vector components are 0 and 0.2425, respectively. Therefore, the magnitude and phase between q_1 and modal velocity vectors are in good correlation, which makes the power efficiency high at $\kappa = 2$. As we knew from previous chapters, the efficiency drops as the frequency goes higher because of the q_1 and modal velocity vectors are not in phase any more. However, Figure 5.13 and Table 5.3 demonstrates that q_1 and modal velocity vectors are still in a very good shape. This explains why the efficiency is still high as the frequency goes up to $\kappa = 6$. As we observed from Figures 5.10 and 5.8, the efficiency is very high at all the frequencies of interest.

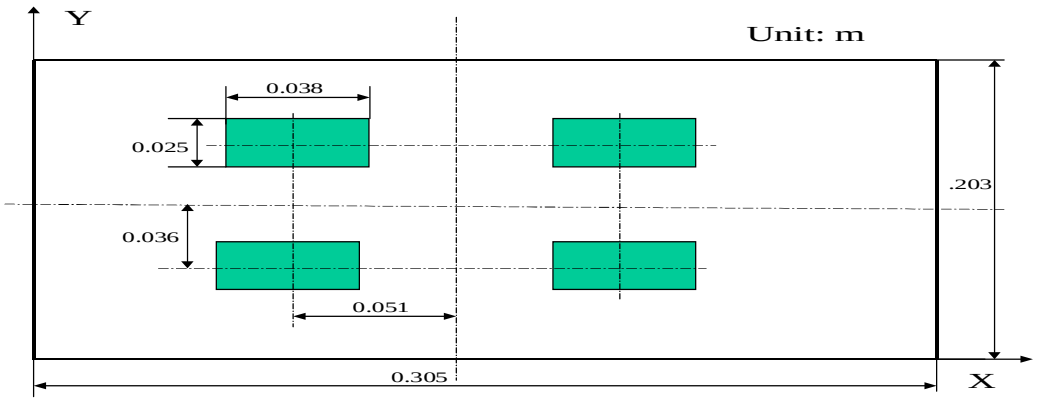

Figure 5.8: The optimized PZT locations for 4 actuators corresponding to κ up to 6.

Table 5.3: A comparison of q_1 and modal velocity vector at $\kappa = 2$

q_1	modal velocity	q_1	modal velocity
	$\kappa = 2$		$\kappa = 6$
0.9207	0.9701	0.9868	0.9166
0.2663	0	0.0377	0
0.2855	0.2425	0.1578	0.3998

If a central PZT patch is added to the other four symmetrically placed PZT patches, we can perform the optimization for these five PZT actuators. The constraints now change to:

$$a_p < dx < \frac{a}{2} \tag{5.19}$$

$$b_p < dy < \frac{b}{2} \tag{5.20}$$

$$1" < a_p < 2" \tag{5.21}$$

$$0.75" < r_p < 1.5" \tag{5.22}$$

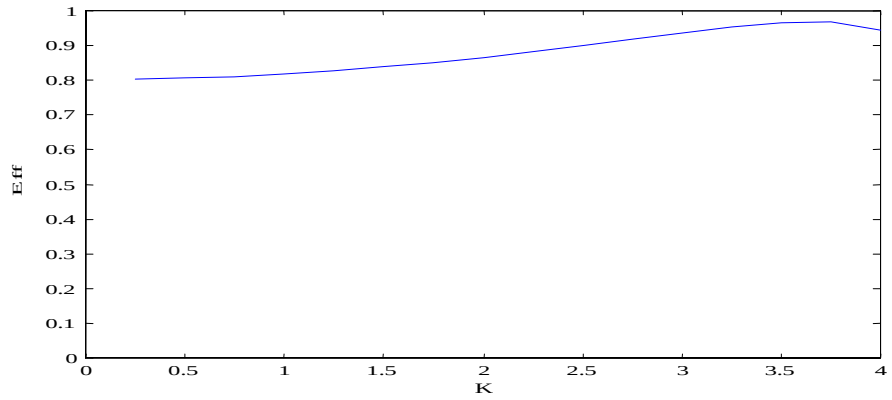

Figure 5.9: The optimization efficiency of PZT actuators corresponding to κ up to 4.

Table 5.4: The optimization of 5 PZT patches for $\kappa < 4$

Initial Conditions	dx	dy	Objective function	note
$a/4, b/4$	0.0928m	0.0547m	0.9825	

Again, the first two constraints will prevent the PZT from overlapping or moving out of the plate surface and these constraints will guarantee that the optimized solution is feasible. Using the same procedure, the constrained optimization problem are performed.

Because of the limitation of PZT sizes, we fix the $a_p = 1.5$" and $b_p = 1$" and optimize the location of center of PZT patches only. Table 5.4 lists the optimized locations for the PZT centers based on the optimization of efficiency at the frequency range up to $\kappa = 4$.

The optimal location can be decided with the optimal results of dx= 0.0928 m (3.6535") and dy=0.0547 m (2.1535"). The corresponding PZT locations are plotted in Figure 5.14.

The optimal function $\eta_{opt} = -0.9825$, i.e. the average efficiency is about 0.9825. The corresponding efficiency was computed at the frequencies of interest and it was

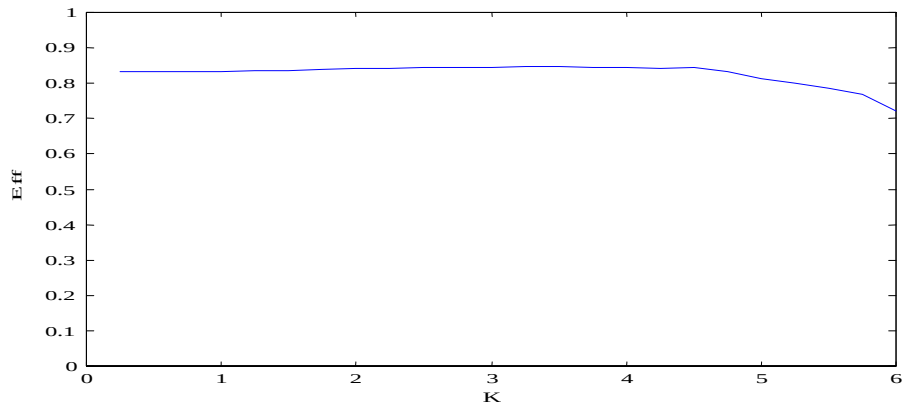

Figure 5.10: The optimization efficiency of PZT actuators corresponding to κ up to 6.

plotted in Figure 5.15. If we compare Figure 5.5 with Figure 5.15, we notice that although the efficiency of 5 actuators (one at the center of plate and the other four at the center of the quarter plate) was higher at high frequencies but it is lower at low frequencies than that of optimized results.

Traditionally, the optimization was focused on the noise reduction level, not the performance of actuators. In addition, the previous power efficiency studies did not focus on the optimization of the multiple distributed moment actuators. Therefore, the research so far shows that the power efficiency can only achieve high efficiency at a very low frequency bandwidth. Nevertheless, this optimization result suggested that even a very limited amount of actuators could greatly expand the high efficiency frequency bandwidth. The significance of this analysis lies in the fact that an optimization could greatly improve actuation efficiency of a multiple actuator array, which will benefit the active noise reduction. In addition, with the optimization, it is very possible to expand the frequency range of noise suppression.

5.5 Summary

In this chapter we focused on the power efficiency analysis of the multiple actuator arrays. The coupled dynamic model and generalized eigenvalue decomposition were

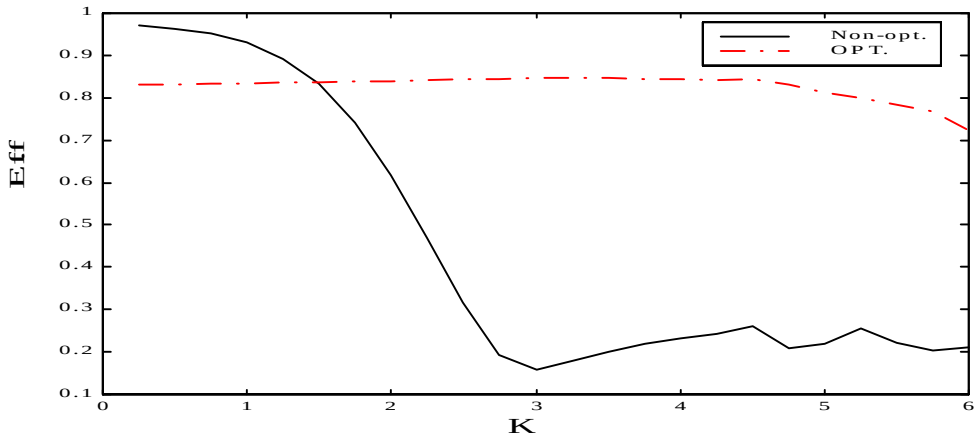

Figure 5.11: The optimization efficiency for four actuators at optimized locations and non-optimized locations, respectively.

integrated to analyze the efficiency. In order to maximize the efficiency of actuator arrays, the PZT locations were optimized for a given pattern of actuator placement. As literature review suggested, the previous optimization of actuator placement was mainly focused on the noise reduction, not the actuator performance. In order to overcome the disadvantages of previous optimization, this optimization procedures were concentrated on the maximization of the actuation performance, i.e. the maximum efficiency. The optimization procedure made it possible that the eigenvector corresponding to the largest eigenvalue of the power transfer matrix in a good match in phase and magnitude with those of the corresponding modal velocity vectors at all the frequencies of interest. Numerical analysis unexpectedly demonstrated that high actuation efficiency of the structure driven by the actuators at an optimized locations have been achieved for a much higher frequency bandwidth than previous analysis suggested. The significance of this optimization procedures lies in the fact the a very few optimally placed PZT actuators could significantly increase not only the efficiency but also the high efficiency bandwidth. This procedure could be easily modified to optimize more complicated PZT actuator placements during control designs.

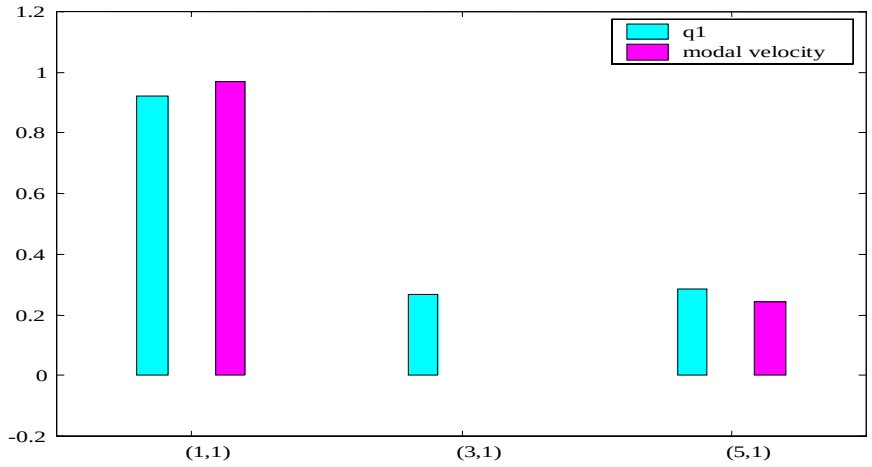

Figure 5.12: The q_1 vector and modal velocity at $\kappa = 2$ of radiated modes for the 4 pair actuator driven plate

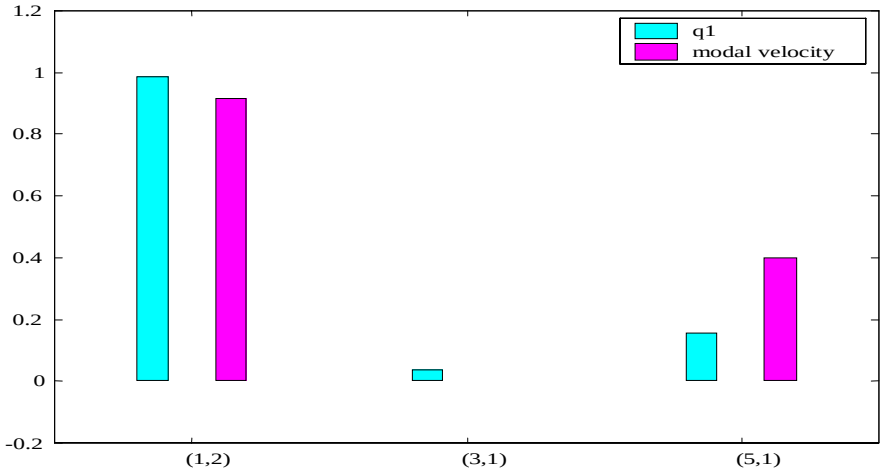

Figure 5.13: The q_1 vector and modal velocity at $\kappa = 6$ of radiated modes for the 4 pair actuator driven plate

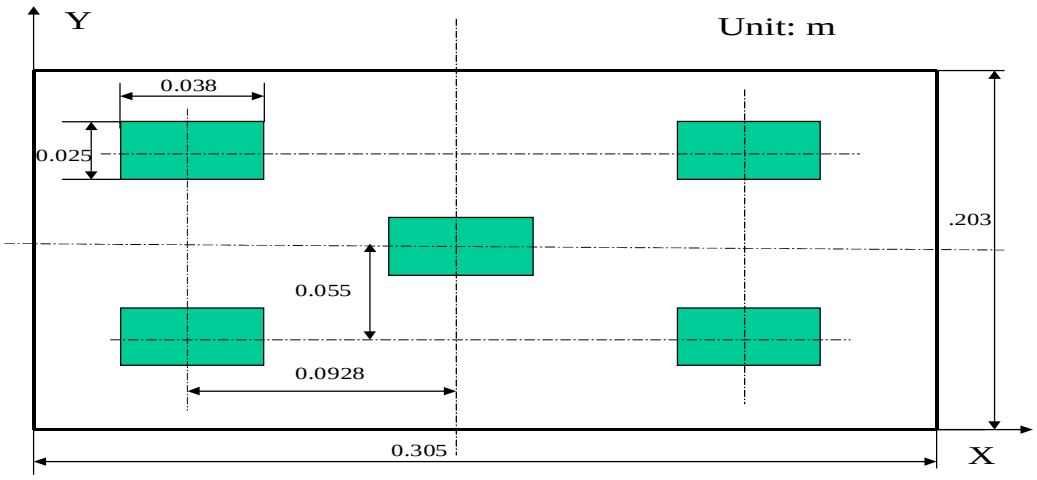

Figure 5.14: The optimized location for five PZT actuators

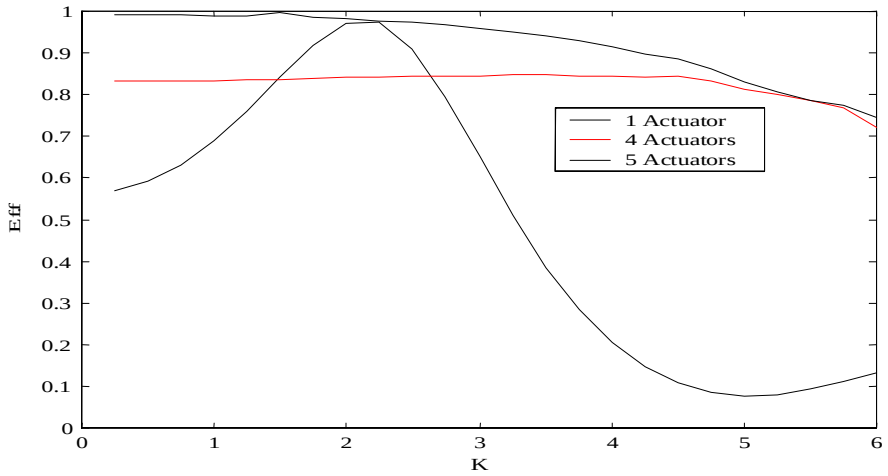

Figure 5.15: The power efficiency of the plate driven by the 5 PZT actuators at optimized locations.

Chapter 6

The Affect of PZT Patches on Power Efficiency

In previous chapters, we have investigated the power efficiency of the patched PZT actuator driven structure. However, the investigation is based on the assumption that the PZT actuators did not change the natural frequencies and modal shapes significantly. Therefore, the power efficiency is evaluated by integrating the weighted mode shapes using mode expansions. For a typical PZT application, the PZT area comprises approximately 0.5% of the total area of the structure. For such applications, the error of modal shape changes caused by PZT patches are small(refer to Table 2.5) and can be ignored if the relative thickness of a single PZT patch to the structure thickness is less than three. Therefore, the previous power efficiency analysis is valid.

Nevertheless, if the thickness of the structure itself is relatively thin comparing to the PZT patch or there are many PZT patches on the surface of the structure, the natural frequency and modal shape changes may be too large to be ignored. In this case, the power efficiency analysis using mode expansions based on the modal shape of the original structure needs further investigation. In this chapter, we will focus on the study of the effect of PZT patches on the power efficiency of the structures, whose PZT patches have a significant influence on the modal shapes and frequencies.

6.1 Mode Shape Effect on Power Efficiency

The expression for the active system equation(see Section 2.5.2) can be simplified as

$$(-\omega^2 M + K)\mathrm{U} = 0; \tag{6.1}$$

where U is the displacement, or the eigenvectors corresponding to the mode shape trial functions ϕ. The mode shape can be evaluated using the variational approach

$$\psi = U^T \phi \tag{6.2}$$

As we know, the PZT patches will change the system stiffness and mass and thus affect the system dynamics. The following is a derivation of the effect of the PZT patches on the actuation power efficiency. Assume the PZT patches cause the natural frequencies to change from ω to $\omega + \Delta\omega$, eigenvectors from U to $U + \Delta U$ and mode shapes from ϕ to $\phi + \Delta\phi$.

The mode shape of the active system could be expressed as the original mode shape plus the terms reflecting the mode shape changes caused by added PZT actuators.

$$\psi = (U + \Delta U)^T(\phi + \Delta\phi) = U^T\phi + U\Delta^T\phi + \Delta U^T\phi + \Delta U^T\Delta\phi \tag{6.3}$$

If we ignore the higher order term $\Delta U^T \Delta\phi$, the above expression can be simplified as

$$\psi = U^T\phi + U\Delta^T\phi + \phi\Delta^T U = \psi_0 + \Delta\psi; \tag{6.4}$$

where $\psi_0 = U^T\phi$ and $\Delta\psi = U\Delta^T\phi + \phi\Delta^T U$.

The power transfer matrix is rewritten as the following:

$$\alpha = \int_S \int_S \psi^T(\boldsymbol{\xi}') \frac{\sin(\kappa\eta)}{\eta} \psi(\boldsymbol{\xi}) d\boldsymbol{\xi}' d\boldsymbol{\xi}, \tag{6.5}$$

Similarly, if we ignores the second order terms, the matrix α for the active system can be expressed as

$$\alpha = \int_S \int_S ((\psi_0 + \Delta\psi)^T(\boldsymbol{\xi}') \frac{\sin(\kappa\eta)}{\eta} (\psi_0 + \Delta\psi))(\boldsymbol{\xi}) d\boldsymbol{\xi}' d\boldsymbol{\xi}, \tag{6.6}$$

and can be simplified as:

$$\alpha = \alpha_0 + \Delta\alpha, \tag{6.7}$$

where $\Delta\alpha$ is the power transfer matrix changes introduced by mode shapes.

$$\Delta\alpha = \int_S \int_S (\psi_0^T \frac{\sin(\kappa\eta)}{\eta} \psi_0 + \Delta\psi^T \frac{\sin(\kappa\eta)}{\eta} \psi_0)(\boldsymbol{\xi}) d\boldsymbol{\xi}' d\boldsymbol{\xi}, \tag{6.8}$$

The corresponding maximum eigenvector for the active structure can also be expressed as:

$$\lambda_1 = \lambda_1 + \Delta\lambda_1, \tag{6.9}$$

In addition, the modal velocity change can also be simplified as

$$v = v_0 + \Delta v, \tag{6.10}$$

Substituting equations (6.7),(6.9),(6.10) into equation (3.12), the power efficiency can be expressed as:

$$\eta = \frac{(v_0 + \Delta v)^H (\alpha_0 + \Delta\alpha)(v_0 + \Delta v)}{(v_0 + \Delta v_0)^H (v_0 + \Delta v)(\lambda_1 + \Delta\lambda_1)} \tag{6.11}$$

If the higher order terms are ignored, this expression can be further simplified as:

$$\eta = \frac{(v_0^H \alpha v_0 + \Delta v^H \alpha_0 v_0 + v_0^H \Delta\alpha + v_0^H \lambda_1 \Delta v_0)}{(v_0^H \lambda_1 v_0 + \Delta v_0^H \lambda_1 v_0 + v_0^H \Delta\lambda_1 + v_0^H \lambda_1 \Delta v_0)}. \tag{6.12}$$

Therefore, we can use the above mode shapes to evaluate the power transfer matrix and efficiency.

6.2 Normal Mode Analysis for Multiple PZT Patched Structure

The above analysis demonstrates that a PZT patch will change the structural modes of the original structure. As we know, changes in the mode shapes will affect the power transfer matrix and therefore the power efficiency. In this section, we will apply the variational approach to analyze the normal mode analysis of the structure.

As an example, the variational approach was applied to analyze the natural frequencies and mode shapes for an aluminum plate, whose dimensions are 12" x 8" x 0.008". A comparison will also be made between the variational method and FEA. As we can see from Table 6.1, for the plate under the simply supported, there is a very good match between the analytical frequencies and those predicted by the variational approach. Furthermore, we will apply this method to analyze the power efficiency of a thin structure, whose mode shapes and frequencies are substantially influenced by the PZT patches.

To model a variety of boundary conditions, the structure's boundary is represented by massless linear springs perpendicular to the plate and torsional springs. By varying the spring constants, the model can represent free, clamped, and simply supported boundary conditions as well as any combination of these extremes. In order to further verify the model accuracy, we will first apply the variational approach to analyze the normal mode analysis of the thin aluminum plate . The natural frequencies and modal shapes for this clamped thin plate without PZT patches are listed in Table 6.1. For the simply supported plate, the nondimensional translational spring constant $k = Ka^3/D$ was chosen as $1e8$ and the rotational spring constant c=0. The 9 terms of truncations of trial function were used in the variational approach. As we can see from the simply supported results from Table 6.1, the natural frequencies obtained from the variational approach agree with those of analytical results. The largest errors occured at $(4, 1)$ and $(4, 2)$ modes with the errors of 3.5% and 2.2%, respectively. For other frequencies, the two methods agree to within 0.0%. The slightly higher error for these two higher modes probably results from the fact that the index of the frequency is higher than others and we did not choose a large number of trial function terms to accurately represent the corresponding mode shape. If we increase the terms of trial functions, higher accuracy is expected.

Now we try to solve the normal modes for the same thin plate but under the clamped support. To simulate clamped boundaries, the rotational spring constant C is chosen as $1e5$, the translational spring constants as K=1e8. The corresponding frequencies of FEA and the variational approach were listed in the same Table 6.2. Re-

Table 6.1: A comparison of frequencies, Hz, of a simply supported thin plate

Freq. Index	Simply Supported *Analytic*	*Variatonal*	Error%
$1,1$	16.9971	16.9971	0.0
$2,1$	32.6867	32.6869	0.0
$1,2$	52.2987	52.2994	0.0
$3,1$	58.8361	58.8457	0.0
$2,2$	67.9883	67.9889	0.0
$3,2$	94.1377	94.1450	0.0
$4,1$	95.4451	98.7585	3.5
$1,3$	111.1348	111.1594	0.0
$2,3$	126.8244	126.8467	0.0
$4,2$	130.7468	133.6226	2.2

sults demonstrated that the frequencies predicted by the variational approach matches with those of FEA results. The percentage errors for all the modes are less than 4.5% except for the $4,1$ mode. The major reason for the larger error of the higher modes is that we do not use a sufficiently large number of trial functions. In the same table, the frequencies with one pair of central PZT patches whose thickness are 0.008" are also listed. As we see, this PZT pair has little influence on the frequencies and therefore, it will not significantly change the actuation power efficiency. As suggested by previous analysis, we could still use the original structural modes and frequencies to compute the power efficiency.

In addition to the frequency comparisons, the corresponding mode shapes of the active structure was also compared with those of the original structure. Figure 6.1 and 6.2 are the mode shapes of the thin plate without PZT patch and with a 1" x 1.5" x 0.008" PZT patch, respectively. As we can see, these two figures are almost identical. Based on the definition given in equation (2.29), the mode shape error for the active structure to its original host structure is 0.74 %. The mode shapes corresponding to those two cases are plotted for the convenience of reference.

Table 6.2: A comparison of frequencies,Hz, of a clamped thin plate

Freq. Index	FEA	woPZT	Error(%)	$w1PZT$	Error(%)
$1,1$	32.11	32.20	0.27	32.22	0.09
$2,1$	49.39	49.73	0.69	49.73	0.00
$1,2$	78.79	78.86	0.09	78.86	0.00
$3,1$	78.89	79.40	0.65	79.65	0.31
$2,2$	94.08	95.19	1.18	95.35	0.18
$3,2$	120.04	123.04	2.50	123.05	0.00
$4,1$	120.52	130.10	7.95	130.10	0.00
$1,3$	149.83	149.64	0.13	149.80	0.11
$2,3$	158.44	165.57	4.50	165.57	0.00
$4,2$	163.71	168.86	3.15	169.06	0.11

6.3 Influence on Power Efficiency

The immediately previous section investigated the PZT patch's influence on the mode shapes for large or thick PZT patches comparing to the size of the host structure. In this section, we will analyze the power efficiency changes incurred by the PZT patches.

As in previous calculations, the power efficiency is computed using the same definition, equation (3.12) but with the mode shapes, modal velocities, and frequencies of the active system instead of those of the plain host structure.

Using the variational approach, the normal modal analysis of the PZT patch driven structure is first evaluated. And then the power transfer matrix and modal velocities are computed. Finally, the power efficiency is calculated, refer to Sections 3.5 and 4.3.

Figure 6.3 is a plot of the efficiency of the simply supported 12" by 8" by 0.008" aluminum plate with one central thick (5 times of the plate's thickness) PZT patch. The solid line is the efficiency of the structure ignoring the PZT patch's influence on the normal mode analysis. The asterisk is the efficiency taking into account the

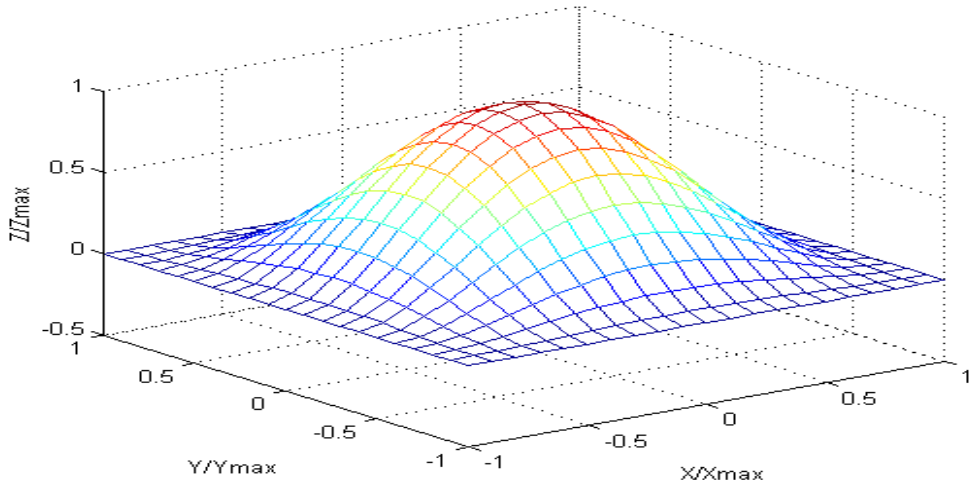

Figure 6.1: The first mode shape of the thin plate without PZT patches.

PZT patch's influence on the system's normal modes. The plot illustrates that these two curves are almost identical. However, detailed numerical analysis does show some errors exist between the efficiencies. The maximum efficiency error occurs at $\kappa = 0.19$ with the absolute error of 0.05, or percentage error of 8.46%. Therefore, we could conclude that ignoring the PZT patch's influence on the actuation power efficiency is not significant and the influence can be ignored if a relatively small piece of PZT patch is employed.

Then comes the question: if we increase the number of PZT patches, will the added amount of PZT patches have a significant effect on the power efficiency? Integrating the variational approach and the generalized eigenvalue technique, we will further investigate the PZT patches' influence on the power efficiency while taking into account the normal mode changes incurred by the PZTs. First, the natural frequencies are evaluated using the variational approach for $h_{pzt} = 5h_{plt}$. The natural frequencies of the structure with or without taking into account the influence of PZT patches on the normal modes are computed using the variational approach. As we could see from Table 6.3, the largest frequency error by ignoring the PZT patches' effect on the frequencies occurs at $(3, 1)$ mode. It is as high as 19%. For other frequencies, the error is very small. The large variation of the error depends on

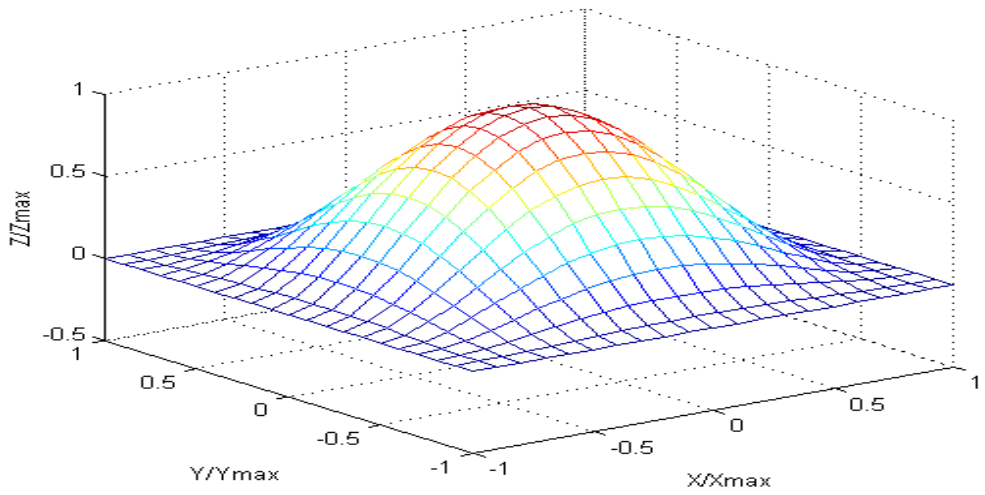

Figure 6.2: The first mode shape of the thin plate with a PZT patch.

the location of PZT patches, the frequency indices, as well as the accuracy of the variational approach, which is related to the number of terms in the trial function.

Integrating the variational approach with the generalized eigenvalue technique, the power efficiency is investigated. The corresponding efficiencies for the thin plate with or without the influence of PZT patches on the normal modes are plotted in Figure 6.7. Among the five PZT patches, one is placed at the center of the plate and the other four are placed in the same positions as specified the optimal location for the 1/8" thick plate in previous chapters. Figure 6.7 illustrates the power efficiency for a group of five actuators whose locations are the same as the optimal positions specified at previous chapters. The solid line is the efficiency of the structure ignoring the PZT patches' influence on the normal mode analysis. The asterisk is the efficiency taking into account the PZT patches' influence on the system's normal modes. As we could see, the difference is very small.

The following is a further analysis of the efficiency of the same group actuators but with the thickness equal to the thickness of the plate. Table 6.3 lists the natural frequencies of the structure with and without PZT patches, respectively. It shows that the PZT patches with a thickness comparable to the thickness of the plate do not cause much frequency change. Detailed numerical analysis demonstrates that

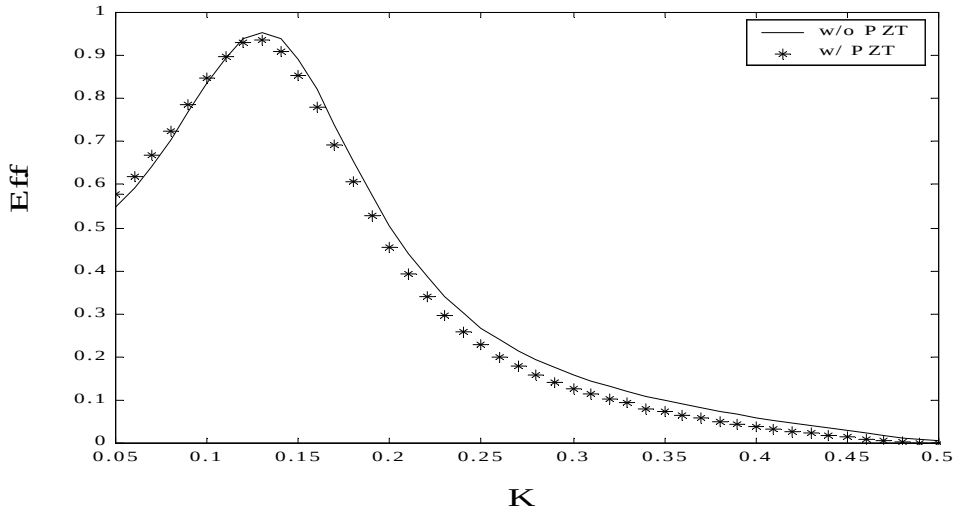

Figure 6.3: Power efficiency of a PZT patch driven thin plate with or with out taking into account the influence of normal modes incurred by PZT patch.

the maximum power efficiency error occurs at $\kappa = 0.36$ with an absolute error of 0.0056, and a corresponding percentage error of 1.09%. In addition, as we can see from Figure 6.4, the thickness does not change the efficiency significantly. In fact, the efficiency is a weak function of PZT patch thickness. The thickness does not change the mode shape much, although the moment generated by the PZT patches is proportional to the thickness of the PZT patch. Due to the cancelation of the influence of thickness in the numerator and denominator in the efficiency expression, it has a very small influence on the efficiency.

After investigated the power efficiency of the thin plate with 5 comparable thickness PZT patches, we now try to further study the relative thick multiple PZT patch on the power efficiency. Figures 6.5 and 6.6 are the first mode shape of the thin plate with 5 PZT patches and the first mode shape for the same plate without PZT patch, respectively. The corresponding natural frequencies are listed in Table 6.3. It's not hard to observe the two mode shapes. The existence of PZT patches causes the displacements near the center of the plate to be flatter than those of plain plate. In order to quantitize the variation of mode shapes caused by multiple PZT

Table 6.3: A comparison of the frequencies for 5 PZT patches ($h_{pzt} = 5 * h_{plt}$) driven structure

Index	fwnoPZT (Hz)	fw5PZT (Hz)	Error %	fw1PZT	Error %
$1,1$	16.9969	18.004	5.93	17.06	0.38
$2,1$	32.6865	33.0142	1.00	32.69	0.02
$1,2$	52.2988	52.5178	0.42	52.30	0.01
$3,1$	58.8449	70.0395	19.02	59.42	0.98
$2,2$	67.9876	76.6971	12.81	68.39	0.59
$3,2$	94.1425	95.6871	1.64	94.18	0.04
$4,1$	98.7567	101.3889	2.67	98.80	0.04
$1,3$	111.1571	122.6098	10.30	111.57	0.37
$2,3$	126.843	128.1702	1.05	126.86	0.02
$4,2$	133.6179	150.0928	12.33	134.19	0.42

patches, the previously defined mode shape error, equation (2.29), is used to evaluate the mode shape error. The corresponding errors for the first ten modes are listed in Table 6.3. As we could see, the largest mode shape error occurs at the first mode with a percentage error of 14.54%.

Figure 6.7 plots the efficiency of the 5 thick PZT patch actuator driven thin plate. As we can see from the plot, the efficiency calculated by taking into account of the mode shape changes caused by PZT patches is higher than that of ignoring the normal mode incurred by PZT patches, since the multiple thick PZT patches changed the system dynamics significantly. The added PZT patches will not only change the original system's natural frequencies and mode shapes, but also the power transfer matrix, which will cause the largest eigenvalue to vary. Therefore, the power efficiency will change. However, the detailed efficiency analysis demonstrated that the thickness of the multiple PZT actuators did not affect the power efficiency significantly. The reason is that the power efficiency is not directly related to the mode shapes, but the integration of mode shapes. The integral will decrease the sensitivity of the mode shapes on the power efficiency. Furthermore, each individual mode has different contributions to the efficiency. The comprehensive influences of the first certain modes

Table 6.4: A comparison of the frequencies for 5 PZT patches ($h_{pzt} = h_{plt}$ driven structure

Index	fwnoPZT (Hz)	fwPZT (Hz)	Error %
$1,1$	16.9969	17.0623	0.385
$2,1$	32.6865	32.6922	0.00
$1,2$	52.2988	52.3016	0.00
$3,1$	58.8449	59.4222	0.01
$2,2$	67.9876	68.3896	0.006
$3,2$	94.1425	94.1767	0.000
$4,1$	98.7567	98.7951	0.000
$1,3$	111.1571	111.5722	0.004
$2,3$	126.843	126.8636	0.000
$4,2$	133.6179	134.1851	0.004

may cancel each other at certain degrees, which further decrease the influence of PZT thickness on the power efficiency.

6.4 Summary

In this chapter, the efficiency of a PZT patch driven structure has been investigated by integrating the variational approach and generalized eigenvalue technique. Special interest is paid to the study of efficiency for the three cases: a relatively thick PZT patch, multiple PZT patches with a comparable thickness, and multiple thick PZT patches.

Numerical analysis illustrates that the relative thickness of the PZT patches has little influence on the power efficiency for the single PZT patch or multiple PZT patches with the comparable thickness to the thickness of the plate. In spite of the fact that the multiple thick PZT actuators may cause large frequency variations and mode shape changes, even for multiple relatively thick PZT patches, they did not cause significant difference on the power efficiency while their influence on the frequencies and mode shapes were compensated in the power efficiency analysis model.

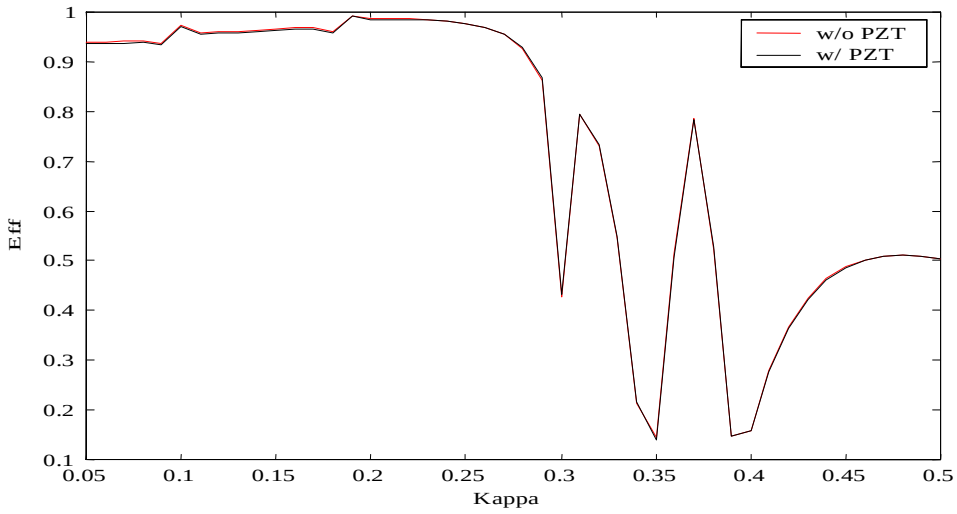

Figure 6.4: Power efficiency of 5 PZT patch ($h_{plt} = h_{pzt}$) driven thin plate with or with out taking into account the influence of normal modes incurred by PZT patch.

The reason is partly due to the fact that the efficiency is not directly proportional to the mode shapes, but to the integration of mode shapes. The integration reduces the sensitivity of the efficiency to the mode shapes. Therefore, we can conclude that the power efficiency analysis discussed previously, based on the original structural modes, is still valid for the multiple PZT actuator driven structures.

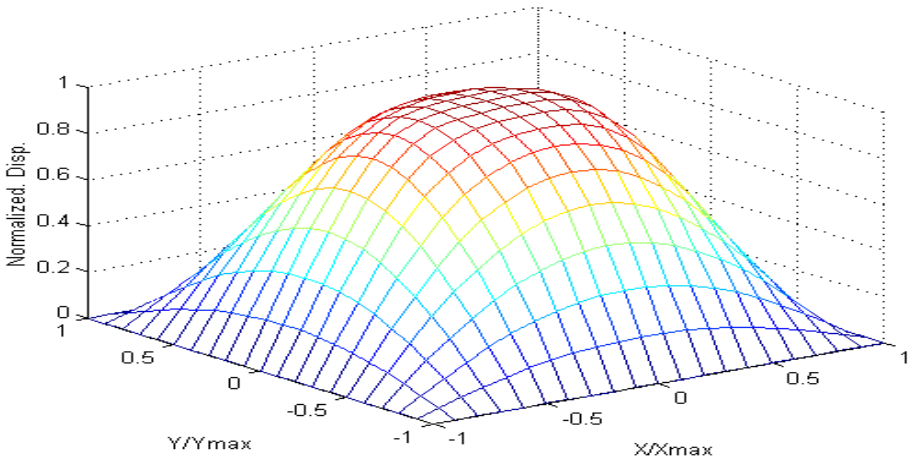

Figure 6.5: First mode shape for the simply supported thin plate with 5 PZT patches.

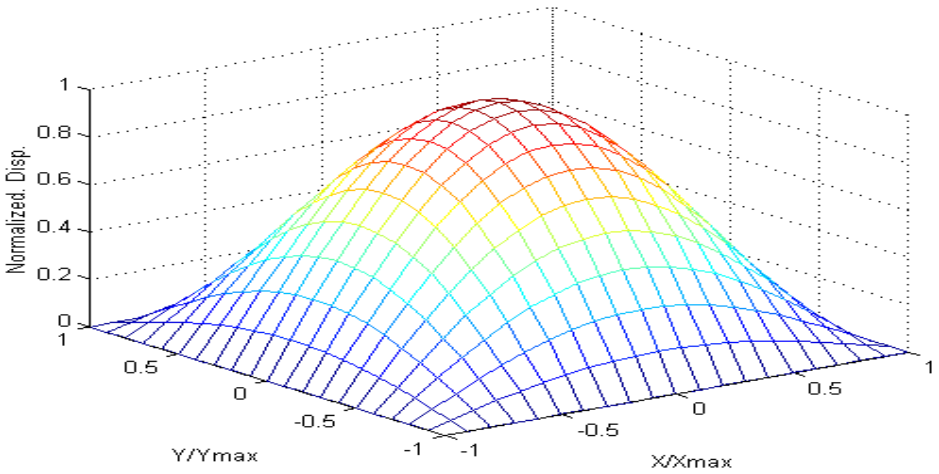

Figure 6.6: First mode shape for the simply supported thin plate without PZT patches.

Table 6.5: A comparison of the mode shape error between the 5 PZT patches ($h_{pzt} = h_{plt}$) driven structure and its plain structure

Index	Error %
$1, 1$	14.54
$2, 1$	-0.23
$1, 2$	1.15
$3, 1$	-7.07
$2, 2$	-7.38
$3, 2$	-11.54
$4, 1$	-3.12
$1, 3$	2.18
$2, 3$	-9.04
$4, 2$	-3.24

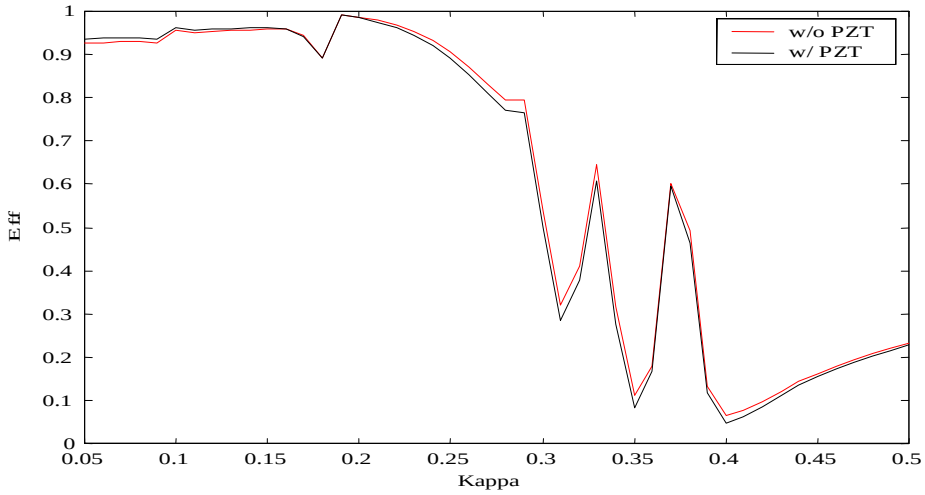

Figure 6.7: Power efficiency of 5 PZT patch ($h_{pzt} = 5h_{plt}$) driven thin plate with or with out taking into account the influence of normal modes incurred by PZT patch.

Chapter 7

Experimental Investigation

In previous chapters we have investigated the sound radiation power and power efficiency of point force and PZT patch actuator-driven structure. In this chapter, we will focus on the experimental investigation on the validation of the theoretical model. First we will briefly investigate the effect of PZT patches on the natural frequencies and damping ratios of the structure. Then, we will verify our analytical acoustic model by comparing the analytical sound radiation power and measured sound radiation power. The 12" by 8" aluminum plates, refer to Figure 7.1, with different thicknesses, 1/8" (actual thickness 0.1235") or 0.008" are respectively used in all of the experiments. Figure 7.2 is a diagram of the modal analysis test setup.

7.1 Modal Testing of the Test Fixture

The first attempt is to verify the feasibility and the accuracy of the fixture of the experimental setup, Figure 7.3. An experimental modal impact testing is served for this purpose. For the 1/8" thick plate, the simply-supported boundary condition is simulated. The plate is machined with grooves along the all four edges. Since the thickness of the groove area is much thiner than that of other areas, therefore, the plate could easily rotate while its edges are fixed by thread fasteners and the simply-supported boundary condition is simulated. An accelerometer is placed on the corner of the bottom left, coordinates (1",1"). A 4 by 6 mesh grid is adopted in the impacting

Figure 7.1: A plate with PZT patches.

test. Alternatively, a laser vibrometer is also used to measure displacement so that a non-contact measurement could improve the accuracy of the frequency response. This is especially important to the testing of a thin plate. The corresponding 24 FRF files are saved using Tektronix analyzer. With these data files, a commercial software package, STAR, is used to identify modes and determine the corresponding damping ratios.

The natural frequencies and damping ratios are listed with those of closed-form solutions in Table 7.1. Figure 7.4 is the FRF of the simply supported plate from 200 Hz to 2,000 Hz.

A comparison of the analytical and experimental frequencies are listed in Table 7.1. As we can see from the table, the first nine experimental natural frequencies upto 2000 Hz agrees with those of analytical results with the largest error of 1.95%. It demonstrates that the setup effectively simulates the simply supported boundary condition.

Secondly, a similar modal testing is performed for the same plate with four pairs of PZT patches bonded on the surface. The purpose of this analysis is to investigate how PZT patches affect the frequencies and damping ratios. The placement pattern of the PZT patches is shown in Figure 5.6. The modal analysis results of the plate

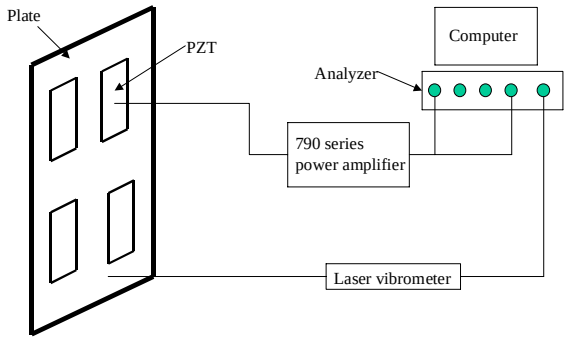

Figure 7.2: The mode analysis experiment setup.

with PZT patches are listed with those of the plate without additional actuators in Table 7.1. As we can see from the table, the PZT patches do cause some minor changes to the frequencies and modal shapes. Apparently, the glued PZT patches add mass to the plate and they also change the stiffness of the plate. Therefore, the natural frequency will change. Results demonstrate that the percentage influence of the PZT on the frequencies is much smaller than on the damping ratios. The largest damping ratio variation occurs at the first frequencies with a value increased from 0.65% of plain plate to 1.19% of the PZT patched plate. A similar modal testing is also performed on the thin plate (0.008"). The corresponding FRF and coherence curves are plotted at Figure 7.5.

Table 7.2 is a comparison of experimental and analytical frequencies of the clamped thin plate. The analytical results were calculated using the variational approach. Generally speaking, there is a good agreement between the experimental and analytical results with the largest errors less than 5.0%. There are many factors contribute to the discrepancy, such as insufficient terms of trial functions. However, one of the significant contributions to the error is that the variation of the mechanical behaviors in different directions of the thin plate. The coatings of the plate are not the same on the two sides. Because of the residual strains from manufacturing, the

Figure 7.3: A plate with PZT patches and fixtures.

plate has the natural bending trend while it is placed on a horizontal plane. Therefore, the plate's stiffnesses along x and y axes are different. In addition, there is no detailed material properties available for the plate.

7.2 Sound Radiation Power

After investigating the effect of PZT patches on the structural frequencies and damping ratios, our next step is to verify the accuracy of our sound radiation predition model. For the 1/8" thick plate, a simply-supported boundary condition is simulated with the same modal testing fixture. Four pairs of PZT patches are collocately placed on both side of the plate, see Figure 5.6. Two separate testings are performed. First, only the bottom left pair of PZT patches and then all the pairs are excited. The control voltage is applied to collocated PZT patches in such a way that they could be excited in phase. A Radio Shack OPTOMS 33-3003 microphone is used as a sensor to measure the sound pressure level. Referring to the Standard of ISO-3477:1994(E), the acoustic test is performed in the anechoic chamber. According to the Standard, a radius of one meter hemisphere is adopted in the testing. The microphone is positioned at ten points as suggested by the standard along the hemisphere surface to

Table 7.1: Frequency and damping ratio comparisons of a plate with or without PZT patches

Index	Ana. Freq.	Exp. Freq.	Error%	Damping ratio%	Exp. w PZT	Damping ratio %
1	262.4	265.87	1.32	0.65	263.07	1.19
2	504.6	500.77	0.76	0.42	500.11	0.615
3	807.4	804.17	0.33	0.32	801.94	0.605
4	908.3	899.02	1.02	0.24	904.41	0.34
5	1049.6	1035	1.39		1030.5	0.347
6	1453.3	1425	1.95		1430.5	0.479
7	1473.4	1465	0.57		1473	0.388
8	1715.6	1695	1.20		1688	0.649
9	1957.9	1960	0.11		1941	0.507
10	2018.4					

record the sound pressure level. The microphone is headed toward to the center of noise source so that the measurement could minimize the pressure error caused by the direction being inconsistent with the direction of the microphone calibration. A random signal is supplied to the actuators after it is amplified 20 times by the 790 series power amplifier. After the test, the signal from the microphone with the pre-amplifier is amplified by 50 times with a bypass mode of the Frequency Function Device. These signals along with the random signal are connected to three different channels of Tektronix analyzer. The corresponding time average signals and FRF, coherence functions are saved. The microphone is calibrated against a B&K calibration device, which generates 94dB sine 1000 Hz signal. The sensitivity is $7mv/Pa$. Since the microphone signal is amplified by 50 times before it is sent to the analyzer, therefore, the micro sensitivity K_1 with the amplifier is $350mv/Pa$.

The sound pressure levels L_p at each point is averaged using the following expression [ISO (1994)]:

$$\bar{L_p} = 10log10\left[\frac{1}{N}\sum_{i=1}^{N} 10^{0.1L_{pi}}\right]; \tag{7.1}$$

Table 7.2: A comparison of experimental and analytical frequencies of a thin clamped plate

Mode Index	$Ana.(Hz)$	$Exp.(Hz)$	Error (%)
$1,1$	32.20	29.00	2.17
$2,1$	49.73	52.53	5.64
$1,2$	78.86	76.86	2.53
$3,1$	79.40	83.13	4.70
$2,2$	95.19	103.78	1.57
$3,2$	123.04	121.11	3.51
$4,1$	130.10	125.53	3.5
$1,3$	149.64	146.18	2.32
$2,3$	158.44	150.60	4.95
$4,2$	168.86	170.88	1.19

where L_{pi} can be evaluated either using time signal or the FRF of microphone signal to input signal. The background noise is ignored since it is relatively weaker than the source. The testing is performed in the anechoic chamber. For convenience, the FRF is used for sound pressure level calculation. The magnitude of each FRF is evaluated using transfer functions. We can alternatively use the following expressions to compute sound pressure levels:

$$L_{pi} = 20log10\left[L_{pi}/L_{ref}\right]; \tag{7.2}$$

where $L_{ref} = 2x10^{-5}$ or approximately,

$$L_{pi} = 94 + 20 * log10\left[mag(FRF_i) * 1000/K1\right]; \tag{7.3}$$

where $mag(FRF_i)$ is the magnitude of FRF while microphone at ith point and the constant 1000 is introduced because the $K1$'s unit is mv/Pa instead of v/Pa. The sound pressure levels L_p at each point is averaged using the following expression:

$$\bar{L_p} = \frac{1}{N}\sum_{i=1}^{N} L_{pi}; \tag{7.4}$$

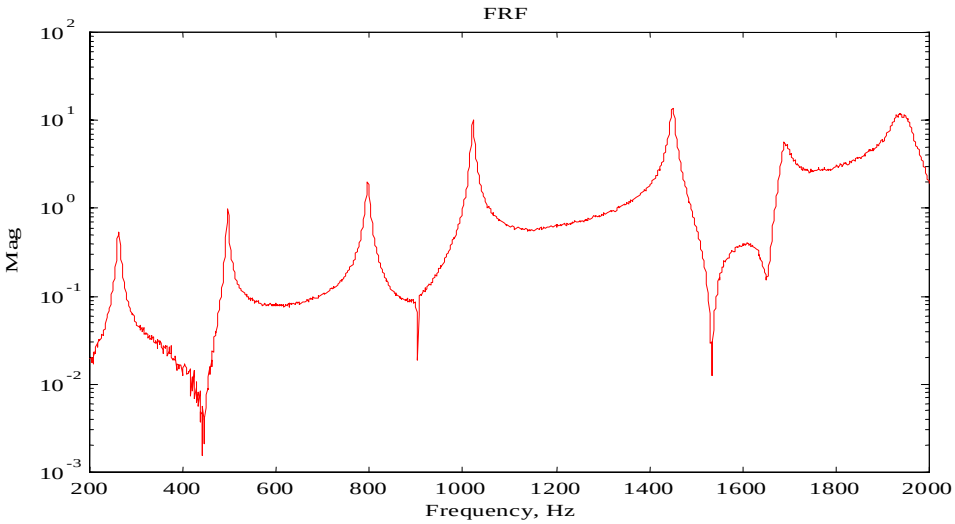

Figure 7.4: Experimental frequency response functions for the simply supported plate at (3", 7").

The sound power level, L_w, can be calculated as follows [ISO (1994)]:

$$L_w = \bar{L_p} + 10log10(\frac{S}{S_0})dB \tag{7.5}$$

where s is the area of the measurement surface of the hemisphere, in square meters, and $s_0 = 1m^2$.

For each plate, the acoustic testing is repeated by exciting the one pair actuators or four pair actuators, respectively.

Figure 7.6 is a diagram of the sound pressure measurement setup. Figure 7.7 and Figure 7.8 are the pictures of the anechoic chamber and the sound pressure measurement test setup inside the chamber, respectively.

In order to make comparison with experimental SPL, the coupled electro-mechanical model, which takes into account the dynamic electro-mechanical coupling, is used to predict SPL of the PZT patch driven plate. As a procedure, the active system's equivalent moments and modal velocities are first computed. Then the generalized eigenvalue technique is used to compute the efficiency. The corresponding value is plotted with experimental results in Figure 7.9. As we could see from this figure, the predicted resonance frequencies and the peaks of SPL match with experi-

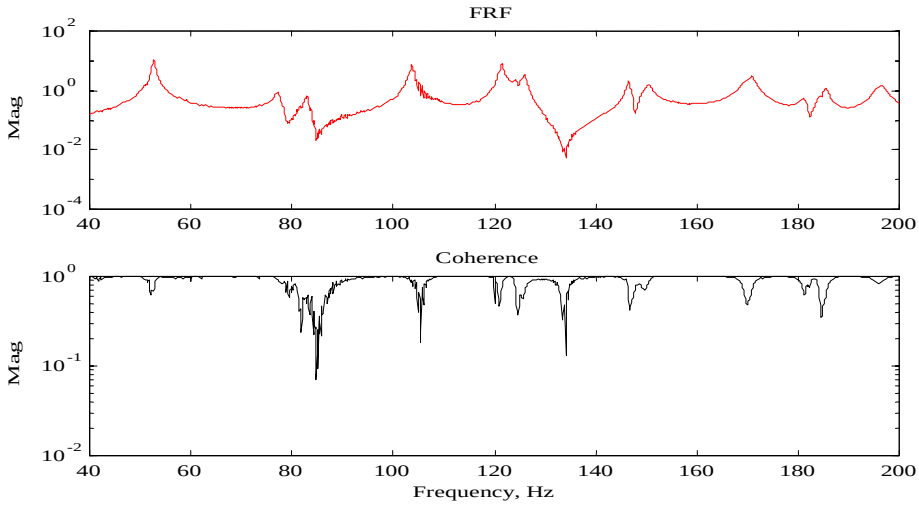

Figure 7.5: Experimental frequency response functions for the clamped thin plate at (3", 7").

mental results. Further numerical results show that the resonance frequency error is less than 1 %. The main reasons for the frequency discrepancies are as following:

1. The experiment setup does not exactly simulate the simply-supported boundary conditions.

2. The material properties may vary from what have been listed.

The possible reasons for the SPL difference are as follows:

1. Damping ratios are not the same as used in the model.

2. The fixture is not exactly symmetric in the normal direction of the plate. Therefore, the acoustic field is not symmetric as we modeled.

3. Low microphone resolution may have negative effect on the accuracy of the measurement.

In general, the coupled impedance model predicts the SPL with a reasonable accuracy, although further adjust material properties and damping ratios may result in a better accuracy.

Table 7.3: Frequencies and damping ratios for the PZT patched plate with or without supplying a voltage

	Without Voltage		With Voltage	
Index	Freq.,Hz	Damping ratio%	Freq.,Hz	Damping ratio %
1	263.07	1.19	263.04	1.01
2	500.11	0.615	495.35	0.368
3	801.94	0.605	795.54	0.544
4	904.41	0.34	904.84	0.245

The acoustic power efficiency with a given excitation at a specific frequency is defined as a ratio of the sound radiation power generated to the maximum achievable radiation power by the structure . According to this definition, the numerator is the sound radiation power, and the denorminator is its maximum achievable value. The maximum achievable radiation power is obtained while all the modal velocity components match with those of eigenvectors, q_1, corresponding to the largest eigenvalue of power transfer matrix. Unfortunately, in current test structure there are not enough inputs to adjust all the modal velocity components to exactly match q_1 components at all locations. In another words, it is not feasible to exactly measure the maximum possible radiation power of the structure based on current test design. Therefore, a direct validation of efficiency model needs furture work. However, not directly validating the efficiency model does not necessary means the model is not acceptable. Since we have verified the power transfer matrix calculation procedure by comparing to previous work, sound radiation by the experiments, and the maximum achievable power mathematically, it is meaningful to use this definition to investigate the performance of actuation and it is especially useful when it is used to make comparison among different actuators. The general conclusions from this work is also validated.

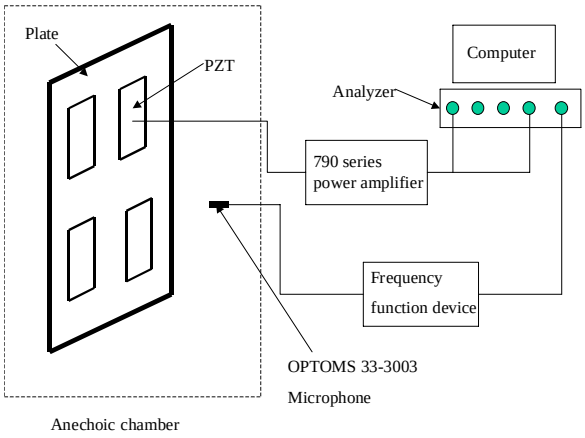

Figure 7.6: SPL measurement setup.

Figure 7.7: Anechoic chamber.

Figure 7.8: Acoustic testing setup inside anechoic chamber.

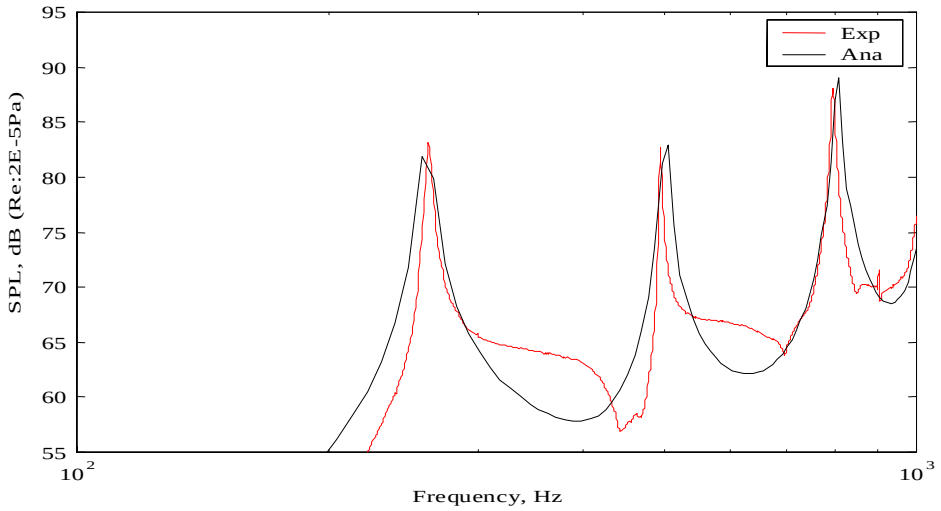

Figure 7.9: A comparison of analytical and experimental SPL of the plate driven by a pair of PZT patches.

Chapter 8

Conclusion and Recommendation

This dissertation studies the sound power radiation and power efficiency of the actuator driven structures. Based on eigenvalue techniques, the purpose of this study is to provide a easy way to compare the effectiveness of different actuators and thereby to help the designers to choose actuators. The major contents and conclusions are highlighted as follows.

8.1 Overall Conclusions

Based on the eigenvalue technique and mode expansions, a general method is proposed to study the sound radiation power of a planar structure. By integrating the variational method into the study, this hybrid approach processes a generality in the analysis of the sound radiation of any planar structure under an arbitrary geometry at any elastic supporting boundaries. This analysis confirms the previous results that the sound power radiation is a strong function of frequency and actuation location and boundary conditions affect the sound radiation.

By defining the maximum power efficiency as the ratio of power radiated from the structure to the maximum achievable power by the structure, the actuation power is reduced to an eigenvalue decomposition technique by Leo (1998). The power efficiency of a point force actuator driving structure is investigated. The power efficiency is simply proportional to the maximum eigenvalue of the power transfer matrix. The

numerical analysis shows that efficiency is a strong function of frequencies and actuator locations. Generally speaking, the single actuator driven structure has a narrow bandwidth of high efficiency. Typically, the efficiency is high at low frequencies and low at high frequencies. The maximum efficiency is near but does not necessary corresponding to the first resonance. In addition, the actuation location influences the efficiency greatly. The efficiency is also related to boundary conditions. It may not necessary change the efficiency value significantly. However, it will shift the power efficiency along the frequency axis, because of the different resonance frequencies for different boundary conditions.

Due to the popular applications of the PZT patches in the noise and vibration control, the power efficiency of a PZT patch driven structure is investigated using the coupled electro-mechanical impedance model [Zhou and Rogers (1995)]. Numerical analyses demonstrate that the efficiency of the PZT actuator driven structure is strongly dependent on the frequency, location, and number of PZT actuators. Generally speaking, the frequency of one PZT actuator has a narrow bandwidth of high efficiency at low frequencies and low efficiency at high frequencies. Changing a PZT actuator position will affect efficiency because it will excite certain modes and therefore influence mode velocity and sound radiation power.

The efficiency of a plate either driven by a point force or PZT patch has a narrow bandwidth of high efficiency. Using the generalized eigenvalue technique, the power efficiency study is extended to a multiple actuator array driven structure for both the point force actuators and PZT patch actuators. Results demonstrate that increasing the number of actuators will not only improve the efficiency but also the bandwidth of high efficiency. In order to increase the efficiency further, an optimization is performed for the PZT patch actuator locations and a relatively higher efficiency at a wider frequency bandwidth is achieved for the optimized multiple PZT locations.

This analysis also suggests that For the typical PZT patch applications the system dynamics of the integrated active structure will not significantly vary from the host structure. Therefore, their influences on the power efficiency analysis ignores

the mode shape change caused by the PZT patch, although the frequency and impedance change are taking into account in the coupled electro-mechanical impedance model. Combining the variational method with the power efficiency analysis, the power efficiency of an extremity, a very thin plate with relatively thick PZT patch driven structure, is investigated. The analysis shows that although a multiple thick PZT patches cause large frequency and mode shape variations, the efficiency variation is not so significant. As our analysis suggests that power efficiency is a function of modal velocity and transfer matrix. The frequency and mode shape changes will indeed cause power transfer matrix change. However, both the numerator and the denominator of the efficiency are proportional to the modal velocity and power transfer matrix or its maximum eigenvalue. Therefore, the efficiency is canceled out at numerator and denominator and make the efficiency not so sensitive to the PZT patch parameter as sound radiation power. Therefore, the previous efficiency analysis ignoring the mode shape variation of the integrated structure from the plain host structure is accurately even for the thick multiple PZT applications.

In addition, different experimental investigations, such as the experimental modal analysis, sound radiation power and structure vibration, are performed. These test results directly verify the coupled electromechanical model and sound radiation power analysis.

8.2 Recommendation For Future Work

Recommendation for further investigation are as follows:

In the experimental investigation, it is found that the thin plate has a natural bending trend even if it is placed on a flat surface. It was probably caused during the manufacturing. In addition, because of the limitation of the fixture, the resonance frequencies are not higher enough for the sound pressure measurement of the thin plate because of the cut-off frequency. For the further experimental investigation, re-designing the fixture of a thin plate and choosing the dimension of the plate in such a way that the first resonance frequency could be above the cut-off frequency of

the anechoic chamber.

Resign a structure to input have enough control inputs to make the modal velocity matches the eigenvectors q_1 as much as possible so that maximum possible sound radiation could be measured.

Integrating the power efficiency into the active structural-acoustic control. This work investigated the power efficiency from a point view of maximizing the actuator performance, which is helpful in actuator design and comparison. However, when a control algorithm is involved as in the ASAC, the control signal will interface the performance of actuators. It is worthwhile to extend the power efficiency analysis methodology presented in this work to analyze the actuator power efficiency of ASAC.

Extended this analysis to study the power efficiency of the sound transmission. Reducing transmission is another type of popular noise control involved in the engineering problem. To maximize the actuator performance and reduce the sound transmission with a few actuators will have practical engineering applications.

Bibliography

Leo, D. J., 1998, "Maximizing the power output of air-acoustic actuator arrays," J. of Intelligent Materials Systems and Structures, 98, p. 534.

Kim, S. J. and Song, K. Y., 1999, "Active control of sound field from plates in flow by piezoelectric sensor actuator," AIAA Journal.

Warnaka, G. E., 1982, "Active attenuation of noise– the state of the art," Noise Control Engineering, pp. 100–109.

C. R. Fuller, S. J. E. and Nelson, P., 1996, Active Control of Vibration, Academic Press, San Diego.

Fuller, C. R., 1990, "Active control of sound transmission/radiation from elastic plates by vibration inputs: I. Analysis," Journal of Sound and Vibration, 136, pp. 1–15.

Jones, L. D. and Fuller, C. R., 1989, "Active control of sound fields in elastic cylinders by force inputs," AIAA Journal, 27, pp. 845–85.

Stevens, J. C. and Ahuja, K. K., 1991, "Recent advances in active noise control," AIAA Journal, 29, pp. 1058–1067.

Widrow, B. and Stearns, S. D., 1985, Adaptive signal Processing, Prentice Hall, Englewood Cliffs, New Jersey.

Burdisso, R. A., , and Fuller, C., 1994, "Design of active structural acoustic control system by eigenproperty assignment," Journal of Acoustical Society of America, 93, pp. 1582–1591.

Ho, W. T. B. F. and Robertshaw, H. H., 1992, "Active structural acoustic control broadband disturbance," Journal of Acoustical Society of America, 91, pp. 1998–2005.

Fahy, F., 1985, Sound and structural vibration: radiation, transmission and responser, Academic Press, New York.

Wallace, C., 1972, "Radiation resistance of a rectangular panel," Journal of Acoustical Society of America, 51, pp. 946–952.

Maillard, G., 1974, "Vibration of and radiative classfications of modes of a baffled finite panel," Journal of Sound and Vbration, 34.

Lomas, N. S. and Hayek, S. I., 1977, "Vibration and acoustic radiation pf elastically supported rectangular plates," Journal of Sound and Vbration, 52.

Keltie, R. F. and Peng, H., 1987, "The effect of modal coupling on the acoustic power radiation from panels," ASME Trans. Journal of Vibration, Acoustic and Stress Reliability Design, 48.

Levine, H., 1984, "On the short wave acoustic radiation from planar panels or beams of rectangular shapes," Journal of Acoustical Society of America.

Elliot, S. J. and Johnson, M. E., 1993, "Radiation modes and the active control of sound power," Journal of Acoustical Society of America, p. 2194.

Naghshienh, K., 1993, "Active control of sound power using acoustic basis functions as surface velocity filters," Journal of Acoustical Society of America, 92, pp. 2740–2752.

Snyder, S. and Tanaka, N., 1995, "Calculating total acoustic power output using modal radiation efficiencies," Journal of Acoustical Society of America, 97, pp. 1702–1709.

Leo, D. J. and Paine, J. S., 1997a, "A comparison of point force and distributed actuators for the active control of structural sound radiation," In Proceedings of the Smart Structures and Materials Conference, San Diego, CA, 97, pp. 1702–1709.

Berry, A., Guyader, J., and Nicolas, J., 1990, "A general formulation for the sound radiation from rectangular, baffled plates with arbitrary boundary conditions," Journal of Acoustical Society of America, 88, pp. 2792–2802.

Song, T., 1995, "The optimal design of transducers for active control of multiple-frequency structural sound radiation," Ph.D. dissertation, Virginia Polytechnic Institute and State University, 88, pp. 2792–2802.

Sung, C. and Jan, C., 1997, "Active control of structurally radiated sound from plates," Journal of Acoustical Society of America, 102, pp. 370–381.

Aksu, G. and Ali, R., 1976, "Free vibration analysis of stiffened plates using finite difference methods," J. of Sound and vibration.

Mead, D., 1988a, "Free vibration of an orthogonally stiffened flat plate," J. of Sound and vibration.

Mead, D., 1988b, "Finite element free vibration of eccentrically stiffened plates," Computers and Structures.

Newbury, K. M. and Leo, D. J., 2000, "Structural dynamics of stiffened plates with piezoceramic sensors and actuators," AIAA/ASME/ASCE/AHS/ASC Structures, structural dynamics and materials conference and exhibit.

Cao, R. and Leo, D., 1998, "An eigenvalue technique for analyzing structural-acoustic power efficiency," Presented at Mathematics and control in smart structures, San Diego, CA.

Fuller, C. R., 1989, "Analysis of active control of sound radiation from elastic plates by force input," proceedings of inter-noise 88, Pittsburgh, p. 2079.

Dimitriadis, E. and Fuller, C., 1989, "Investigation on active control of sound transmission through elastic plates using Piezoelectric actuators for distributed vibration excitation of thin plates," Proceeding of the AIAA 12th Aeroacoustics conference, AIAA 89-1062.

Snyder, S. D. and Hansen, C. H., 1991, "The effects of the transmissio of sound," proceedings of the first conference on recent advances in active control of sound and vibration, p. 708.

Dimitriadis, B. T. W. E. K. and Fuller, C. R., 1990, "Active control of structually radiated noise using muitiple piezoelectric actuators," Proceedings of the AIAA/ASME/ASCE/AHS 31st Structural Dynamics and Materials Conference, Long Beach, CA.

Fuller, B. T. W. C. R. and Dimitriadis, E. K., 1991, "Active control of structually radiated noise using muitiple piezoelectric actuators," AIAA Journal, 29, pp. 1802–1809.

Clark, R. L. and Fuller, C. R., 1991, "Control of sound radiation with adaptive structures," Journal of Intelligent Material System and Structures, pp. 431–452.

Clark, R. L. and Fuller, C. R., 1992, "Optimal placement of piezoelectric actuators and polyvinvlidence fluoride error sensors in active structural acoustic control approaches," Journal of Acoustical Society of America, 91, pp. 1521–1533.

Varadan, V. V., Kim, J., and Varadan, V. K., 1997, "Optimal placement of piezoelectric actuators for active noise control," AIAA, 35, pp. 526–533.

Meirovitch, L. and Thangjithan, S., 1990, "Active control of sound radiation pressure," Journal of Vbration and Acoustics, 112.

Cunefare, K. A., 1991, "The minimum multimodal radiation efficiency of baffled finite beams," Journal of Acoustical Society of America, p. 2521.

Naghshineh, K. and Koopmann, G. H., 1992, "A design method for achieving weak radiator structures using active vibration control," Journal of Acoustical Society of America, 92, pp. 856–870.

Suanders, W. T. B. W. R. and Robertshaw, H. H., 1991, "Active suppression of acoustic radiation from impulsively excited structures," Journal of Acoustical Society of America, 90, pp. 3202–3208.

Palumbo, D. and Cabell, R., 2000, "Optimizing sensor and actuator arrays for ASAC noise control," SAE Technical Paper Series.

Feng, L., 1995, "Active control of structurally radiated sound using multiactuator method," Journal of Acoustical Society of America, pp. 397–402.

Leo, D. J. and Paine, J. S., 1997b, "Maximizing the power output of air-acoustic actuator array," In the Proceedings of the Adaptive Structures and Materials Symposium, International Mechanical Engineering Congress and Exposition, Dallas, TX, 97, pp. 1702–1709.

Crawley, E. and Luis, J., 1989, "Use of piezoelectric actuators as elements of intelligent structures," AIAA, 25, pp. 1373–1385.

Dimitriadis, E., Fuller, C., and Rogers, C., 1991, "Piezoelectric actuators for distributed vibration excitation of thin plates," Journal of Vibration and Acoustics, 113, p. 100 107.

Pan, J., Hansen, C. H., and Snyder, S. D., 1992, "A studey of the response of a simply supported beam to excitation by a piezoelectric actuator," Journal of intelligent material system and structures, pp. 3–15.

Liang, C. and Rogers, C. A., 1992, "Behavior of shape memory alloy actuators embedded in composites," Procedding of 1989 composites conference, Beijing, China.

Liang, C. and Rogers, F. S. C., 1994, "An impedance method for dynamic analysis of active material systems," Transactions of ASME, 116, pp. 120–128.

Hagood, N. M., Chung, W. H., and von Flotow, A., 1990, "Modeling of piezoelectric actuator dynamics for active structural control," Proceddings of the AIAA/ASME/ASCE/AHS/ASC 31st Structures, Structural Dynamics, and Materials Conference (Long Beach, CA), AIAA washinton, DC, pp. 2242–2256.

Zhou, S. W. and Rogers, C. A., 1995, "Power flow and consumption in piezoelectrically actuatored structures," AIAA, pp. 1305–1311.

Molyet, K., Peelamedo, S., Yu, Y., Naganathan, N., and Dukkipati, R., 1998, "Investigation of strain transfer in an induced strain actuator," Presented at Mathematics and control in smart structures, San Diego, CA.

Sun, C., Sun, F. P., and Roger, C. A., 1993, "Coupled electro-mechanical analysis of piezoelectric cermic actuator power consumption and system energy transfer," Proceddings of Smart Structure and Materials, SPIE, Albuquergue,NM, pp. 229–235.

Zhou, S.-W., 1994, "Coupled electro-mechanical system modeling and experimental investigation of piezoelectric actuator-driven adaptive structure," Ph.D. dissertation, Virginia Polytechnic Institute and State University.

Chattopadlyoy, 1999, "Coupled thermo-piezoelectric-mechanical model for smart composite laminates," AIAA Journal.

Giurgiutiu, V. and Rogers, C., 1996, "Comparison of solid-state actuators based on power and energy criteria," SPIE conference, 116, pp. 120–128?

Giurgiutiu, V., 2000, "Active-materials induced-strain actuation for aeroelastic vibration control," Shock and Vibration Digest, p. 355.

Snyder, S., Tanaka, N., and Kikushima, Y., 1995, "The use of optimally shaped pizeo-electric film sensors in the active control of free field structural radiation, part 1: Feed forward control," Journal of Vibration and Acoustics, 117, pp. 311–322.

Liang, C., Sun, F., and Rogers, C. A., 1992, "Investigation of the energy transfer and consumption of adaptive structure," Proceedings, IEEE Tucson Conference, Tucson, AZ.

Charette, F. and Berry, A., 1997, "Dynamic effects of Piezoelectric actuators on the vibration response of a plate," Journal of Intelligent Material Systems and Structures, 8.

Inman, D. J., 1994, Engineering Vibration.

Meirovitch, L., 1997, Principles and Techniques of Vibration, Prentice Hall.

Cao, R. and Leo, D. J., 1999a, "A matrix method for analyzing structural-acoustic power efficiency," 6th SPIE conference, New Beach, CA.

Cao, R. and Leo, D. J., 1999b, "A matrix method for analyzing astructral-acoustic power efficiency," Submitted to Journal of Sound and Vibration.

Lancaster, P., 1969, Theory of Matrices, Academic Press, New York, pp. 108–109.

Pierce, A., 1994, Acoustics: an introduction to its physical principles and applications, published by Acoustical Society of America, New Yorks.

Kinsley, 1982, Fundamentals of acoustics, Academic Press.

Morse, P. M. and Ingard, U., 1968, Theoretical acoustics, Journal of the Audio Engineering Society.

Bank, G. and Wright, J. R., 1995, "Radiation impedance calculations for a rectangular piston," Journal of the Audio Engineering Society, 38.

Clark, R. L., 1992, "Modal sensing of efficient acoustic radiators with polyvinylidene fluoride distributed sensors in active structural acoustic control approaches," Journal of Acoustical Society of America, 91, pp. 3321–3329.

Leo, D. J., 1999, "Energy analysis of piezoelectric-actuated structures driven by linear amplifers," Proceddings of the AIAA/ASME/ASCE/AHS/ASC 31st Structures, Structural Dynamics, and Materials Conference (Long Beach, CA), AIAA washinton, DC.

ISO, 1994, "Acoustics Determination of sound power levels of noise sources using sound pressue," Produced by GLOBAL ENGINEERIGN DOCUMENTS with the permission of ISO under royalty agreement.

Appendix A

Extrme Eigenvalues of

$max < X, AX >$

Let A be an n x n real symmetric matrix and define the unit sphere, θ, in R_n to be the set of all vectors in R for which $< X, X >= 1$, where X is vector. Consider the problem of finding the maximum value of $< X, AX >$ subject to the condition that $< X, X >= 1$. We write the quantities:

$$\begin{gathered} max < X, AX > \\ < X, X >= 1 \end{gathered} \tag{8.1}$$

Suppose that the eigenvalues of A are $\lambda_1 \geq \lambda_2 \geq ...\lambda_n$, that $\Omega = diag\{\lambda_1, ..., \lambda_n\}$, and let T be a real orthogonal matrix for which

$$T^T A T = \Omega. \tag{8.2}$$

We observe that if $X = TY$, then

$$< X, X >= X^T X = Y^T T^T T Y = Y^T Y =< Y, Y > . \tag{8.3}$$

Furthermore, since T is necessarily nonsingular, $RT^T = R_n$ and it follows that as X varies over all vectors in θ, so Y varies over all the vectors in θ and

$$\begin{gathered} max < X, AX >= max < TY, ATY >= max(Y^T T^T A T Y) = max(Y^T \Omega Y) = max(\sum_{j=1}^{n} \lambda_j y_j^2). \\ < X, X >= 1 \end{gathered} \tag{8.4}$$

Because of the ordering of the eigenvalues,

$$\sum_{j=1}^{n} \lambda_j y_j^2 <= \lambda_1 y_j^2 = \lambda_1 < Y, Y >= \lambda_1. \tag{8.5}$$

if $Y \in \theta$. Furthermore, with $Y = q_1$ we obtain $\sum \lambda_j y_j^2 = \lambda_1$. Hence, since $q_1 \in \theta$,

$$\begin{aligned} max < X, AX >= \lambda_1 \\ < X, X >= 1 \end{aligned} \tag{8.6}$$

Vita

The author, Renfang Cao, was born on June 10, 1963, in Changzhou, Jiangsu Province, China. He obtained his Bachelor of Science degree in Dynamic Machine from North China Institute of Technology, Taiyuan, China, in 1984. Later on he received his Master of Engineering degree in Mechanical Engineering from Mechanical Engineering Department, Nanjing University of Science and Technology. His master thesis was on the vibration and noise reduction of an aircraft gun. After graduation in 1987, he joined the faculty of the Department of Mechanical Engineering in the same University and worked as an Assistant Professor. In 1989 he moved to Jiangsu Institute of Chemical Technology, Changzhou, China, and worked as a Lecturer first and later the Associated Chairman of the Department of Mechanical Engineering. His eight years of work experience includes teaching and research on Machine Design and Analysis, Dynamics and Vibration, and Optimization. He moved to West Virginia University in August 1995 and quickly transferred to The University of Toledo in September the same year, where he conducted research on active structural-acoustic control. He received his second Master Degree of Science in Mechanical Engineering from the Mechanical, Industrial, Manufacturing Engineering in 1998. Then he moved to Virginia Polytechnic Institute and State University , in Blacksburg, Virginia, to continue to pursue his Ph.D. degree in the same year. He completed the requirements for the degree of Doctor of Philosophy in Mechanical Engineering in May 2001.

Permanent Address: 770 Coachman Dr, Apt. 2

Troy, MI 48083

This dissertation was typeset with LaTeX 2_ε[1] by the author.

[1] LaTeX 2_ε is an extension of LaTeX. LaTeX is a collection of macros for TeX. TeX is a trademark of the American Mathematical Society. The macros used in formatting this dissertation were written by Greg Walker, Department of Mechanical Engineering, Virginia Tech.